

# **The interaction of mitochondrial Uncoupling Protein-1 with regulatory ligands**

by

Riccardo Cavalieri

Thesis submitted for the Degree of Doctor of  
Philosophy

Norwich Medical School  
Biomedical Research Centre  
University of East Anglia, Norwich, UK

Date of submission: 31<sup>st</sup> December 2021

This copy of the thesis has been supplied on condition that anyone who consults it is understood to recognise that its copyright rests with the author and that use of any information derived there-from must be in accordance with current UK Copyright Law. In addition, any quotation or extract must include full attribution.

## Declaration of Authorship

I declare that the contents of my thesis entitled “The interaction of mitochondrial Uncoupling Protein-1 with regulatory ligands” are my original work, unless otherwise acknowledged, and have not been submitted for another degree in this or any other university. No parts of this research have been published prior to submission.

  
Riccardo Cavalieri

## **Abstract**

Brown adipose tissue of mammals possesses the specialised ability to oxidise nutrients to generate heat for thermoregulation. In adult humans, the thermogenic capacity of the tissue has attracted much interest for its potential to help combat obesity and metabolic disease. Brown fat thermogenesis relies on the Uncoupling protein 1 (UCP1), a member of the mitochondrial carrier family of metabolite transporters. When activated, UCP1 catalyses proton leak across the mitochondrial inner membrane, uncoupling mitochondrial nutrient oxidation from ATP production, releasing energy as heat. The protein is inhibited by cytosolic purine nucleotides and activated by free fatty acids, generated in brown adipocytes when stimulated. Through biochemical analysis of purified UCP1, these studies investigated the interaction of UCP1 with regulatory ligands to gain insight into the activation mechanism.

Assessment of ligand binding to native UCP1 by protein thermostability shift analysis, indicated that fatty acid activators likely interact as transport substrates of UCP1. Specific UCP1 thermostability shifts were used to identify ligands in screens, which revealed novel activators of UCP1, including the drug ibuprofen. The analysis also identified an interaction of UCP1 with the metabolite acyl-Coenzyme A, which could compete off the GDP inhibitor from the protein, representing a possible regulatory mechanism.

Yeast-expressed isoforms of human, mouse, and ovine UCP1 were generated, to show similar nucleotide binding and fatty acid-dependency for proton leak, suggesting that past claims of an inherent proton leak activity in only rodent UCP1 might be unlikely.

Finally, the generation of homology models of UCP1 isoforms, utilising recently available crystal structures of the related ADP/ATP carrier, suggests that UCP1 retains key structural features consistent with a conventional carrier transport mechanism. Novel state-specific bonding networks were also identified, potentially linking transport state shifts with changes in nucleotide affinity, leading to a structural hypothesis of how di- and tri-phosphopurine nucleotides interact with UCP1.

## **Access Condition and Agreement**

Each deposit in UEA Digital Repository is protected by copyright and other intellectual property rights, and duplication or sale of all or part of any of the Data Collections is not permitted, except that material may be duplicated by you for your research use or for educational purposes in electronic or print form. You must obtain permission from the copyright holder, usually the author, for any other use. Exceptions only apply where a deposit may be explicitly provided under a stated licence, such as a Creative Commons licence or Open Government licence.

Electronic or print copies may not be offered, whether for sale or otherwise to anyone, unless explicitly stated under a Creative Commons or Open Government license. Unauthorised reproduction, editing or reformatting for resale purposes is explicitly prohibited (except where approved by the copyright holder themselves) and UEA reserves the right to take immediate 'take down' action on behalf of the copyright and/or rights holder if this Access condition of the UEA Digital Repository is breached. Any material in this database has been supplied on the understanding that it is copyright material and that no quotation from the material may be published without proper acknowledgement.

# Table of contents

---

<b>Abstract .....</b>	<b>3</b>
<b>Table of contents .....</b>	<b>4</b>
<b>List of figures .....</b>	<b>7</b>
<b>List of tables.....</b>	<b>8</b>
<b>List of abbreviations.....</b>	<b>9</b>
<b>1. Introduction.....</b>	<b>11</b>
1.1 UCP1 is a characteristic feature of brown adipose tissue. ....	11
1.2 Brown Adipose Tissue (BAT).....	12
1.2.1 BAT in mammals .....	12
1.2.2 BAT in adult humans .....	13
1.2.3 BAT physiology and activation .....	15
1.2.4 UCP1 independent thermogenesis.....	18
1.2.5 Therapeutic activation of BAT and Ucp1 .....	19
1.3. Uncoupling Protein 1 .....	20
1.3.1 Discovery and early studies.....	20
1.3.2 UCP1 mechanism of activation .....	22
1.3.3 Activation of UCP1 by Reactive Oxygen Species (ROS).....	25
1.3.4 UCP1 structure – SLC25 conserved structural characteristics .....	26
1.3.5 The properties of UCP1 .....	28
1.3.6 UCP2 and the other uncoupling proteins UCP3-5 .....	30
1.4. General aim and objectives of the project .....	33
<b>2.Materials and Methods .....</b>	<b>35</b>
2.1 SDS PAGE .....	35
2.2 Western Blot.....	35
2.3 Silver stain .....	36
2.4 Protein thermostability assay.....	36
2.5 Purification of UCP1 .....	37
2.6 Proteoliposome formation .....	39
2.7 Flux assays.....	41
2.8 Homology modelling and sequence alignments .....	42
2.9 UCP1 gene cloning in plasmid and yeast transformation .....	42

2.10 UCP1 isoforms expression in yeast.....	44
2.11 Isolation of mitochondrial membranes from yeast.....	44
2.12 Sample quantification .....	45
2.13 Statistical analysis .....	45
2.14 Compounds used in screens .....	46
<b>3.The regulatory ligands of native ovine UCP1 .....</b>	<b>51</b>
3.1 Introduction.....	51
3.2. Aims.....	52
3.3. Results .....	52
3.3.1. UCP1 thermostability shifts and ligand interactions.....	52
3.3.2. UCP1 ligands exploration – thermostability based screen .....	58
3.3.3. UCP1 activators - transport assays.....	61
3.3.4. Ibuprofen activates UCP1-dependent proton transport.....	63
3.3.5 Oleoyl-CoA and UCP1.....	65
3.4 Discussion.....	67
3.4.1 Fatty acids as transport substrates of UCP1 .....	67
3.4.2 Novel activators of UCP1 .....	68
3.4.3 Low structural specificity of UCP1 activators .....	68
3.4.UCP1 and acyl-CoAs .....	69
<b>4. Characterisation of the human, mouse, and ovine UCP1 isoforms .....</b>	<b>72</b>
4.1 Introduction.....	72
4.2 Aims.....	73
4.3 Results .....	73
4.3.1 UCP1 isoforms expression in yeast .....	73
4.3.2 UCP1 isoforms purification .....	73
4.3.3 UCP1 isoforms thermostability analysis .....	76
4.3.4 UCP1 isoforms reconstitution in proteoliposomes .....	78
4.4 Discussion.....	82
4.4.1 Isoform purification and behaviour in the thermostability shift assay.....	82
4.4.2 UCP1 isoforms basal proton transport rates.....	83
<b>5. Homology modelling and systematic analysis of key structural features of UCP1</b>	<b>85</b>
5.1 Introduction.....	85
5.2 Aims.....	86
5.3 Results .....	86

5.3.1 Creating homology models .....	86
5.3.3 Analysis by symmetry .....	91
5.3.4 The common carrier substrate binding site in UCP1, the arginine triplet R <sup>84</sup> -R <sup>183</sup> -R <sup>277</sup> .....	93
5.3.5 UCP1 has the potential to form cytoplasm and matrix interaction networks.....	94
5.3.6. A novel structural feature: a secondary cytoplasmic network .....	97
5.3.7 Residues in the central cavity: a hydrophobic triplet.....	100
5.3.8 Residues in the central cavity: additional gating bonds relevant to nucleotide binding.....	102
5.3.9 Other carrier structural features .....	104
5.3.10. Other notable UCP1 amino acid residues.....	107
5.4 Discussion.....	110
5.4.1 Where do fatty acids bind on UCP1? .....	110
5.4.2 The secondary cytoplasmic network and nucleotide binding .....	111
<b>6. Discussion and conclusion.....</b>	<b>115</b>
6.1 Key experimental findings .....	115
6.1.1 The regulatory ligands of native ovine UCP1.....	115
6.1.2 Characterisation of the human, mouse, and ovine UCP1 isoforms.....	115
6.1.3 Homology modelling and systematic analysis of key structural features of UCP1 .....	116
6.2 General discussion.....	117
6.2.1. Acyl-CoAs interaction with UCP1 .....	117
6.2.2. UCP1 mechanism of transport: reconciling structural features and transport assay data .....	119
6.2.3 Novel UCP1 activators and possible translational avenues .....	121
6.2.4 Homology models and AlphaFold models of UCP1.....	121
<b>7.References.....</b>	<b>123</b>
<b>Appendix .....</b>	<b>139</b>

## List of figures

Figure 1.1 UCP1 uncoupling.....	11
Figure 1.2 Acute thermogenesis in brown adipocytes.....	16
Figure 1.3 Models of UCP1 mechanism .....	23
Figure 1.4 AAC structures in its two states .....	26
Figure 2.1 pYES2/CT vector map .....	43
Figure 3.1 UCP1 thermostability assay, the effect of activators and inhibitors .....	53
Figure 3.2 UCP1 activators profiles, a specific destabilizing effect.....	54
Figure 3.3 Trends in thermostability with fatty acids' acyl chain length.....	56
Figure 3.4 Trends in thermostability with alkyl sulphonates chain length .....	57
Figure 3.5 UCP1 thermostability screen for detection of interacting ligands.....	59
Figure 3.6 Thermostability ligand screen – ligands inducing significant changes in melting temperature. ....	60
Figure 3.7 The activation of UCP1 in proteoliposomes by novel ligands.....	62
Figure 3.8 Ligands increasing the melting temperature are non-inhibitors in flux assays..	63
Figure 3.9 Ibuprofen metabolites do not induce proton transport.....	64
Figure 3.10 Oleoyl CoA ligand interactions with UCP1.....	66
Figure 4.1 Coomassie gels and western blots of purification profiles .....	74
Figure 4.2 Silver stain gels of UCP1 profiles.....	75
Figure 4.3 The thermostability of recombinant UCP1 isoforms .....	76
Figure 4.4 T <sub>m</sub> values of the recombinant UCP1s compared to native UCP1 upon GDP or CATR addition .....	77
Figure 4.5 Determination of UCP1 reconstituted in liposomes.....	79
Figure 4.6 Flux assays with recombinant UCP1 isoforms .....	80
Figure 5.1 Distribution of generated homology models for HsUCP1 c-state, according to RMSD and estimated overlap to the template AAC structure.....	88
Figure 5.2 Example of quality control with QMEANbrane with a OaUCP1 model.....	90
Figure 5.3 The arginine triplet.....	93
Figure 5.4 Human UCP1 model as seen from the membrane in c and m-states .....	94
Figure 5.5 Cytoplasmic and matrix gates of AAC and UCP1 with their relative network strength.....	95
Figure 5.6 The secondary cytoplasmic network.....	98
Figure 5.7 FIW triplet and its position in OaUCP1.....	101
Figure 5.8 The interaction between R92 and E191 in HsUCP1.....	104
Figure 5.9 Overview of carrier features possessed by UCP1, shown on HsUCP1 models .....	106

Figure 5.10 Further important residues in UCP1, shown on HsUCP1 models.....	109
Figure 5.11 A model for the regulation of binding of triphosphopurine nucleotides to UCP1, involving residues of the secondary cytoplasmic network .....	112

### List of tables

Table 2.1 Buffer composition for flux assays.....	40
Table 2.2 Molecules for thermostability screens.....	46
Table 5.1 Overview information of the creation and refinement process for generating UCP1 homology models .....	87
Table 5.2. Model refinement – MolProbity score.....	89
Table 5.3. Example of residue interactions analysis in HsUCP1.....	92
Table 5.4 Sequence alignment – secondary cytoplasmic network .....	100

## List of abbreviations

12MNG: lauryl maltose neopentyl glycol detergent  
4HNE: 4-hydroxy-2-nonenal  
AAC: ADP/ATP carrier  
ATF2: activating transcription factor-2  
ATGL: adipose tissue triglyceride lipase  
ATP: adenosine triphosphate  
BAT: brown adipose tissue  
BMCP1: brain mitochondrial carrier protein  
BMI: body mass index  
CAC: carnitine/acyl-carnitine carrier  
cAMP: cyclic adenosine monophosphate  
CATR: carboxyatractyloside  
CCCP: [(3-chlorophenyl) hydrazono]malononitrile  
CK: mitochondrial creatine kinase  
CPM: 7-Diethylamino-3-(4'-Maleimidylphenyl)-4-Methylcoumarin  
CRE: cAMP responsive elements  
CREB: cAMP responsive element binding protein  
DDM/12M: n-dodecyl- $\beta$ -D-maltoside  
dH<sub>2</sub>O: distilled water  
DIC: dicarboxylate carrier  
DIO2: iodothyronine 5'-deiodinase  
DNP: 2,4-dinitrophenol  
DOPC: 1,2-dioleoyl-sn-glycero-3-phosphocholine  
FDG: fluorodeoxyglucose (<sup>18</sup>F)  
FFAs: free fatty acids  
GDP: guanosine diphosphate  
HSL: hormone sensitive lipase  
IMM: inner mitochondrial membrane  
IMS: intermembrane space  
LDL: low-density lipoprotein  
log*P*: partition coefficient of a molecule between an aqueous and a lipophilic phase  
M2OM: 2-oxoglutarate/malate carrier  
MANT-ATP: 2'/3'-O-(N-Methyl-anthraniloyl)-adenosine-5'-triphosphate

NMR: nuclear magnetic resonance

p38MAPK: p38 mitogen-activated protein kinase

PBFI: 1,3-Benzenedicarboxylic acid, 4,4'-[1,4,10,13-tetraoxa-7,16-diazacyclooctadecane-7,16-diylbis(5-methoxy-6,2-benzofurandiyl)]bis-tetrakis[(acetyloxy)methyl] ester

PET: positron emission tomography

PET-CT: positron emission tomography-computed tomography

PKA: protein kinase A

PP $\gamma/\alpha$ : peroxisome proliferator activated receptor  $\gamma$  and  $\alpha$

RAR: 9-cis retinoic acid receptor

RMSD: root mean square deviation

ROS: reactive oxygen species

SC-ura: synthetic complete supplement mixture of amino acids without uracil

SL+G: selective lactate + glucose culture medium

RXR: retinoid X receptor

SDS: sodium dodecyl sulphate

SERCA: sarco-endoplasmic reticulum Ca<sup>2+</sup> ATPase

SPQ: 6-Methoxy-N-(3-Sulfopropyl)Quinolinium, Inner Salt

T<sub>m</sub>: protein melt temperature

TNPs: triphosphopurine nucleotides

TOCL: tetraoleoyl cardiolipin

TR: thyroid hormone receptor

TRE: thyroid hormone responsive elements

TTNPB: (4-[(E)-2-(5,6,7,8-Tetrahydro-5,5,8,8-tetramethyl-2-naphthalenyl)-1-propenyl]benzoic acid

UCP: uncoupling protein

VLDL: very low-density lipoprotein

WAT: white adipose tissue

# 1. Introduction

## 1.1 UCP1 is a characteristic feature of brown adipose tissue.

UCP1 is a characteristic protein of brown fat, representing about 5 % of total mitochondrial protein in the tissue [1]. Brown fat, or brown adipose tissue (BAT) is a particular type of adipose tissue, which, while acting similarly to white adipose tissue as a storage for energy (in the form of triglycerides stored in lipid droplets), is also capable of dissipating the stored energy into heat [2]. BAT acts physiologically as a secondary thermogenic source, distinct from muscle contraction (shivering) for mammals, especially small hibernators, and neonates of larger ones. It is the source of non-shivering thermogenesis, generating heat through the activity of UCP1, the mitochondrial uncoupling protein 1 [3, 4]. UCP1, which is not inherently active, being inhibited by cellular concentrations of purine nucleotides [5, 6], uncouples the oxidation of respiratory substrates from ATP production by catalysing proton leak across the mitochondrial inner membrane, thus dispersing the electrochemical proton gradient created by the electron transport chain with the energy received from the Krebs cycle and  $\beta$ -oxidation (in the form of electrons), as illustrated in figure 1.1.

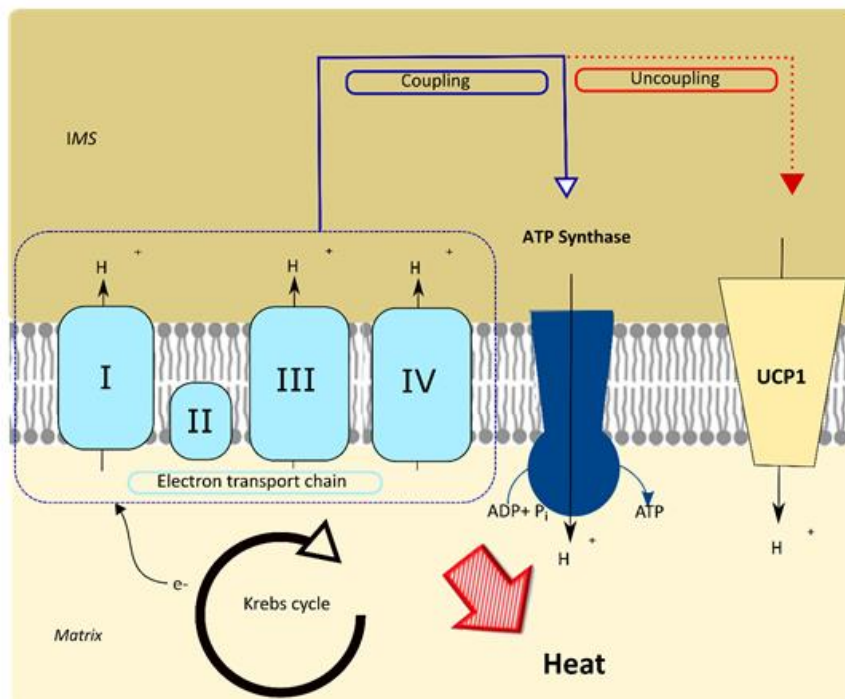


**Figure 1.1 UCP1 uncoupling.** UCP1 uncouples the oxidation of nutrients from the synthesis of ATP. The energy stored in the form of an electrochemical gradient across the

inner mitochondrial membrane is instead dispersed by the system as heat. IMS = intermembrane space; ATP = adenosine triphosphate; ADP = adenosine diphosphate;  $P_i$  = inorganic phosphate; UCP1 = uncoupling protein 1;  $H^+$  = proton;  $e^-$  = electron.

## **1.2 Brown Adipose Tissue (BAT)**

### **1.2.1 BAT in mammals**

The original discovery of BAT in mammals dates back to the 16<sup>th</sup> century [7, 8]. A Swiss naturalist named Conrad Gessner first described in 1551, in his text "*Tigurine Historie Animalium*", the existence in marmots of a particular kind of fat in the back area, which he described as being neither flesh nor fat and bearing a similitude to an endocrine gland [9]. BAT was then "rediscovered" in the early 1960s and recognized for its heat-producing function when physiologists investigated the origin of non-shivering thermogenesis in hibernating mammals [7]. In the early sixties, studies in rats and bats identified the thermogenic function of BAT in small mammalian hibernators [10, 11]. Smith and Hock [10] described the thermogenesis in BAT, and how heat was then distributed to the thoracic and spinal areas through the vascular system, to protect the organism from cold. The tissue is unique to eutherian (placental) mammals, particularly those that hibernate [12]. Small rodents, such as mice, hamsters, and rats, have been the first model organisms in which BAT properties have been studied [13].

BAT is a morphologically distinct type of adipose tissue, differing from the subcutaneous white adipose tissue on several features. The tissue presents a lobulated structure rich in capillaries, which supports its high metabolic rate and the necessity to quickly spread the generated heat to the whole body through the vascular system [2, 9]. Brown adipocytes contain numerous lipid droplets for storage, in contrast with the unilocular lipid deposits of white adipocytes [2, 12, 14]. Moreover, brown adipocytes are rich in mitochondria, and thus of cytochromes and iron, which confer their characteristic brown colour [2, 9]. Brown mitochondria also possess an extended inner membrane with an increased number of cristae protruding into the matrix, helping them to sustain a higher respiratory rate [15].

BAT is present in several areas of the body, both subcutaneous and intraperitoneal, but with a marked predominance in the thoracic region. BAT depots are present in the interscapular (forming up to 50 % of total BAT in mice [16]), subscapular, intercostal, periaortic and perirenal regions, as well as the dorsal cervical area [2, 8, 17].

### **1.2.2 BAT in adult humans**

Although it had been known since the 1980s that BAT is present in humans, it was originally thought that depots of tissue were limited to infants [18, 19]. These depots would help to combat cold exposure, protecting vital organs, but would later disappear during adulthood. However, between 2007 and 2009 BAT was discovered in adult humans, as reported in three articles published in early 2009 in the *New England Journal of Medicine* [20-22]. Positron emission tomography (PET) scans, routinely used in oncology studies and diagnosis, detected high uptake of glucose in adult subjects in symmetrical areas in the sub clavicular and neck regions of healthy tissue. PET scans use a radioactive form of glucose, fluorodeoxyglucose ( $[^{18}\text{F}]$  FDG), to track the metabolic rate of tissues based on the quantity of glucose consumed, since neoplastic formations have high metabolic needs [23]. The areas identified in the scans did not show abnormal growths, and tumours metastasis are not symmetrical. Using PET- CT scans (which can estimate the density and composition of a tissue) it was determined that the areas were not muscles and were similar to adipose tissue [20-22]. Further investigation, including immunostaining of bioptic samples from the areas, revealed that the areas identified were functioning BAT deposits [19-22].

Although there are few main locations of BAT depots in humans, the cervical and supraclavicular areas are by far the most studied, constituting around 66 % of total BAT and about 70 % of tissue activity [24, 25]. Strikingly, PET-CT studies on patients of both sexes and a wide range of age groups revealed the absence of any sexual dimorphism in BAT depots distribution, in contrast with white adipose tissue (WAT) [20]. White adipose tissue tends to accumulate on the thighs in women while on the abdomen in men [26]. The presence of BAT showed a marked inverse correlation with the body mass index (BMI) of patients (i.e., the leaner the patient, the higher

the chance they possessed significant depots of BAT) and their age (younger patients possessed more BAT, while almost none was detected in patients over 70 years old) [20]. Moreover, from the intense study that began in the last decade a further characteristic has emerged, BAT can be differentiated in two distinct types: classical brown fat and “beige” fat or “brite” (brown in white) [27, 28]. Stemming from studies on rodents it has been clarified in recent years that both humans and rodents possess a second type of brown adipocyte, defined as beige (or brite) adipocytes, interspersed in the white adipose tissue (WAT) [29]. The first studies on the subject raised the possibility that human BAT could be more similar to mouse beige fat than to conventional brown adipocytes, a hypothesis supported by similarity in gene expression profiles between the two tissues [27, 29]. However, studies of the interscapular BAT of infants [30] and of BAT in the neck area of adults [25] confirmed that, similarly to rodents, humans possess both types of brown adipocytes, and it seems that human classical BAT resembles mouse BAT [31]. Brown adipose tissue is present only in low amounts in adult humans (when it is present at all), about 15 - 250 mL [32]. Beige fat contains about 10% of the UCP1 that is in classical brown fat [32].

Beige adipocytes differ firstly on their anatomical location. They occur in WAT, in subcutaneous regions, and their differentiation is inducible in response to an external adrenergic stimulus [28]. They are rich in mitochondria and possess multilocular lipid droplets in the cytoplasm, making them functionally similar to conventional brown adipocytes. Furthermore, it has been determined that classical brown adipocytes and beige have different developmental origins [14, 33]. While brown adipocytes differentiate from precursor cells expressing the Myf5 marker [34], beige adipocytes derive from bipotential progenitor stem cells located in the perivascular areas of WAT, and express markers such as PDGFR $\alpha$ /sca-1 and CD34 [35, 36], typical of white fat.

Myf5 is a marker found in myocyte progenitors, encoding a regulatory factor for muscle development [34]. Its presence shows how conventional brown adipocytes are related to skeletal muscle cells rather than to white adipocytes, which is also reflected in one of their morphological characteristics, i.e. the high density of mitochondria in which energy is transduced for these two types of metabolically active cells [9]. Beige adipocytes, on the other hand, derive from Myf5 negative cells,

which can either differentiate into white adipocytes or into beige adipocytes, if subject to a  $\beta$  adrenergic stimulus. Hence, beige adipocytes are more closely related to white adipocytes, although capable of expressing the same functional capabilities of conventional brown adipocytes [9, 29, 34].

### **1.2.3 BAT physiology and activation**

UCP1 activity is strictly regulated in BAT. Activation of non-shivering thermogenesis to maintain thermoneutrality in a colder environment is initiated when the sympathetic nervous system is stimulated by the centres in the brain perceiving changes in environmental temperature (or increased food uptake) [2, 37]. The generated excitatory stimulus is then transmitted to BAT by release of noradrenaline, and intracellular signalling cascades ensue. These cascades are cAMP dependent and include both an acute response and a chronic response, with an increase in UCP1 gene expression and brown adipocyte proliferation [2].

Acute activation (figure 1.2) occurs simultaneously to chronic activation in response to an external stimulus. Postganglionic sympathetic nerve terminals, which are situated near BAT, release catecholamines, mainly norepinephrine, to stimulate adrenoceptors [38, 39]. Brown adipocytes possess all 3 types of  $\beta$ -adrenergic receptors, as well as both types of  $\alpha$ -receptors [2]. However, the pivotal receptor involved in the thermogenic response is the  $\beta_3$  [40]. In humans, in contrast, mature brown adipocyte activation seems to rely more on the  $\beta_1$ , as well as  $\beta_2$  adrenoceptor, as BAT activation is inhibited at amounts of propranolol tailored for  $\beta_1$  rather than  $\beta_3$  [19, 41].

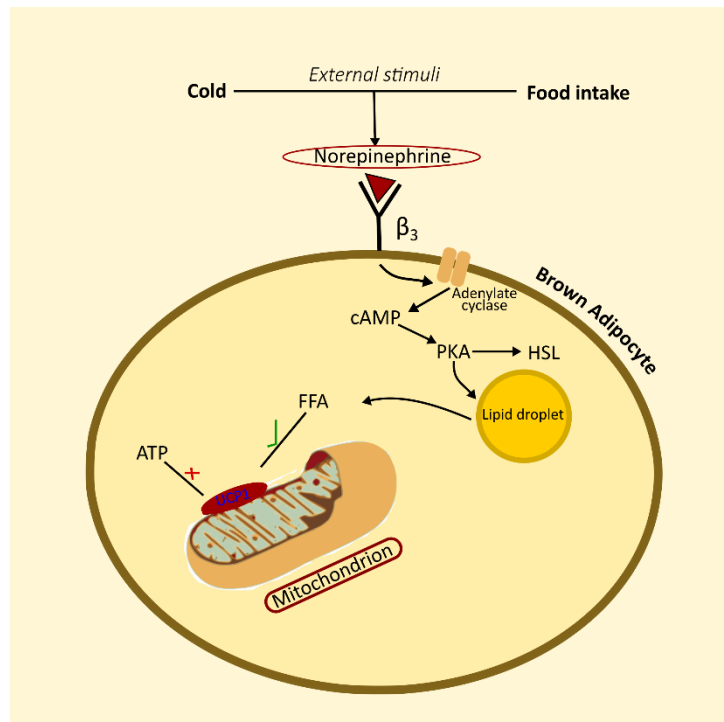


**Figure 1.2 Acute thermogenesis in brown adipocytes.** Noradrenaline is released in BAT, where it binds  $\beta$ -adrenergic receptors on the adipocytes' surface and begins an intracellular signal cascade. This leads to lipolysis of the stored lipid droplets, generating free fatty acids, which act both as an energy source for  $\beta$ -oxidation, and to activate UCP1, overcoming inhibition of the protein by purine nucleotides (e.g. ATP); cAMP = cyclic adenosine monophosphate; PKA = protein kinase A; HSL = hormone sensitive lipase; FFA = free fatty acids; ATP = adenosine triphosphate.

When noradrenaline binds to the receptor,  $G_{\alpha s}$  coupled proteins dissociate and stimulate the enzyme adenylate cyclase, which converts cytosolic ATP to the cyclic compound cAMP. The rise of cytoplasmic cAMP levels activates the phosphokinase A (PKA) complex, which, through the phosphorylatory subunit, begins a further signalling cascade [2, 42]. Once activated, as well as other targets, PKA possibly activates the adipose tissue triglyceride lipase (ATGL), which transforms triglycerides into diglycerides plus free fatty acids, and the hormone sensitive lipase (HSL) [43] which breaks down diglycerides into monoglycerides and fatty acids; finally, the monoglyceride lipase is also activated, turning monoglycerides into free fatty acids [44]. The protein perilipin, which protects the external surface of stored lipid droplets, is also phosphorylated, deactivating it. Lipolysis, the breakdown of triglycerides into glycerol and free fatty acids (FFAs), is thus stimulated, and free fatty acids are released into the cytosol [2, 45]. The free fatty acids are converted to

acyl-CoA and transported via the carnitine-acyl carnitine shuttle to the mitochondrial matrix for  $\beta$ -oxidation, providing energy for oxidative phosphorylation, but also acting as primary activators of UCP1, switching on uncoupling [46] and initiating thermogenesis. UCP1 is inhibited by cytosolic purine nucleotides (e.g. ATP) [47, 48]. Though this inhibition is overcome by the fatty acid interaction to begin thermogenesis, although the exact molecular mechanism of the event is still not clear and is debated (see [49] and section 1.3.2).

As well as the acute response,  $\beta$  adrenergic activation induces chronic activation [2]. The amount of brown adipose tissue and UCP1 in the organism can be increased to respond to the necessity for thermogenesis;  $\beta$  adrenergic activation stimulates not only thermogenesis but also UCP1 expression, mitochondrial biogenesis and brown adipose tissue growth [46]. When the stimulus is first received brown adipocytes have fewer mitochondria and express lower amounts of UCP1 [50], which has a half-life of around 30 hrs [51]. Tissue growth and increases of the amounts of UCP1 and mitochondria, are enhanced as part of this adaptive, slower response, which is also initiated by the rise of cytoplasmic cAMP concentration. Among the proteins phosphorylated by the cAMP activated PKA is p38MAP kinase [52], which participates in a pathway that targets nuclear receptors. The UCP1 gene possesses two main regulatory regions, both at the 5' non-coding end of the gene: a proximal region and a distal enhancer [53]. The proximal region contains the binding sites for the cAMP responsive element binding protein (CREB), an activator of transcription which mediates the nuclear response caused by the increase in cAMP levels and the activation of PKA [54]. The distal enhancer situated 2.5 kb upstream from the transcription site contains an activating transcription factor-2 binding site (ATF2), which confers p38MAPK responsiveness to gene transcription [46, 52]. Importantly on the distal enhancer numerous response elements for hormone nuclear receptors are present, specifically the retinoic X receptor (RXR), 9-cis retinoic acid receptor (RAR), peroxisome proliferator activated receptor  $\gamma$  and  $\alpha$  (PPAR $\gamma/\alpha$ ) and thyroid hormone receptor (TR) [55]. Thyroid hormones T3 and T4 are also involved in UCP1 transcription modulation [56]. The T4 hormone is converted into T3 by the enzyme iodothyronine 5'-deiodinase (DIO2) [57], which is among the downstream targets of the PKA signalling cascade and is highly inhibited by its own substrate, and thus linked in its activity to cAMP concentration once again

[56]. The UCP1 distal enhancer contains thyroid hormone responsive elements (TRE) for binding of the complex T3-thyroid receptor, which stimulate UCP1 transcription [56].

#### **1.2.4 UCP1 independent thermogenesis**

In section 1.2.3 an overview of the UCP1 dependent non-shivering thermogenesis was presented. However, other mechanisms of thermogenesis, which do not rely on UCP1 mediated uncoupling, were proposed (see [58] for an extensive review). They are creatine cycling, re-esterification of lipids, calcium cycling and proton leak through the ADP/ATP carrier.

Kazak et al. [59] proposed a futile cycle of creatine inducing increased respiration in mitochondria of beige fat through the coupling of creatine phosphorylation by the mitochondrial creatine kinase (CK) to respiration through the ADP/ATP carrier [59]. In this model ATP usage would be driven by the continuous phosphorylation of creatine to phosphocreatine by the mitochondrial CK [60], depleting the pool of mitochondrial ATP and thus stimulating increasing production of ATP from complex five.

The futile cycle of lipids consists of the cycle of lipolysis, the lysis from triglycerides to fatty acids plus glycerol, and the inverse process of re-esterification of fatty acids to triglycerides [61]. The required fatty acids could come from the internal storage lipid droplets in brown adipocytes or potentially from circulating lipids [62, 63]. Interestingly, evidence shows that cold and adrenergic stimulus increase the expression of genes for both lipolysis and lipid esterification [46, 64].

In muscles  $\text{Ca}^{2+}$  is transported into the sarcoplasmic reticulum by the sarco/endoplasmic reticulum  $\text{Ca}^{2+}$ ATPase (SERCA) pump (with the sarcolipin protein), with hydrolysis of ATP [65]. Ryanodine receptors, instead release the accumulated  $\text{Ca}^{2+}$  from the sarco/endoplasmic reticulum. The sarcoplasmic reticulum acts as the storage of  $\text{Ca}^{2+}$  for muscle cells, while the endoplasmic reticulum has the same function in other cells [66]. Calcium cycling, which has been proposed to occur in both muscle tissue, WAT, and BAT consists in the futile cycle of  $\text{Ca}^{2+}$  transport into the lumen of the sarcoplasmic/endoplasmic reticulum through the SERCA pump and its transport out of the lumen by the ryanodine receptor [65].

Mitochondria can present proton leak in the absence of UCP1 [67, 68]. While other UCPs have been proposed to mediate proton transport in the absence of UCP1 the literature is controversial (see section 1.3.6). Moreover, proton leak is rather ubiquitous, and UCP2-5 are not ubiquitously expressed. The ADP/ATP carrier, the most abundant and ubiquitous mitochondrial carrier, has instead been proposed to mediate UCP1-independent proton leak [69, 70].

### **1.2.5 Therapeutic activation of BAT and Ucp1**

Enhancing mitochondrial thermogenesis had already been explored as a means to provoke weight loss as far back as in the 1930s, when it was attempted using DNP (2, 4 - dinitrophenol), a small non-polar molecule which acts as a proton shuttle across the IMM, effectively acting similarly to UCP1 [71]. This drug, however, was soon withdrawn from the market, due to its significant side effects, including many fatalities, as the effective dose was too close to the lethal dose [72].

Due to its ability to dissipate the energy obtained from oxidation of nutrients as heat, BAT has been long suspected to play a role in metabolism and to offer therapeutic avenues in its regulation (see [73, 74] for a review). For example, early studies in the late seventies associated overfeeding of rodents with a marked activation of BAT [75]. UCP1 ablation in mice induces an obese phenotype [76]. Furthermore, increasing the total number or the activity of brown/beige adipocytes provokes a decrease in weight and counteracts insulin resistance in mice strains prone to obese phenotypes [77]. When BAT is activated by adrenergic stimuli it starts consuming the tissue's internal supplies of fatty acids contained in the cytoplasmic lipid droplets [2]. Once these reserves are finished, which occurs rapidly, the tissue begins to uptake free fatty acids from circulating lipoproteins (chylomicrons, VLDL, LDL etc.) [78]. BAT activation has consequently been shown to increase clearance of circulating triglycerides and improved glucose homeostasis and uptake in human subjects [62, 79, 80]. It is not surprising that BAT has become the subject of research focused on increasing energy expenditure in order to combat metabolic disease [81].

After the rediscovery of BAT in adult humans, different and safer pharmacological approaches to BAT activation have been explored. So far, the research has not focused on direct activation UCP1, but on activation of the adrenergic response. For

example, the effects of several  $\beta$  adrenergic agonists, such as L796568, CGP-12177, CL 316243 [78, 82, 83], have been explored. Continuous treatments of mice with these agonists stimulates UCP1 expression and induces browning of white adipocytes in WAT [84]. However, permanent treatment with  $\beta$ -adrenergic agonists can eventually lead to desensitization of the receptor and inhibition of the cAMP pathway [85], with a consequent decrease in effectiveness. Another recent example is constituted by the  $\beta$ 3 adrenergic receptor agonist Mirabegron [86], a licensed oral drug used in the treatment of overactive bladder. Despite increasing BAT metabolic activity and effectively stimulating thermogenesis Mirabegron unfortunately also provoked serious cardiovascular side effects and could thus not be used.

Another alternative to pharmacological activation, is physiological - cold induced activation, which can be achieved through either exposure to intermittent cold or lowering of ambient temperature to around 19 °C [87]. Cold acclimation experiments with human subjects exposed to temperatures of 16-19 °C for 6 hrs a day for a period of 10 days reported increased amounts of brown adipose tissue in both lean and obese subjects, as well as improved insulin sensitivity in subjects affected by type 2 diabetes [16, 88, 89]. Intermittent cold acclimation could represent a cheaper and safer alternative, avoiding the problematics connected to drugs 'side effects [8, 78], although it is not practical and can have other negative side effects.

### **1.3. Uncoupling Protein 1**

#### **1.3.1 Discovery and early studies**

Brown adipose tissue extreme capacity of producing heat, superior to that of any other tissue, including the liver, proved disconcerting as it did not respect the rules of control of respiration (see [90] and [91, 92] for a review). Later experiments revealed that in BAT respiration was not coupled to oxidative phosphorylation [93], but could be recoupled by purine nucleotides, a baffling aspect. Early studies on isolated mitochondria from BAT also observed that they were unusually permeable to chloride and bromide, showing uncommon ion transport properties [94].

In 1975-6 Ricquier and Kader [95], examined with gel electrophoresis if the protein content of BAT mitochondria would undergo changes after cold acclimation [90].

They therefore compared the protein composition of BAT mitochondria from rats kept at 23 °C and cold acclimated (6 °C for 3 weeks). They encountered “*a striking increase in the content of an unknown polypeptide, apparent molecular weight 32 kDa*” after cold acclimation [95]. Furthermore, this marked increase disappeared after the cold acclimated animals were re-exposed to regular ambient temperature. Ricquier et al. [95] also demonstrated that this alteration of protein profile was specific only to BAT. Repeats of the same analysis on liver mitochondria did not record any change in protein composition.

David Nicholls et al. [96] identified through 8 azido-ATP labelling on the cytosolic side of the inner mitochondrial membrane in BAT an ion uniport responsible for energy dissipation and determined that it corresponded to the protein identified by Ricquier and Kader.

The next challenge was purifying the isolated protein, a non-trivial matter for a transmembrane protein, which is highly hydrophobic. UCP1 was first purified exploiting its nucleotide binding capacity. Rat UCP1 was purified, albeit only partially, by covalent agarose affinity chromatography with GDP [97]. Complete purification from BAT hamster mitochondria was achieved shortly afterwards by the Klingenberg group [98]. Klingenberg et al. [99] built upon their knowledge of the biochemical characteristics of a similar carrier (the ADP-ATP carrier (AAC), then called the CATR binding protein) for which they had established a purification procedure from mitochondria based on filtration chromatography with hydroxyapatite resin [99].

Ricquier and Bouillaud [100] developed a library of bacterial clones with the aim to isolate those producing a complete gene sequence for the protein, using immunological probes previously obtained by injecting rat UCP1 into ewes. They succeeded in isolating the desired clone and extracted the cDNA, thus obtaining a probe for detecting, with Northern blot techniques, the presence of UCP1 mRNA in any sample [101]. In the following years between 1988 and 1991 the Ricquier group gradually identified the sequences of rat [102] and human UCP1 [103], which, in addition to the new PCR techniques being developed, allowed for a more precise description of the gene's transcription regulation.

It was soon clear that UCP1 is a membrane protein that is related to the ADP/ATP carrier (AAC) [104], though with different nucleotide binding properties [48], and more stable than AAC [98]. Both proteins are members of mitochondrial metabolite transporters SLC25, a family of carriers that share the same basic structural features and membrane disposition. Klingenberg et al. [105] in the mid-1980s managed to reconstitute UCP1 into liposome vesicles and study its transport properties. They demonstrated it was a both the site of nucleotide binding and a proton translocator with liposome assays [105]. They subsequently named the protein, so far called nucleotide binding protein, as uncoupling protein. The following reconstitution efforts focused on examining UCP1 uncoupling properties in the context of BAT physiology and its regulation, clarifying how the protein was inhibited by nucleotides and activated by FFAs after lipolysis of internal cellular storages [106, 107].

More recently, in the late 1990s new homologues of UCP in different tissues were also identified, such as UCP2 and 3 [108], which led to renaming the brown adipocyte protein UCP1 (see section 1.3.6 for a discussion of UCP2-5).

### **1.3.2 UCP1 mechanism of activation**

As seen in section 1.2.3 UCP1 activity is tightly regulated. The protein is inhibited by bound purine nucleotides and is activated only in response to an adrenergic stimulus upon release of stored fatty acids [2]. Although there have been claims of other molecules acting as cofactors and activators for UCP1, such as coenzyme Q [109] or superoxide [110], fatty acids are currently accepted as the principal and most important activators. However, the actual mechanism of UCP1 activation by fatty acids and transport of protons from the intermembrane space to the mitochondrial matrix has long been debated. Four main models have been proposed (reviewed in [111]), all of which were based on studies using different techniques and approaches, from UCP1 proteoliposomes to isolated mitochondria. The mechanistic models are the following: the functional competition model, the cofactor model, the cycling model, and the shuttle model (see figure 1.3).

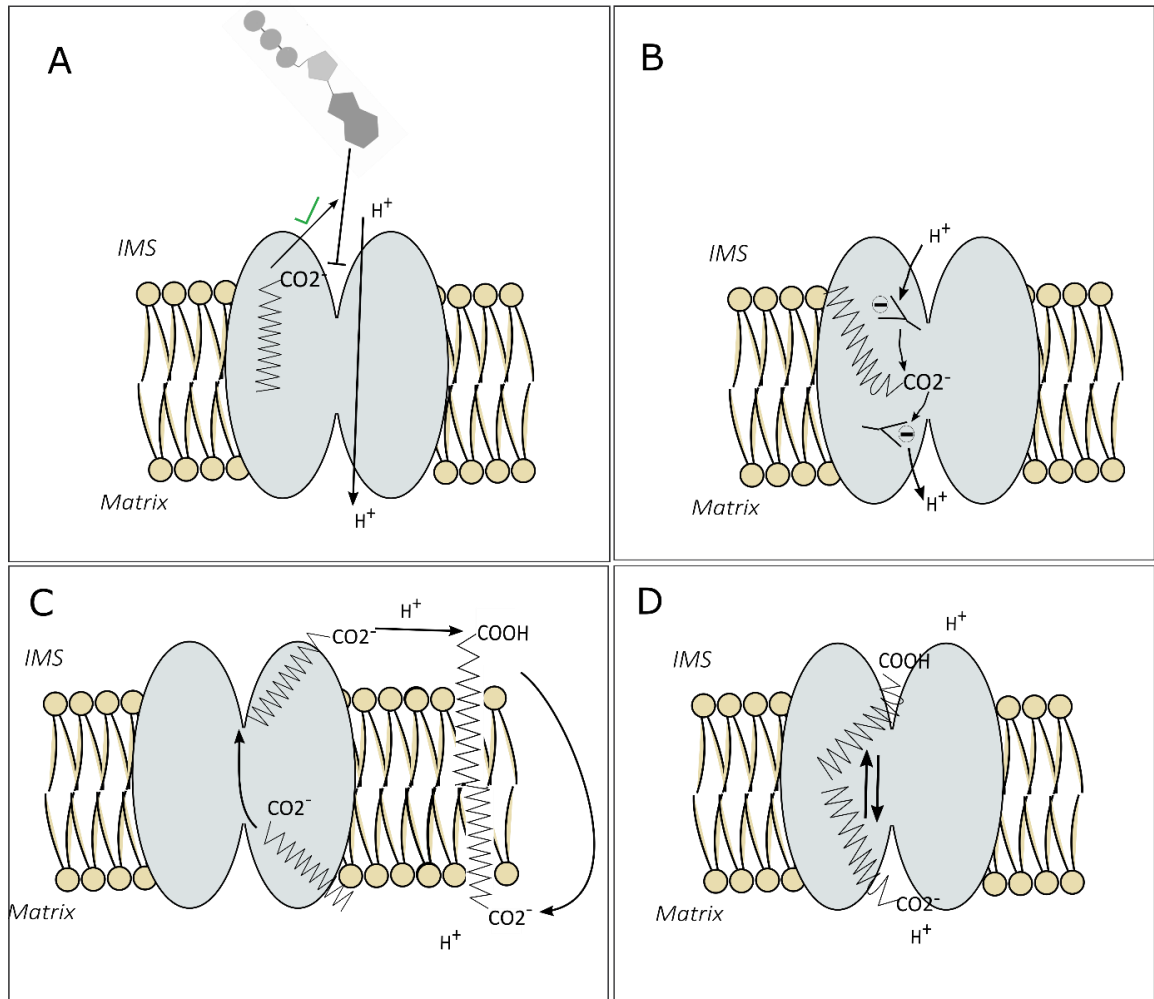


**Figure 1.3 Models of UCP1 mechanism.** A single UCP1 monomer is represented as two joined grey transmembrane oval shapes. IMS = intermembrane space;  $H^+$  = proton. **Panel A.** Functional competition model. Fatty acids act on UCP1 to displace purine nucleotides. **Panel B.** Cofactor model. Fatty acids are cofactors of UCP1 that create a proton pathway within the protein. **Panel C.** Cycling model. Fatty acids flip-flop independently into the matrix and fatty acid anions are exported by UCP1 into the intermembrane space. **Panel D.** Shuttling model. Long-chain fatty acids remain bound to UCP1 and the carboxylic head cycles between the two sides of the inner mitochondrial membrane, alternatively protonated and unprotonated.

The functional competition model, formulated by working on isolated mitochondria, states that fatty acids act on UCP1 purely to displace purine nucleotides and thus overcome inhibition [112]. This hypothesis assumes, therefore, that fatty acids act on UCP1 by competing, directly or allosterically, with purine nucleotides, and that the protein should be inherently active and kept in its inhibited state by the elevated ATP and ADP concentration in the cytosol. However, it has been demonstrated with

reconstituted UCP1 in liposomes that the carrier is not inherently active as it is not possible to detect a proton current before the addition of fatty acids [113, 114]. The same proof of principle has been established with patch-clamp technique on isolated mitochondria in more recent studies: UCP1 has no constitutive activity [115].

The cofactor model, proposed by Klingenberg [113, 116], hypothesizes that fatty acids act by associating with UCP1 as cofactors and providing a carboxylic acid group as an acceptor (alongside other acceptor groups provided by UCP1 amino acids) to create a proton path within the protein. Supporting this hypothesis is the  $pK_a$  of physiologically relevant fatty acids being quite similar to the pH dependency for activation that has been observed in UCP1.

The cycling model (reviewed in [117]) was initially proposed by Vladimir Skulachev [118] almost at the same time of the cofactor model, and then championed by Keith Garlid [107, 119]. This hypothesis, however, has a striking difference compared to the previous two: it assumes that fatty acids are substrates for UCP1, which means that UCP1 transports protons indirectly, as a secondary element. According to the cycling model UCP1 transports, as substrates, non-protonated fatty acid anions from the mitochondrial matrix to the intermembrane space. Once in the intermembrane space fatty acids become protonated and independently flip-flop through the membrane to the matrix side, where they release the protons and are once again ready to act as UCP1 substrate. Fatty acids have been shown to be able to independently flip-flop across a lipid membrane, in a timescale of microseconds [120, 121]. The result of the cycle is the net transport of protons to the matrix side of the IMM. The model, therefore, predicts that fatty acid can be transported by UCP1 only when introduced by the matrix side. Support for this model is based on a particular class of fatty acid analogues, alkyl sulfonates. These molecules mimic fatty acids with one important difference: their head groups contain sulphates, meaning that they are low  $pK_a$  analogues of fatty acids, and cannot become protonated at physiological pH. Using undecansulfonate (the analogue of lauric acid) Garlid et al. [119] demonstrated that although the molecule is transported by UCP1 there is no associated proton transport. The authors argued that this happens because undecansulfonate is unable to bind protons and flip-flop across the membrane back to the matrix side at physiological pH [119]. Moreover, the model is supported by the well-established ability of UCP1 to transport anions, specifically

chloride [111], as well as anionic analogues of fatty acids, with similar transport rates [122].

More recently Kirichok [115, 123] has proposed a new model, the shuttling model, containing many elements of the cycling model as well as some of the cofactor model. The model proposes that UCP1 is an anion transporter with fatty acids as a substrate, but that it can transport both protonated and non-protonated fatty acid species. Patch clamp records of isolated mitochondria showed the occurrence of a current even when fatty acids, or their analogues, were introduced from the cytoplasmic side, in contrast with what predicted by the cycling model [115]. Bertholet et al. [123] propose that net transport of proton is achieved because once a long chain fatty acid is bound to UCP1, the protein is unable to release it and the carboxylic head group keeps cycling between the two sides of the inner mitochondrial membrane, being alternatively protonated and unprotonated. In short, the model describes UCP1 as both a symporter of fatty acid anions and protons and a fatty acid anion uniporter. The protein, however, has a restricted capability to release long chain fatty acids following transport, resulting in net transfer of protons across the inner mitochondrial membrane.

### **1.3.3 Activation of UCP1 by Reactive Oxygen Species (ROS)**

In 2003 Echtay et al. reported that UCP1 was activated by superoxides [110]. Later Echtay et al. also reported that the reactive alkenal 4-hydroxy-2-nonenal (4HNE), in concentration of 10-50  $\mu\text{M}$ , was the mediator of UCP1 activation. The authors claimed that 4HNE was capable of inducing GDP-sensitive proton conductance in BAT, kidney, and skeletal muscle mitochondria [124, 125]. The finding could not be replicated [126]. Also Fedorenko et al. [115] tested 4HNE in patch clamp experiments and found no evidence of proton transport. Recently Chouchani et al. [127] claimed that an increase of mitochondrial ROS following thermogenesis shifted UCP1 to a more active state, making the protein more sensitive to fatty acid activation. This process would involve specific sulfenylation of the cysteine residue in position 254 (human UCP1 residue numbering) of UCP1 (on one of the matrix helices). However, studies have reported that cysteine residues are not essential for the activity of UCP1 [128]. Moreover, a cysteine residue in the equivalent position

of C254 is conserved in other mitochondrial carriers, including AAC, the oxoglutarate carrier, and the citrate carrier and is not important for function [111, 129].

#### 1.3.4 UCP1 structure – SLC25 conserved structural characteristics

UCP1 is a member of the mitochondrial carrier family (SLC25) of metabolite exchangers and shares structural features with the other members. These proteins are responsible for the exchange of energy and small metabolites across the mitochondrial inner membrane [130-132].

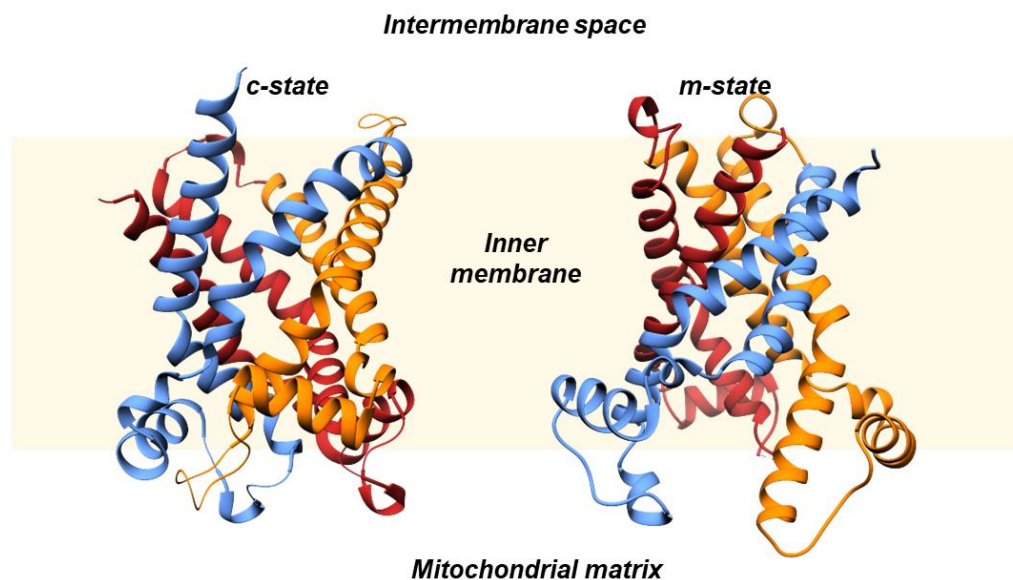


**Figure 1.4 AAC structures in its two states.** Representative mitochondrial carrier (AAC) structure, with three-fold pseudo-symmetry, in its two states. Structures 4C9H (ScAAC) for c-state AAC; structure 6GCI (TtAAC) for m-state AAC. Each of the three ~100 amino acid domains of the protein is coloured differently, in blue, red and orange.

The structure of UCP1 has not been solved, however all mitochondrial carriers share the same basic fold, and many characteristics of UCP1 have been postulated from studies with AAC, due to their homology [111]. Mitochondrial carriers are formed by three homologous domains, each of approximately 100 aminoacid residues, composed of two alpha helices, organized in a three-fold pseudosymmetry where each residue at a given position of a domain is related by symmetry to a residue on each of the other two domains (figure 1.4) [133]. The tertiary structure is organized in a barrel transmembrane structure with three-fold pseudo symmetry. Each helix is

connected to the next by a loop and a smaller alpha helix on the matrix side [134-136]. Robinson et al. [137] have proposed that the mechanism of transport of mitochondrial carrier must take into account, and is likely to be based on, the symmetrical properties of these proteins. Mitochondrial carriers would enact a transport cycle based on the alternate access of substrate to a binding site located in the central cavity of the protein [137-139]. This model, based on studies with AAC, postulates that mitochondrial carriers conserve two salt bridge networks, situated at the protein to water interface at either side of the membrane and able to alternatively close the access to the central cavity of the proteins [140]. Mitochondrial carriers would then cycle between two states, one in which the substrate binding site is open to the cytosol (called a c-state), and one where the substrate binding site would be accessible from the mitochondrial matrix (called an m-state). The binding of a substrate (for instance ADP) from the cytosol to the central binding site would provide the energy for the protein to switch from one state to the other. In the new state the binding of another substrate from the opposite direction (for example ATP) from the matrix would provide the energy to switch back and complete the transport cycle [133, 141-144].

Structures of the ADP/ATP carrier have shown that these salt bridge networks form on the mitochondrial carrier at the matrix and cytosolic side of the protein and that AAC can indeed assume two conformations: an m-state and a c-state [135, 136].

On the odd numbered alpha helices of AAC is located the signature motif, Px[DE]xx[RK], shared by the members of the SLC25 family. The proteins also present a second conserved motif, Fx[DE]xx[RK], on the even numbered helices [133, 140]. These conserved motifs form the two salt bridges networks and sequence analysis has shown that these motifs are also conserved in UCP1 [111]. The residues on the odd numbered helices form the salt bridge on the matrix side when the protein is in its cytosolic state (c-state). The other residues on the even numbered helices form the cytosolic network of salt bridges when the protein is in its matrix state (m-state) [136]. The matrix network of AAC, consists of 3 salt bridges and one additional hydrogen bond provided by a glutamine residue, (called a glutamine brace). The network on the cytosolic side of the protein on the other hand consists of two salt bridges and one hydrogen bond provided by a tyrosine residue (called a tyrosine brace). The formation of the salt bridge networks is aided by the

L-shaped form of the transmembrane helices, created by the presence of some helix breaker residues (mainly prolines). UCP1 is also predicted to possess these interaction networks at the matrix and cytosolic side of the protein [111]. Among other conserved features are the “matrix tethers”, interactions between charged residues at the end of the matrix helices and residues at the matrix side of the transmembrane helices [111]. Several other conserved structural features have been identified in the SLC25 family of mitochondrial membrane carriers, after the recent solution of a structure of AAC in the m-state [136], all of which are presumed to be conserved in UCP1 [133]. Among these are the hydrophobic plug (a group of hydrophobic residues) and the GxxxG and  $\pi$ xxx $\pi$  motifs. To aid occluding the internal cavity to the cytoplasm when the protein is in the m-state, underneath the cytoplasmic salt bridge network, toward the matrix side are three conserved bulky aromatic residues that forms a hydrophobic “plug”, a layer of highly hydrophobic residues preventing water entering the internal cavity from the cytoplasmic side. Helix packing in membrane proteins is tighter than in soluble protein, particularly transmembrane helix–helix interfaces [136, 145]. Common residues with high packing values are small hydrophobic aminoacids such as alanine and glycine [145]. The m-state structure of AAC from a thermophilic fungus (TtAAC) [136] has revealed tight packing of the transmembrane helices at the cytoplasmic side, necessary to close the cytoplasmic gate. This has led to the identification of conserved small hydrophobic residues at the interdomain interfaces on the odd numbered alpha helices, which were not evident in the more open c-state conformation. These conserved motifs have been named the GxxxG (from the presence of conserved glycines) and  $\pi$ xxx $\pi$  (from the presence of conserved small aminocids, identified by the Greek letter  $\pi$ ) motifs [136].

### **1.3.5 The properties of UCP1**

UCP1 was originally thought to be a dimer, as were all mitochondrial carriers [146-148]. Studies using techniques such as analytical centrifugation and cross-linking experiments initially supported this model [98, 147]. This notion was challenged after the solution of the AAC carrier structure in complex with its inhibitor CATR [134] and further refuted through molecular and structural studies on the AAC2 carrier from yeast, confirming that AAC was a monomer [129, 149, 150]. Given the similarity

between AAC and UCP1 the same hypothesis was tested for the uncoupling protein and found valid again [151].

The binding of purine nucleotides (ATP, GTP, ADP and GDP) to UCP1 is highly pH dependent, showing a tighter binding at pH < 6 [152]. This binding behaviour has been proposed to depend on the structural conformation and amino acid composition of the nucleotide binding pocket. Mutation studies by the Klingenberg group [153, 154] identified a glutamic acid residue, E191 (human UCP1 amino acid residue numbering), which was proposed to be responsible for the pH dependence of nucleotide binding. Furthermore, this nucleotide binding model [155] assumed the presence of a binding pocket able to adapt to accommodate the binding of di- or triphosphopurine nucleotides through the retraction or exposure of a His residue, His 215 (human UCP1 residue numbering), which protrudes into the binding pocket [156]. Upon protonation of two close residues, D210-D211 (human UCP1 residue numbering), a positive charge is supposed to retract His 215 allowing the docking of triphosphopurine nucleotides (TNPs). Reinterpreting these early mutation studies in light of recent structural information, it has been proposed that, since UCP1 does not possess any evident adaptation to allow nucleotide binding [137], nucleotides are likely to bind in the central cavity [157], probably to three intrahelical arginines providing the positive charge for binding the phosphates of the nucleotide [158]. The role of E191 as a “gatekeeper” would be compatible with this hypothesis, as the residue is predicted to be situated in the cavity near the cytosolic side, from which nucleotides would bind. Original research concerning the nucleotide to UCP1 binding stoichiometry proposed that one purine nucleotide binds each UCP1 dimer (a 1:2 ratio) [48]. These studies, largely based on Lowry assays to quantify the purified protein, were recently confuted by re-examining the issue with new techniques. Using isothermal titration calorimetry Crichton et al. [157] measured the exact binding ratio by titrating purified UCP1 with carefully determined concentrations of GDP. The results clearly pointed to a 1:1 binding ratio of purine nucleotides to protein.

Cardiolipin, a phospholipid formed by a glycerol backbone, phosphatidic acid moieties and acyl chains is an important cofactor lipid for many mitochondrial proteins (see [159] for a review). For instance, cardiolipin is a pivotal cofactor for the assembly and function of complex 5, the ATP synthase [160-162] as well as the

other complexes of the respiratory chain [163, 164]. Cardiolipin is also necessary for the functioning of many mitochondrial carriers, such as AAC [165-168]. However, it was initially thought that UCP1 did not bind cardiolipin [168], contrary to other carriers which were known to bind three molecules [105] required for activity [113]. UCP1 was reported not to retain cardiolipin following purification or require it to be reconstituted into vesicles, to the point that the addition of cardiolipin seemed to inhibit activity [116]. The role of cardiolipin with UCP1 was reinvestigated in recent years. New purification methods by covalent chromatography produced native protein which retained endogenous cardiolipin, as measured by phosphorus quantification assays [157], in quantities compatible with three molecules per protein. Furthermore, cardiolipin was demonstrated to be necessary for UCP1 stability [169] and activity in reconstituted vesicles [157]. Cardiolipin molecules had binding sites on AAC structures, which appear conserved in other mitochondrial carriers including UCP1 [134, 135]. Cardiolipin phosphate groups, which are negatively charged, bind to positively charged regions on AAC helices, both on the matrix and cytoplasmic side, forming hydrogen bonds. Of particular importance for binding are two conserved motifs of AAC, constituting crucial parts of the binding site, [YF]x[G] and [YWF][RK]G [135]. The aromatic residues in these motifs constitute the bridge to the hydrophobic acyl chains of cardiolipin, while the ending glycine residues, and serine residues in UCP1, act as helix-breakers [170, 171] favouring contact.

### **1.3.6 UCP2 and the other uncoupling proteins UCP3-5**

Other than UCP1, there are other mitochondrial carriers named uncoupling proteins (UCPs), which were found by sequence identity to UCP1 in cDNA libraries [172]. In 1997 a gene coding for a protein with 59 % amino acid identity to UCP1 was identified and named UCP2 [173]. Contrary to UCP1, the expression of UCP2 mRNA was observed not only in brown adipose tissue but was rather ubiquitous, though initially reported to be higher in skeletal muscle and white adipose tissue [174]. However, the tissues and organs where UCP2 protein was observed by Pecqueur et al. [175] were stomach, lungs, thymus, spleen, and bone marrow. UCP2 was also present in leukocytes [176]. The highest expression was reported in spleen, and was much lower than UCP1, about 1 % of UCP1 expression levels in

BAT. The protein appeared unstable with a much shorter half-life than UCP1, of around 30 min to 1 hr [177].

Due to the sequence identity with UCP1, UCP2 was initially thought to be another uncoupling protein, and early studies in isolated mitochondria [178] and with the reconstituted protein from yeast found the protein responsive to lauric acid and reported uncoupling upon activation [179]. UCP2 was also found to be responsive to alkylsulfonate, catalysing the transport of the fatty acid analogue undecanesulphonate, although being much less sensitive to purine nucleotides inhibition ( $K_i$  of ATP at pH 7.2 was 710  $\mu\text{M}$  for UCP2 versus 125  $\mu\text{M}$  for UCP1;  $K_i$  for GDP at pH 7.2 1.2 mM for UCP2 vs 17  $\mu\text{M}$  for UCP1) [180]. Later studies observed that these earlier experiments reporting UCP2 mediated uncoupling were prone to artifacts. Overexpression of UCP2 in yeast expression systems produced damaged mitochondrial membranes with consequent loss of integrity and production of uncoupling artifacts [181, 182]. Thus, it was proposed that UCP2 is not an uncoupler, at least at physiological amounts of expressed protein [183, 184]. Another characteristic of UCP1 is the ability to bind purine nucleotides, which have an inhibitory effect. The capacity of UCP2 to bind nucleotides has been tested with different results. Jekabson et al. [185, 186] reported that UCP2 refolded from bacterially expressed inclusion bodies had a  $K_d$  at pH 6.8 for ATP of 3-5  $\mu\text{M}$  and in the nanomolar range for the fluorescent MANT-ATP (2'/3'-O-(N-Methyl-anthraniloyl)-adenosine-5'-triphosphate), whilst the affinity for GDP was around 10 times lower. However, Jaburek et al. [187] found with bacterially expressed UCP2 and UCP1 reconstituted in liposomes,  $K_i$  at pH 7.2 of 70 and 50  $\mu\text{M}$  for ATP respectively; reconstituted UCP1 from native material had a similar affinity of 65  $\mu\text{M}$ .

A mouse UCP2 structure, solved by solution NMR by Berardi et al. [188], was published in 2011. The same authors also later proposed that UCP2 functions as a proton transporter, similarly to UCP1 [189]. However the integrity of the protein sample was challenged [190] due to the method of expression and reconstitution chosen (expression in bacteria and refolding from solubilised inclusion bodies) and particularly the choice of detergent to solubilise the protein, highlighting the importance of ensuring the correct folding of the protein sample in the detergent and the excessive harshness of the zwitterionic detergent, deoxyphosphocholine [191, 192].

The function of UCP2 remains a controversial topic, with some proposals of UCP2 having a different function more similar to other mitochondrial carriers, of transporting small metabolites (specifically C4 molecules [193]). UCP2 may also play some role in brain function, UCP2 KO mice models showed impaired brain function and an anxious behavioural phenotype [194]. Considering the evolution of UCPs homologs it has been proposed that the function of UCP2-5 may not be in thermogenesis or proton uncoupling [195].

A third uncoupling protein, UCP3, with 57 % identity to UCP1, and 73 % identity to UCP2 has been reported [196]. UCP3 was found to be expressed in skeletal muscle in humans and in brown adipose tissue and skeletal muscle in rodents [197, 198]. Similarly to UCP2, UCP3 has a much shorter half-life than UCP1, around 0.5 to 4 hrs [199]. Early studies, often performed in parallel with UCP2, proposed an uncoupling role for UCP3 [180, 187, 197], which was also put in doubt by the following experiments. UCP3 expressed in hamster ovary cells did not initiate uncoupling upon addition of retinoic acid, and UCP3 overexpression in muscle cells did not affect membrane potential, although it increased fatty acid metabolism [200, 201]. Similarly to UCP2 other functions have been proposed for UCP3. For instance, early studies suggested that UCP3 could mediate fatty acid export during elevated fatty acid oxidation requirements, to maintain mitochondrial CoA availability for energy production [202, 203]. However later experiments showed that UCP3 was more likely to play a role in the regulation of fatty acid metabolism but not fatty acid anion export from the mitochondrial matrix [204].

UCP4 and UCP5 (also called BMCP1 – brain mitochondrial carrier protein) were also found in cDNA libraries by sequence identity to UCP1, and thus named uncoupling proteins [205, 206]. Both proteins have low identity to UCP1 (30 - 40 %) and are expressed mainly in neural tissue, predominantly in the brain [207]. Phylogenetic analysis showed that UCP4 and UCP5 are more distantly related to UCP1, compared to the other UCPs, and they are not part of the core group of UCPs (UCP1-2 and 3) [195, 208]. In contrast, UCP4 and 5 are more closely related to the oxoglutarate/malate carrier and the dicarboxylate carrier. Studies testing UCP4 and 5 abilities to act as ion transporter do not abound in the literature: Hoang et al. [209] expressed UCP4 and UCP5 in *Escherichia coli*, and reconstituted the protein in

liposomes. Both proteins conducted protons across the liposome membrane when stimulated by lauric acid addition.

#### **1.4. General aim and objectives of the project**

There is much that is still to be clarified regarding UCP1, the protein central to BAT thermogenesis, even after more than 40 years from when it was first purified by Lin and Klingenberg [98]. For instance, the nature of the interaction between UCP1 and fatty acids that is required for the induction of UCP1-mediated proton transport, or the exact mechanism by which the protein transports protons have been challenging to resolve [91, 111, 210, 211]. The UCP1 literature also contains a wealth of structure-function information from mutation studies, the interpretation of which has been limited by the lack of a suitable structural framework for carriers to effectively rationalise findings (e.g. on nucleotide binding [128, 153, 156, 212]).

The overall aim of this PhD project was to advance our understanding of the molecular mechanism of UCP1 function and regulation by ligands, through biochemical analysis of the purified protein. Specifically, the project investigated the interaction between UCP1 and the small molecules effectors (e.g. fatty acids) and determined that UCP1 has substrate-like interactions with fatty acids and other activators. Importantly, characterising the interaction has led to the identification of novel ligands that may regulate UCP1, or have potential to, therapeutically (e.g. acyl-CoA or ibuprofen, respectively). Different isoforms of UCP1 that have been used in past research investigations were also characterised and found to be generally similar in their ability to carry out fatty acid-activated proton transport and bind inhibitory purine nucleotide. Furthermore, within the signal to noise of the experiments performed, mouse UCP1 does not appear to have an inherent proton leak activity in the absence of activators that is different from human UCP1, as claimed in the past [213]. Moreover, in this thesis homology models of UCP1 were created, taking advantage of new carrier structural information [133, 136], to re-examine and clarify the likely structural mechanism of UCP1, utilising the wealth of existent information on UCP1 structure-function relations. This analysis has

revealed important correlations that have allowed new structural hypothesis to be developed to explain how regulators may interact with UCP1.

## **2. Materials and Methods**

### **2.1 SDS PAGE**

Protein samples were diluted in 3x loading buffer (150 mM Tris-HCl pH 6.8, 30 % (v/v) glycerol, 6 % (v/v) SDS, 3 mM EDTA, 0.03 % (v/v) bromophenol blue, 3 % (v/v)  $\beta$ -mercaptoethanol) and loaded on either hand cast (10-15 wells, 12 % (v/v) acrylamide) or pre-cast polyacrylamide gels (10/15 wells 4-15 % (w/v) Mini PROTEAN TGX precast gels (Bio-rad 4561086-3)). Separation was achieved running gels for ~50 min at a fixed current of 25 mA per gel in a Mini-PROTEAN Tetra Vertical Electrophoresis Cell with 1 L of running buffer (25 mM Tris, 0.192 M glycine, 0.1 % (w/v) SDS). After electrophoresis protein bands were developed using Coomassie-based stains (high sensitivity Imperial stain, (ThermoFisher, 10006123) or Instant Blue Protein stain (Sigma, ISB1L)), or silver staining (see paragraph 2.3 for details). The stained gels were visualized on a ChemiDoc XRS+ Gel Imaging System. Gel densitometry was performed with Fiji (version 1.52p).

### **2.2 Western Blot**

Protein Gels were transferred onto PVDF membranes (Fisher #15269894) cut to size (8.5 x 6.5 cm) and preactivated for 20 s in 100 % methanol, with a wet blotting system (Bio-Rad Mini Trans-Blot Cell). Transfers were run with transfer buffer (250 mM Tris, 1.92 M glycine) at 120 V for 1 hr in a cold room at 4 °C with the addition of an ice pack within the transfer cell to avoid overheating. Membranes were rinsed in distilled water and incubated in blocking buffer (5 g dry milk powder in 100 mL TBST: 1.5 M NaCl, 200 mM Tris base pH 7.4, 1 % (v/v) Tween-20) for 30 min at room temperature on an orbital shaker. All antibody incubations were performed for 1 hr at room temperature. The following primary antibodies, diluted in blocking buffer as indicated, were used: rabbit 'anti-UCP1' (Sigma U6382) 1:5000 dilution for human/mouse UCP1 detection and 1:2000 dilution for ovine UCP1; chicken 'anti-AAC' (AgriSera, custom manufactured) 1:10'000 dilution. The following HRP-conjugated antibodies were used: goat 'anti-rabbit HRP' (Millipore AP132P), 1:5000 dilution for human/mouse/ovine UCP1; rabbit 'anti-chicken HRP' (Sigma A9046),

1:10'000 dilution for AAC. Membranes were visualized on a ChemiDoc XRS+ Gel Imaging System and the signal developed with an Amersham ECL Western Blotting detection kit (Fisher 10340125). Gel densitometry was performed with Fiji (version 1.52p).

### **2.3 Silver stain**

Protocols were developed based on [214]. Protein gels were washed thoroughly in distilled water 3 times for 5 min and then placed in a plastic container and covered with fixing solution (50 % (v/v) methanol) at room temperature for 1 hr on a shaker. The gels were then rinsed for 15 min in distilled water and transferred to a clean plastic container, pre-washed in 100 % ethanol, and submerged in staining solution (47 mM AgNO<sub>3</sub> (Sigma 204390), 27 mM NaOH, 146 mM NH<sub>4</sub>OH) and placed on a shaker for 7 min. The gels were then quickly rinsed twice in distilled water and left on a shaker for 5 min. After transferring the gels to a fresh container pre-washed in 100 % ethanol, the developing solution (0.35 mM citric acid, 0.1 % (v/v) formalin (Sigma 252549)) was applied for max ~30 s. The gels were immediately rinsed with distilled water several times as the first sight of a visible signal, and the stop solution applied (1.46 % (w/v) EDTA). The gels were visualized on a ChemiDoc XRS+ Gel Imaging System. Gel densitometry was performed with Fiji (version 1.52p).

### **2.4 Protein thermostability assay**

A fluorescence based thermostability assay [215] optimized for mitochondrial membrane carriers [169, 216] was used to assess folding and ligand interactions of purified protein in a Rotor-Gene Q HRM 2-plex PCR cycler, using the CPM dye (7-Diethylamino-3-(4'-Maleimidylphenyl)-4-Methylcoumarin, Invitrogen D346). Aliquots of CPM diluted in DMSO at a concentration of 5 mg/mL were prepared in advance and stored at -80 °C. The CPM dye was diluted 1:50 in assay buffer (20 mM Hepes pH 7.5; 0.1 % (v/v) lauryl maltose neopentyl glycol detergent (12MNG) / n-dodecyl- $\beta$ -maltoside detergent (12M)) and incubated for 10 to 15 min after mixing protected from light. The samples with ligand additions were made up to a total volume of 45  $\mu$ L in thin wall PCR tubes (Fisher 10161391) and kept on a metal plinth on ice to maintain constant temperature. 2  $\mu$ g of UCP1 were used for each sample and 1  $\mu$ L

additions of ligands at the required concentration were used to minimize the amount of solvent added to the assay mixture (distilled water (dH<sub>2</sub>O), DMSO or ethanol). For one of the ligands, octadecanesulphonate (C18-S, see chapter 3), the solvent was dH<sub>2</sub>O with methyl- $\beta$ -cyclodextrin (m $\beta$ CD, Sigma C4555) added to increase the solubility of hydrophobic compounds. Finally, 5  $\mu$ L of diluted CPM were added to each sample to give a 50  $\mu$ L final volume, mixed, and incubated on ice for 10 to 15 min. The samples were put in a 36-position rotor placed in the Rotor-Gene Q HRM 2-plex PCR cycler. The sample underwent a high-resolution melt (HRM) procedure in the thermocycler, consisting of a 90 s wait to reach equilibration temperature (18 °C) and subsequent stepwise increase in temperature of 1 °C over 15 minutes with measurements recorded between 25 to 90 °C, to progressively unfold the protein contained in the samples. The instrument's gain was set as -1 to obtain a suitable signal within the detection range. As the temperature rises the buried cysteine residues inside the protein are exposed to the external environment, and bind CPM, which forms a fluorescent adduct, emitting at ~470 nm. The fluorescence changes are visualized as a sigmoidal curve, and from peaks in the derivative of the profile, the protein melt temperature (T<sub>m</sub>) is obtained using the high-resolution melt (HRM) analysis with the Rotor-Gene Q software. The melt temperature (T<sub>m</sub>) or 'denaturation temperature' provides a relative measure of protein stability.

## **2.5 Purification of UCP1**

Native UCP1 was purified from ovine (lamb) BAT mitochondria, while recombinant UCP1 was purified from yeast mitochondria. Native or recombinant UCP1 were purified from mitochondrial membranes using a protocol combining negative chromatography with hydroxyapatite resin and covalent chromatography with the thiol-reactive resin TPS (Thiopropyl Sepharose) [98, 157].

Hydroxyapatite chromatography: 100 mg of isolated mitochondrial membranes were thawed from liquid nitrogen storage and centrifuged at 313000 x *g* for 20 min at 4 °C in a TLA 120.2 rotor on a benchtop ultracentrifuge. The pellet obtained was resuspended in hydroxyapatite (HA) buffer (20 mM MOPS pH 6.7, 20 mM Na<sub>2</sub>SO<sub>4</sub>, 0.16 mM EDTA) and solubilized with 3 % (v/v) TritonX-100 while being rotated in a cold room for 20 min. Membranes were pelleted with a second ultracentrifugation at

313000 x *g* for 20 min at 4 °C. The supernatant was recovered and loaded onto a hydroxyapatite column prepared previously. The column was prepared at room temperature on the day or the day before, stored at 4 °C but raised to room temperature at least 2 hrs prior to use. About 7 g of hydroxyapatite (Biorad 130-0420) were hydrated for ~30 min in HA buffer at room temperature. The obtained HA slurry was loaded onto a 20 mL Biorad PolyPrep column and packed to 15 mL by peristaltic flow, using a minipulse pump with a 1.65 mm PVC tube attached to the column via a 4 cm silicon tube (1 cm overlap). The column was run at 0.7 mL/min until all the supernatant had bound to the column. Once loaded, the flow was stopped for 15 min in order to unfold other less stable carriers, particularly AAC. The column was then topped up with fresh HA buffer and the flow resumed. The first 10 mL were discarded whilst the second 10 mL containing UCP1 were collected on ice and labelled as the post hydroxyapatite sample ('post-HA'), which was flash frozen and stored in liquid nitrogen until further use.

TPS chromatography: 300 mg of thiopropyl Sepharose (Sigma T8387) were weighed, added to an empty PD-10 column and hydrated in degassed distilled water for 20-30 min at room temperature on a roller. The post-HA sample was thawed from storage and supplemented with 50 mM Tris pH 8.0 and 1 mM EDTA, before being incubated with TPS for 1 hr at 4 °C rotating for the protein to bind to the resin. The column containing the sample was attached to a peristaltic pump and the protein washed with 30 mL wash buffer 1 (20 mM Tris pH 8, 50 mM NaCl, 1 mM EDTA and 0.5 % (v/v) 12MNG with or without tetraoleoyl cardiolipin (TOCL – Avanti Polar lipids 710335) at a 10:1 detergent to lipid ratio) at ~2.5 mL/min. Then 30 mL wash buffer 2 (20 mM Tris pH 8, 50 mM NaCl, 1 mM EDTA and 0.005 % (v/v) 12MNG with or without TOCL at a 10:1 ratio) were applied to the column. Finally, the column was detached from the pump, briefly spun at 500 x *g* to dry to dampness, topped up with 1 mL of elution buffer (wash buffer 2 supplemented with 150 mM DTT) and agitated in a cold room for 15 min. The eluate containing UCP1 was collected centrifuging 1 min at 500 x *g* and remaining protein in the column incubated again with a further 0.8 mL of elution buffer for 15 min. The second eluate was collected by centrifugation at 2000 x *g* for 2 min. The two eluate fractions were poured sequentially on to a PD-10 desalting column and eluted in the final PD10 buffer (20 mM Tris pH 8, 0.005 % (v/v) 12MNG with or without TOCL at a 10:1 ratio).

The final sample obtained was immediately flash frozen in the case of native material used for thermostability assays. Native protein destined for thermostability assays did not have TOCL added in the TPS step of the purification process. Recombinant protein and native protein used for liposome reconstitution was purified with TOCL (to stabilise the sample) supplemented to the TPS wash buffers and PD10 buffer and concentrated 5-fold with 0.5 mL Pierce centrifugal concentrators (30 MWCO 88502) before being flash frozen.

## 2.6 Proteoliposome formation

Native and recombinant UCP1 were reconstituted into liposomes following previously described methods [105, 153, 157, 217]. Lipid mixtures of phosphatidyl choline 18:1 (1,2-dioleoyl-sn-glycero-3-phosphocholine - DOPC) and cardiolipin 18:1 (tetraoleyl cardiolipin - TOCL) were dried down in 10 mg aliquots (9.5 mg DOPC and 0.5 mg TOCL) under a nitrogen stream, resolubilized in 100 % methanol, redried and stored sealed under nitrogen at -20 °C. Liposomes were formed by stepwise detergent removal with adsorbent beads: lipids were resolubilized in a total of 600 µL of aqueous medium comprising the internal buffer (see table 2.1 detailing buffers for proton and anion transport assays), the appropriate fluorescent probe - 2 mM of SPQ ((6-Methoxy-N-(3-Sulfopropyl)Quinolinium, Inner Salt) (Fisher M440) for proton transport tests or 0.5 mM PBF1 (1,3-Benzenedicarboxylic acid, 4,4'-[1,4,10,13-tetraoxa-7,16-diazacyclooctadecane-7,16-diylbis(5-methoxy-6,2-benzofurandiyl)]bis-, tetrakis[(acetyloxy)methyl] ester) for anion transport tests, and 55 µL of 25 % (v/v) polyoxyethylene detergent (C<sub>10</sub>E<sub>5</sub>, Sigma 76436).

20 µg of purified protein was added to the reconstitution mix, and the solution was vortexed. The samples were immediately transferred to 4 °C, onto a rotating mixer, where they were kept gently mixing. 8 additions (4 x 30 mg and a further 4 x 60 mg) of adsorbent beads (Bio-Beads SM-2), were applied in 20-minute intervals to progressively remove the detergent and encourage the formation of proteoliposomes. After the final bead addition, samples were left mixing overnight at 4 °C.

The following morning the formed proteoliposomes were removed from the cold room, and the adsorbent beads were removed by brief centrifugal filtration using an empty ~1 mL spin column cartridge. The eluate containing proteoliposomes was pretreated with 20 or 40 mM m $\beta$ CD (Methyl- $\beta$ -cyclodextrin, Sigma C4555) to collect free fatty acids and passed onto a PD10 desalting column to substitute the internal buffer with the appropriate external (assay) buffer, to establish a potassium concentration gradient, relevant for generating a membrane potential in the downstream assay. The internal and external buffers, detailed in table 2.1, were set to give a ratio of potassium (K<sup>+</sup>) concentration of 1000:1 to allow the generation of a membrane potential ( $\Delta\Psi$ ) in the desired direction in accordance with the Nernst equation ( $\Delta\Psi = 2.3 \frac{RT}{zF} \log_{10} \left( \frac{[K^{+}_{\text{outside}}]}{[K^{+}_{\text{inside}}]} \right)$ , where  $R$  is the universal gas constant,  $T$  the temperature in Kelvin,  $z$  the charge of the ion and  $F$  the Faraday constant) through the selective movement of K<sup>+</sup> using valinomycin in the assay [218]. The final liposome sample was eluted from the desalting columns in 1.4 mL, sufficient for 12-14 single traces in the fluorimeter.

**Table 2.1 buffer composition for flux assays**

<b>Proton influx assay – internal buffer</b>	<b>Anion influx assay – internal buffer</b>
100 mM K(PO <sub>4</sub> ) pH 7.5	100 mM TEA(PO <sub>4</sub> ) pH 7.5
30 mM (TEA)TES pH 7.5	30 mM (TEA)TES pH 7.5
0.5 mM (TEA)EDTA pH 7.5	0.5 mM (TEA)EDTA pH 7.5
0.1 mM TEA(PO <sub>4</sub> ) pH 7.5	0.1 mM K(PO <sub>4</sub> ) pH 7.5
<b>Proton influx assay – external buffer</b>	<b>Anion influx assay – external buffer</b>
100 mM TEA(PO <sub>4</sub> ) pH 7.5	100 mM K(PO <sub>4</sub> ) pH 7.5
30 mM (TEA)TES pH 7.5	30 mM (TEA)TES pH 7.5
0.5 mM (TEA) EDTA pH 7.5	0.5 mM (TEA) EDTA pH 7.5
0.1 mM K(PO <sub>4</sub> ) pH 7.5	0.1 mM TEA(PO <sub>4</sub> ) pH 7.5

## 2.7 Flux assays

Proton and anion transport were measured respectively with SPQ and PBFI fluorescent probes [219, 220]. 75  $\mu\text{L}$  of liposome samples were diluted in a quartz cuvette with 425  $\mu\text{L}$  of external buffer (either  $\text{TEA}^+$  or  $\text{K}^+$  based depending onto the direction of the assay). Fluorescence was measured at 334/443 nm for SPQ and 380/500 nm for PBFI. Unless otherwise stated, 100  $\mu\text{M}$  of compound/effector or 1 mM GDP in an appropriate solvent, was added to the cuvette in  $< 5 \mu\text{L}$  volumes, where control tests with an equivalent amount of solvent alone were also carried out. Fluorescence was measured on a Carey Eclipse fluorimeter at 22  $^\circ\text{C}$ , over 140 seconds total time. A membrane potential was induced after 40 s of baseline by the addition of 2.5  $\mu\text{M}$  of the ionophore valinomycin to drive proton transport across the membrane. In-assay additions were made via a culture inoculation loop containing the measured volume as a droplet at the tip. Transport was recorded for a further 60 s before addition of 1  $\mu\text{M}$  CCCP ([3-chlorophenyl) hydrazono]malononitrile) as a control to determine the maximum proton capacity of the liposome system. For the SPQ probe, the signal to proton change ratio was calibrated by stepwise additions of 1 M  $\text{H}_2\text{SO}_4$  to a fresh liposome sample in the presence of 10  $\mu\text{M}$  Nigericin with an external buffer used that matched the internal potassium buffer composition (i.e. no membrane potential would be generated). For the PBFI probe, a similar process was carried out, where the signal to charge moved ratio was calibrated by stepwise additions of 1 M potassium phosphate. The signals recorded from these calibrations give a linear relationship in Stern-Volmer plots ( $1/F$  vs  $\delta[\text{H}^+]$ ). The observed linear relationship was modelled by linear regression to obtain signal conversion [219]. The entrapped 'internal' volume was calculated assuming the original concentration of probe added to the reconstitution was retained as the entrapped concentration. The internal liposome volume was determined by solubilising a fresh 75  $\mu\text{L}$  sample of liposomes in assay buffer with 0.2 % (v/v) Triton X-100 detergent, releasing the fluorescent probe. The associated fluorescence signal was recorded and quantified with a standard curve obtained from the signal associated with 5 x 1  $\mu\text{L}$  subsequent additions of the appropriate fluorescent probe at known concentration. The amount of protein per 75  $\mu\text{L}$  of sample was not experimentally determined for all experiments in chapter 3 using native protein, where instead a 100 % reconstitution of the 20  $\mu\text{g}$  of UCP1 added was assumed.

For the experiments in chapter 4 with recombinant UCP1, the protein content of proteoliposomes samples was determined by detection through western blot analysis and interpolation using a calibration curve fitted to UCP1 standards. From assay recordings, the signal 10 s before to 59 s after the addition of valinomycin (calibrated to relative proton or anion concentration) was fitted with a 'plateau-one phase association' exponential fit using GraphPad Prism (version 8.0) software, to estimate the initial rate at valinomycin addition, which was used to calculate the specific transport rate in  $\mu\text{mol}/\text{min}/\text{mg}$  protein.

## **2.8 Homology modelling and sequence alignments**

Target sequences (ovine, mouse and human UCP1 - W5PSH7, P12242, P25874) were obtained from the Uniprot database [221]. Template structures were selected by sequence identity [222] from available ADP/ATP carrier structures on the Protein Database (PDB) [223]. Template structures for the c-state were 1OKC (BtAAC1) and 4C9G (ScAAC2); the template structure for the m-state was 4C9G (TtAAC). Homology modelling was performed with the MODELLER [224] software using the extension provided in UCSF Chimera (version 1.13.1) [225]. 100 homology models were generated per isoform per conformation. These models were scored by Estimated RMSD/Overlap, the top 2 models selected and further refined. Optimization was performed by using GalaxyRefine 2 on the Seok Server [226]. The best scored models underwent quality control checks with MolProbity [227] and QMEANBrane [228]. The final models were analysed in UCSF Chimera, and all images were also taken in UCSFChimera. Sequence alignments and analysis performed with Jalview (version2.11.0) and MEGA-X. See chapter 5 for further details.

## **2.9 UCP1 gene cloning in plasmid and yeast transformation**

Ovine, mouse, and human UCP1 genes were cloned into pYES2/CT vectors by Paul Crichton and Danielle Copeman (University of East Anglia) using conventional molecular biology methods.

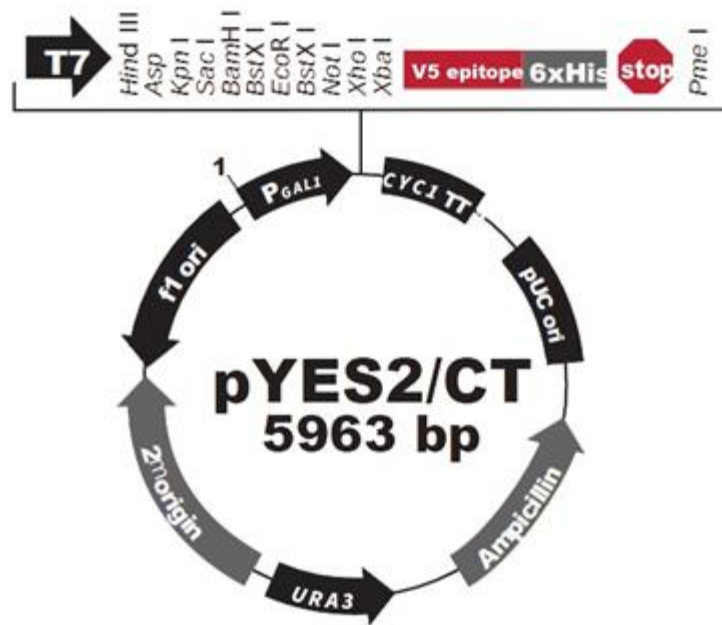


**Figure 2.1. pYES2/CT vector map** (adapted from Invitrogen user manual, catalogue no. V8251-20), showing restriction sites, cloning site, promoters and genes comprising the plasmid.

UCP1 genes were cloned into pYES2/CT vectors containing an ampicillin resistance gene for *Escherichia coli* transformant selection, a URA3 gene for *Saccharomyces cerevisiae* transformant selection, and a pGAL1 promoter for galactose-inducible expression of the genes cloned into the multiple cloning site. The restriction enzymes used were *Sac I* and *Xba I*. Stop codons had been included with the inserted gene to avoid the addition of a C-terminal V5 epitope and His-tag, as UCP1 is purified with a thiol reactive resin through a cysteine residue near its C-terminus, and detected on western blots with UCP1 specific antibodies.

UCP1 constructs (codon optimized for *S. cerevisiae* expression by GenScript) were amplified by PCR, cut with the designed restriction enzymes, *Xba I* and *Sac I*, and ligated into the multiple cloning site of pYES2/CT, before being transformed into competent *E. coli* cells (TOP10 or XL1-blue). The successful transformation was first checked by colony PCR, then the vector extracted and sequenced to ensure correct insertion of UCP1 gene and absence of mutations.

The vectors were finally transformed into *S. cerevisiae* (W303.1B strain) [136]. Colonies that were successfully transformed were stored at -80 °C in 10 % (v/v) glycerol, ready to be used for starter cultures for large scale expression.

## 2.10 UCP1 isoforms expression in yeast

4 to 5 days before expression, transformed yeast cells (W303.1B) were streaked from glycerol stocks onto plates (synthetic complete supplement mixture (SC) of amino acids without uracil (SC-ura) + 2 % (w/v) glucose) and incubated at 30 °C for 48 - 72 hours. A single colony from each plate was grown overnight (30 °C, 225 rpm) in 10 mL of selective lactate + glucose (SL+G) media (0.67 % (w/v) yeast nitrogen base, 0.077 % (w/v) complete supplement mixture (CSM) of amino acids without uracil (CSM-ura), 30 mg/L adenine, 2 % (v/v) lactic acid, 0.1 % (w/v) glucose, (pH corrected to pH 5.5 with concentrated KOH)) in 50 mL tubes (loosely capped). For each construct, 80 mL of SL+G media was inoculated with 3-5 mL of the 10 mL pre-culture and grow overnight again (30 °C, 225 rpm). In the afternoon of the day before expression (-15/17 hr) OD<sub>600nm</sub> readings of the cultures were taken to assess yeast growth. In tunair flasks (Sigma 710822-4EA) 1 L of pre-warmed YPL media (1 % (w/v) yeast extract, 2 % (w/v) peptone, 3 % (v/v) DL-lactic acid, (pH corrected to 5.5 with concentrated KOH)) was inoculated at a 100x dilution (i.e. 10 mL per flask) from the 80 mL starter cultures, and grown overnight (30 °C, 200 rpm) for ~15-17 hours, depending on the isoform expressed. After 15 to 17 hrs of growth 10 mL of each culture ("t = 0") were collected, and protein expression was induced by addition of 1 % (v/v) galactose to the remaining culture. Expression time was between 6 hrs to 7 hrs, depending on optimal time for each isoform (determined with small-scale expression screens, courtesy of Danielle Copeman). At the end of the expression period a final sample ("t = 6 to 7 hrs") was collected for OD<sub>600nm</sub> measurements. The cells were then immediately transferred from the tunair flask to centrifuge tubes and pelleted by centrifugation (4500 rpm, 10 min, 4 °C). Because the obtained pellet was very soft, ice cold dH<sub>2</sub>O was added and the pellet recentrifuged (4000 rpm, 2-5 min at 4 °C) to remove excess buffer. The final pellet was transferred to 50 mL falcon tubes and weighed to estimate the amount of pellet before being snap frozen and stored at -80 °C.

## 2.11 Isolation of mitochondrial membranes from yeast

Frozen cell pellets from 6 L cultures were thawed and resuspended in 100 mL of breaking buffer (100 mM Tris-HCl pH 8.0, 0.65 M D-sorbitol, 5 mM Na-EDTA (pH 8.0), 5 mM aminocaproic acid, 5 mM benzamidine HCl, 1 mM PMSF). The

resuspended pellet was poured into a beadbeater (Stratech, 1107900EUR-BSP) 250 mL chamber filled 2/3 with ice cold glass beads (Sigma G8772) and homogenized with 5 x 30 seconds pulses. The lysate was decanted and transferred into JLA 16.250 Beckman tubes and centrifuged for 20 min, 4300 x *g* (6,500 rpm) at 4 °C, the supernatant was then centrifuged again. The resulting supernatant was recovered and ultracentrifuged at 28000 x *g* (15,749 rpm) for 50 min at 4 °C to pellet the membranes. The resulting membranes were resuspended in 30 to 40 mL of wash buffer (50 mM Tris-HCl pH 8.0, 0.65 M D-sorbitol, 5 mM aminocaproic acid, 5 mM benzamidine HCl) with a paintbrush. The mixture was ultracentrifuged again at 28000 x *g* (15,749 rpm) for 50 min at 4 °C and the pellet resuspended in as small as possible volume of TBG buffer (10 mM Tris-HCl pH 8.0, 10 % (w/v) glycerol, 500 μM PMSF), the final buffer in which the membranes were stored in. The protein content of the membranes was assessed with a BCA assay and the isolated membranes were flash frozen and stored in liquid nitrogen.

### **2.12 Sample quantification**

Isolated membranes and purified protein concentrations were determined with the bicinchoninic acid BCA Protein Assay Kit colorimetric method (ThermoFisher, 23227), using bovine serum albumin standards. Readings were taken on 96 wells plates with a plate reader at 562 nm. GDP (Sigma G7127) purity was estimated by spectrophotometry using GDP extinction coefficient ( $\epsilon_{253}$ : 13700 M<sup>-1</sup> cm<sup>-1</sup>) and the molecular weight to ensure maximum accuracy of the GDP working concentration added to each assay.

### **2.13 Statistical analysis**

The statistical analysis of data was performed with GraphPad Prism (version 8.0). Paired or unpaired two tailed Student-t tests, one sample t-tests, or one-way ANOVA were used for the comparison of averages from experimental groups. Initial proton or anion transport rates were determined by fitting with a non-linear curve using an exponential fitting (using the function called “plateau followed by one phase association”).

## 2.14 Compounds used in screens

**Table 2.2 Compounds used in thermostability screens**

<i>Compound</i>	<i>Manufacturer</i>	<i>Product code</i>
Lorglumide	Sigma	L109
Ibuprofen	Alexis/Sigma	550-249/i4883
Bezafibrate	Sigma	B7273
Indomethacin	Cayman	70270
2-amino-2-norbornenecarboxylic acid	Sigma	A7902
Cantharidic acid	Calbiochem	210150
Celecoxib	LKT Laboratories	C1644
NSC 23766	Tocris	13196
Sodium orthovanadate	Sigma	S6508
U-73122	Cayman	70740
Acetylsalicylic acid	Sigma	A5376
Meclocycline sulfosalicylate	Sigma	M1388
Myriocin	Cayman	63150
Adapalene	Sigma	A7486
Tazarotene	Sigma	T7080
Acitretin	Sigma	44707
Citrate	Sigma	71498
Trimesic acid	Sigma	482749
Maleic acid	Sigma	M5757
Succinic acid	Sigma	224731
L-aspartate	Fluka	11195
Isocitric acid (DL)	Sigma	I1252
Sodium malate	Sigma	M9138

Cis-aconitate	Sigma	A3412
2-oxoglutarate	Sigma	K1875
Sodium malonate	Sigma	M4795
Oxaloacetate	Sigma	O4126
Fumarate	Sigma	F1506
Prostaglandin E2	Cayman	14010
All trans retinoic acid	Cayman	11017
(±)12,13-DiHOME	Chemcruz	sc204985
Cholic acid	Sigma	C1129
L-Carnitine	Sigma	C0283
Oleoyl CoA	Sigma	O1012
Potassium pyrophosphate	Sigma	322431
3,3',5-triiodo-L-thyronine (T3)	Sigma	T2752
L-Thyroxine (T4)	Sigma	T2376
4-aminobutyric acid	Fluka	7329
Cefamandole nafate	Sigma	C0682300
Pentasodium tripolyphosphate	Sigma	T5633
Adenine	Fluka	8130
Cyclo-dextrin (alpha)	Sigma	C4642
DIDS	Sigma	D3514
Tetradecanedioic acid	Sigma	D221201
tetradecylthioacetic acid	Sigma	T1698
Perfluorononanoic acid	Sigma	394459
Perfluorotridecanoic acid	Sigma	654973
7-amino heptanoic acid	Sigma	284637
Farnesyl acetate	Sigma	W421350
Bromodecanoic acid	Sigma	541397

12-hydroxylauric acid	Sigma	198781
Behenic acid	Sigma	216941
6-Phenylhexanoic acid	Sigma	333603
Agaric acid	Sigma	01387
Adipic acid	Sigma	09582
Lipoic acid	Sigma	T5625
16-hydroxyhexadecanoic acid	Sigma	177490
5-Amino-n-valeric acid	Fisher	153910050
4-Heptylbenzoic acid	Sigma	230642
Medica 16	Cayman	90290
TUG-891	Cayman	17035
Palmitic Acid methyl ester	Cayman	10007358
N-Arachidonoyl-3-hydroxy- $\gamma$ -Aminobutyric Acid	Cayman	10158
N-Oleoyl-L-Serine	Cayman	13058
Linoleoyl Glycine	Cayman	9000326
TTNPB	Cayman	16144
MJ33	Cayman	90001844
Pyrophenone	Santa Cruz	sc-296161
1-oleoyl lysophosphatidic acid	Cayman	10010093
RSC-3388	Santa Cruz	sc-296281
Methyl Arachidonyl Fluorophosphonate	Cayman	70660
1-Octadecyl Lysophosphatidic Acid (sodium salt)	Cayman	10010291
Oleyloxyethyl Phosphorylcholine	Cayman	70560
Bodipy FL ATP-g-S	Invitrogen	A22184
Bodipy FL GDP-g-S	Invitrogen	A22360
Sodium sulphate	Fisher	A19890.0B
Sodium phosphate	Fisher	BP329-1

Salsalate	Cayman	11911
Malonyl-CoA	Cayman	16455
Oleoyl-L-carnitine	Sigma	19945
Acetyl CoA	Sigma	A2076
Palmitoyl-CoA	Sigma	P9716
CoA	Sigma	C3144
L-Citrulline	Sigma	C7629
Butyric acid	Sigma	B103500
Heptanoic acid	Sigma	75190
Nonanoic acid	Sigma	N5502
Dodecanoic acid	Sigma	W261408
Nonadecanoic Acid	Cayman	19723
Propanesulfonate	Sigma	358959
Hexanesulfonate	Sigma	106410
Octanesulfonate	Sigma	74884
Undecanesulfonate	Alfa Aesar	B20332.14
Octadecanesulfonate	Insight Biotechnology	sc-250992
Oleic acid	Sigma	O1008



## **3.The regulatory ligands of native ovine UCP1**

### **3.1 Introduction**

Since brown fat was discovered in adult humans [20-22] its thermogenic properties have attracted interest for possible therapeutic uses. The presence of BAT in adults correlates with leanness and euglycemia and studies have shown that BAT positive humans, after cold exposure, present higher resting energy expenditure and improved levels of whole-body glucose disposal as well as accelerated lipid oxidation and mobilization [80, 229, 230]. Therefore, the activation of endogenous brown fat constitutes a promising therapeutic avenue for combating metabolic disease [37, 81, 231].

Brown fat thermogenic properties are mediated by UCP1 which catalyses proton leak across the mitochondrial inner membrane, uncoupling mitochondrial substrate oxidation from the phosphorylation of ADP to ATP. However, BAT and UCP1 must be specifically activated for thermogenesis to occur. Research on exploiting brown fat thermogenic properties has mainly focused on stimulating brown fat proliferation (browning) and activation through the adrenergic stimulation of adipocytes [8, 78, 232, 233] (see chapter 1, section 1.2.3 on the activation process). However, the direct pharmacological activation of the UCP1 protein could allow the activation of thermogenesis in the absence of upstream stimuli (e.g. cold exposure or  $\beta$ -adrenergic targeting), avoiding the associated issues. However, targeting UCP1 requires a better understanding of how UCP1 interacts with its regulatory ligands, fatty acid activators and purine nucleotide inhibitors. While nucleotide binding is to some degree understood, how fatty acid activators bind to UCP1 is not known [111, 210]. Recent studies have demonstrated that ligand interactions of isolated carriers can be detected by thermostability shift analysis using an assay tailored for membrane proteins, which has proved effective in studying mitochondrial carriers [140, 169, 216]. This chapter sets out to characterise the interactions of native ovine (lamb) UCP1 with activators by thermal shift analysis and identify novel regulatory ligands of the protein.

## 3.2. Aims

1. To detect and clarify the specific interactions of native ovine UCP1 with activators by thermostability shift analysis
2. To identify new ligands of native ovine UCP1 from an array of drugs, fatty acid analogues and physiologically relevant metabolites, utilising thermostability shift analysis for compound screening

## 3.3. Results

### 3.3.1. UCP1 thermostability shifts and ligand interactions

Shifts in the stability of proteins associated with changes in covalent and non-covalent bonding upon ligand binding can be detected through a protein thermostability assay and provide information on substrate and inhibitor ligand interactions [169, 216]. The thermostability assay used here is a fluorescence-based assay suitable for membrane proteins that uses the properties of the thiol sensitive dye N-[4-(7-diethylamino-4-methyl-3-coumarinyl) phenyl] maleimide (CPM) to create a profile, tracking the unfolding of an isolated protein [215]. The assay is based on denaturing the protein by progressively increasing the temperature from 25 to 90 °C; as the protein unfolds, the cysteine residues buried within the protein are exposed to the external environment, where they react with CPM to generate a fluorescent adduct.

Figure 3.1 shows typical denaturation profiles of native ovine UCP1 (upper panel). The traces start with a low plateau and transition to a higher one as the temperature increases. Using the first derivatives of the recorded signal, the inflection point can be identified (the peak in the profile), corresponding to the temperature where the unfolding rate is highest, which provides an apparent melting temperature ( $T_m$ ) for the protein as an indicator of relative stability. The starting fluorescence at 25 °C is not 0, suggesting that the protein has at least 1 of its 9 cysteines exposed in its folded conformation. In the assay, at pH 7.5 with 0.1% of the non-ionic detergent lauryl maltose neopentyl glycol (12MNG), ligand-free native UCP1 had an average  $T_m$  of  $51.5 \pm 0.4$  °C (see the derivative peak, lower panel, figure 3.1). UCP1

interactions with known activators and inhibitors, such as oleic acid and GDP induce a shift in the unfolding transition and corresponding  $T_m$  measured (“ $\Delta T_m$ ”). The presence of the UCP1 activator oleic acid induces a shift to a lower  $T_m$  (dotted line), whereas the presence of GDP induces an increase in  $T_m$  (dashed line). Binding of a fatty acid activator (25  $\mu$ M oleic acid) caused a  $\Delta T_m$  of  $-5.7 \pm 1.9$  °C, while binding of the inhibitor GDP caused a  $\Delta T_m$  of  $+ 14.9 \pm 0.3$  °C (1 mM working concentration).

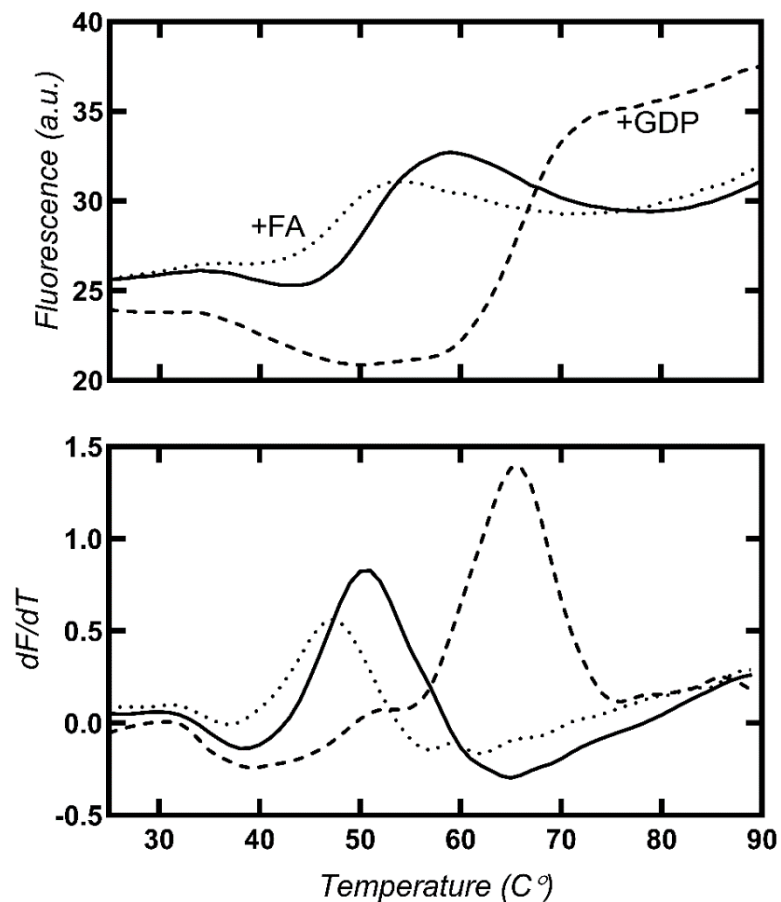


**Figure 3.1. UCP1 thermostability assay, the effect of activators and inhibitors.** Assays performed at pH 7.5 in 0.1 %12MNG. (Upper panel) typical raw fluorescence traces of native ovine UCP1 with a fatty acid (FA; 25  $\mu$ M oleic acid; dots) and a purine nucleotide (GDP; 1 mM; dashes). (Bottom panel) corresponding derivative peaks from which the melting temperature ( $T_m$ ) was measured. Average  $T_m$  (3 repeats), -ADD =  $51.5 \pm 0.4$  °C; +FA =  $44.9 \pm 1.8$  °C; +GDP =  $64.9 \pm 1.4$  °C. Repeats, showing variation of the traces in different experimental runs, are shown in appendix figure A1.

Previous research has demonstrated that fatty acid addition decreases the  $T_m$  of UCP1 in a similar manner to what happens to the yeast ADP/ATP carrier (ScAAC2) with the binding of a substrate, such as ADP, at micromolar concentrations [169]. However, it could be argued that the decrease in  $T_m$  of UCP1 by fatty acids is a

consequence of general denaturation of the protein by adding a harsh ionic detergent, since fatty acids act as soaps at physiological pH, rather than being the result of a specific substrate-like effect. To address this possibility, the dependence of the  $T_m$  change ( $\Delta T_m$ ) with variable activator concentration was determined for four different established activators of UCP1 [113, 234, 235]: lauric acid, oleic acid, retinoic acid and the retinoid TTNPB (4-[(E)-2-(5,6,7,8-Tetrahydro-5,5,8,8-tetramethyl-2-naphthalenyl)-1-propenyl]benzoic acid [234]) (figure 3.2).

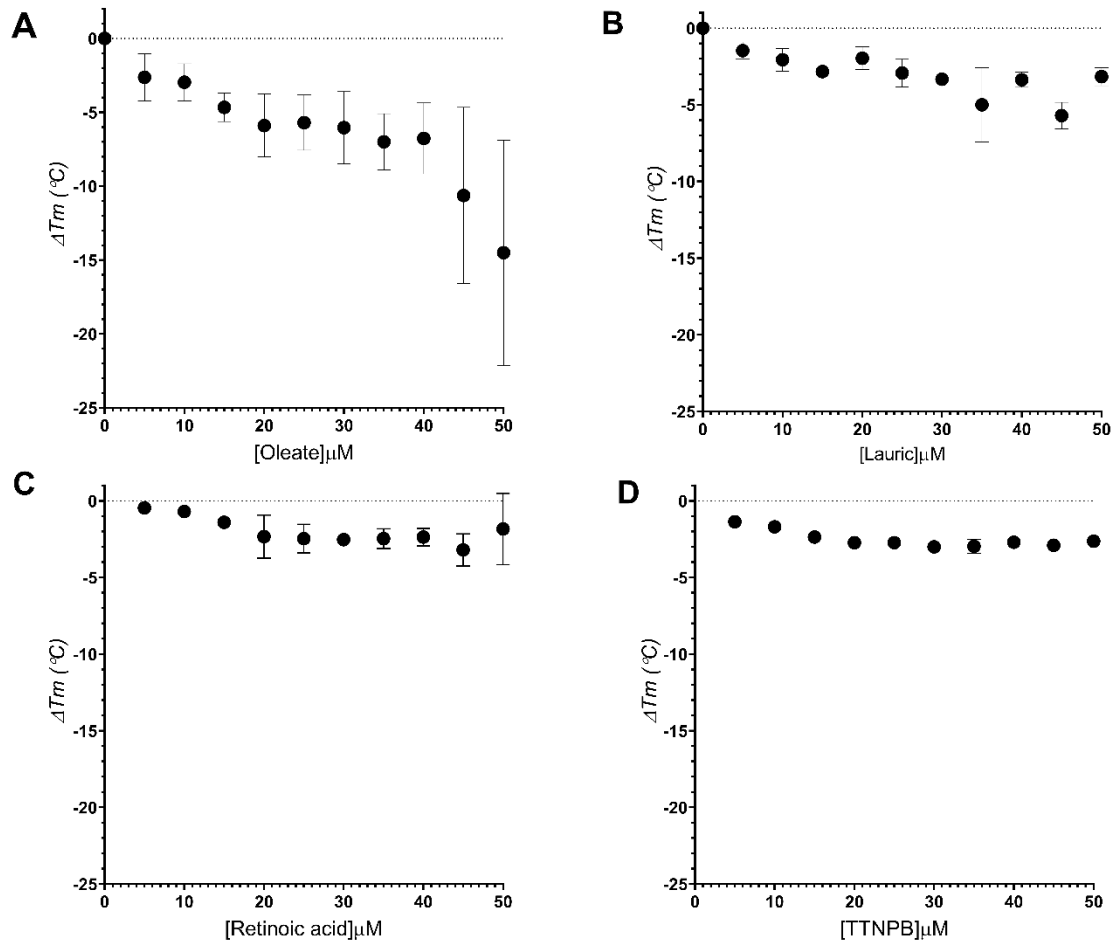


**Figure 3.2. UCP1 activator profiles, a specific destabilizing effect.** Assays performed at pH 7.5 in 0.1 % 12MNG **Panel A.** Oleic acid titre,  $\Delta T_m$  (difference between  $T_m$  of no addition trace and  $T_m$  + ligand) 0-50  $\mu\text{M}$ ; **Panel B.** lauric acid titre,  $\Delta T_m$  0-50  $\mu\text{M}$ ; **Panel C**  $\Delta T_m$  retinoic acid titre 0-50  $\mu\text{M}$ ; **Panel D.**  $\Delta T_m$  retinoid TTNBP titre 0-50  $\mu\text{M}$ . Values given are averages ( $\pm$ SD) of three independent experiments.

The activators, with the exception of lauric acid (panel B), exhibited a saturation profile, where the  $T_m$ , after an initial drop at low concentrations (often up to 15  $\mu\text{M}$ ), plateaued with little or no further decrease with increasing ligand concentration, thus likely representing a specific interaction. In the case of oleic acid (panel A), the

plateau ended around 50  $\mu\text{M}$ , with a more rapid drop of the  $T_m$  at higher concentrations to below the measurable threshold (25  $^{\circ}\text{C}$ ), which probably represents non-specific denaturation of UCP1 by fatty acids as harsh ionic detergent. In contrast, the trend for lauric acid was an almost linear decrease in stability of UCP1 with increasing concentration of the acid. The absence of a clear plateau for lauric acid is consistent with it being a harsher detergent than the other activators tested, and so more likely to denature the protein at lower concentrations, where  $T_m$  changes associated with specific interactions may have otherwise been observed. Although for each compound the exact size of the drop in melting temperature was different, the presence of a plateau showed that the specific binding of a fatty acid activator to UCP1 can be distinguished from non-specific denaturing effects, which take place at higher concentrations, as exemplified in the oleic acid trace in panel A.

Tests with other known activators of UCP1 over similar ranges of concentrations showed similar destabilising effects. Three linear fatty acids of different chain lengths, representative of short chain fatty acids - heptanoic acid (C7), medium chain - dodecanoic acid (C12), and long chain fatty acids - nonadecanoic acid (C19), were tested (Figure 3.3 Panel A). Only the long chain nonadecanoic acid (C19) destabilised UCP1 with a saturating behaviour, similarly to retinoids. The shorter chain lauric acid (C12) caused a drop in  $T_m$  but did not produce a plateau, while the shortest fatty acid, heptanoic acid (C7) showed almost no destabilising effects. It was also determined that the decrease in UCP1 stability (negative  $\Delta T_m$ ) correlated with the length of the acyl chain (Figure 3.3, panel A). A clear trend could be observed when comparing the species at 25  $\mu\text{M}$  concentration (Figure 3.3, panel B), where a UCP1  $\Delta T_m$  is of  $-0.5 \pm 0.5$   $^{\circ}\text{C}$  for heptanoic acid (7 carbons),  $-2.9 \pm 0.9$   $^{\circ}\text{C}$  for lauric acid (12 carbons), and  $-4.1 \pm 1.6$   $^{\circ}\text{C}$  for nonadecanoic acid (19 carbons) was observed.

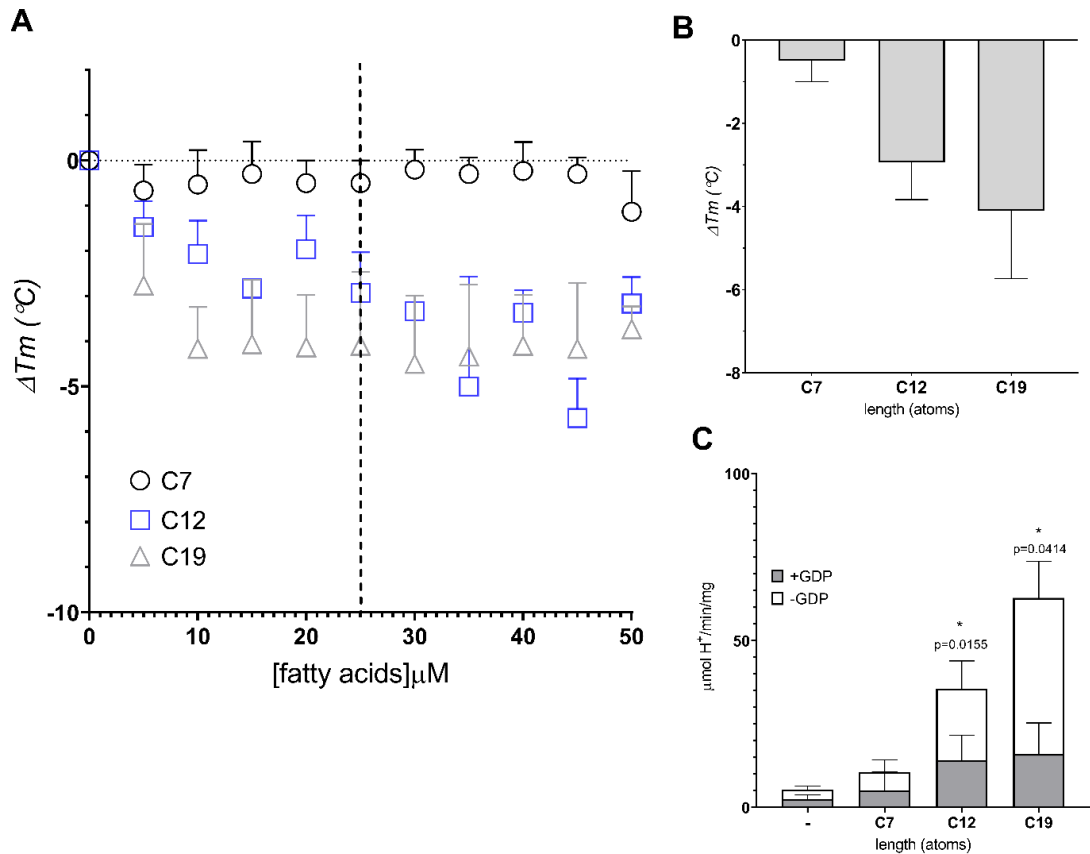


**Figure 3.3. Trends in UCP1 thermostability with fatty acids' acyl chain length. Panel A.** Titre of increasing concentration of heptanoic (C7), lauric (C12) and nonadecanoic (C19) acid, comparing  $\Delta T_m$  trends. **Panel B.**  $\Delta T_m$  of heptanoic (C7), lauric (C12) and nonadecanoic (C19) acid at 25  $\mu\text{M}$ ; **Panel C.** Proton transport rates after addition of 100  $\mu\text{M}$  heptanoic (C7), lauric (C12) and nonadecanoic (C19) acid, compared to no addition control. Values expressed as averages  $\pm$ SD, statistical analysis performed by one-way ANOVA (\* $p < 0.05$ , \*\* $p < 0.02$ , \*\*\* $p < 0.001$ ).

Proton transport in liposomes was monitored using an entrapped fluorescent probe (SPQ) (see chapter 2, Materials and Methods). Fatty acid chain length and the decrease in  $T_m$  also correlated with the potency in activating UCP1-mediated proton influx in proteoliposomes (Figure 3.3, panel C); heptanoic acid induced very low rates of  $10.6 \pm 3.6 \mu\text{molH}^+/\text{min}/\text{mg}$ , which were not significant. Lauric acid and nonadecanoic acid stimulated proton influx in a significant manner (with rates of  $35.6 \pm 8.3 \mu\text{molH}^+/\text{min}/\text{mg}$  and  $62.8 \pm 10.9 \mu\text{molH}^+/\text{min}/\text{mg}$  respectively).

Similar trends in thermostability were observed with a class of known transport substrates of UCP1, alkyl sulphonates (figure 3.4). Alkyl sulphonates are linear fatty acid analogues with non-protonable head groups at physiological pH, and have

been used to investigate the UCP1 proton transport mechanism by Keith Garlid and collaborators (e.g. [236]) and more recently by Fedorenko et al. [115]. The alkyl chain length was matched to those of the linear fatty acids tested to give equivalent species of similar length.

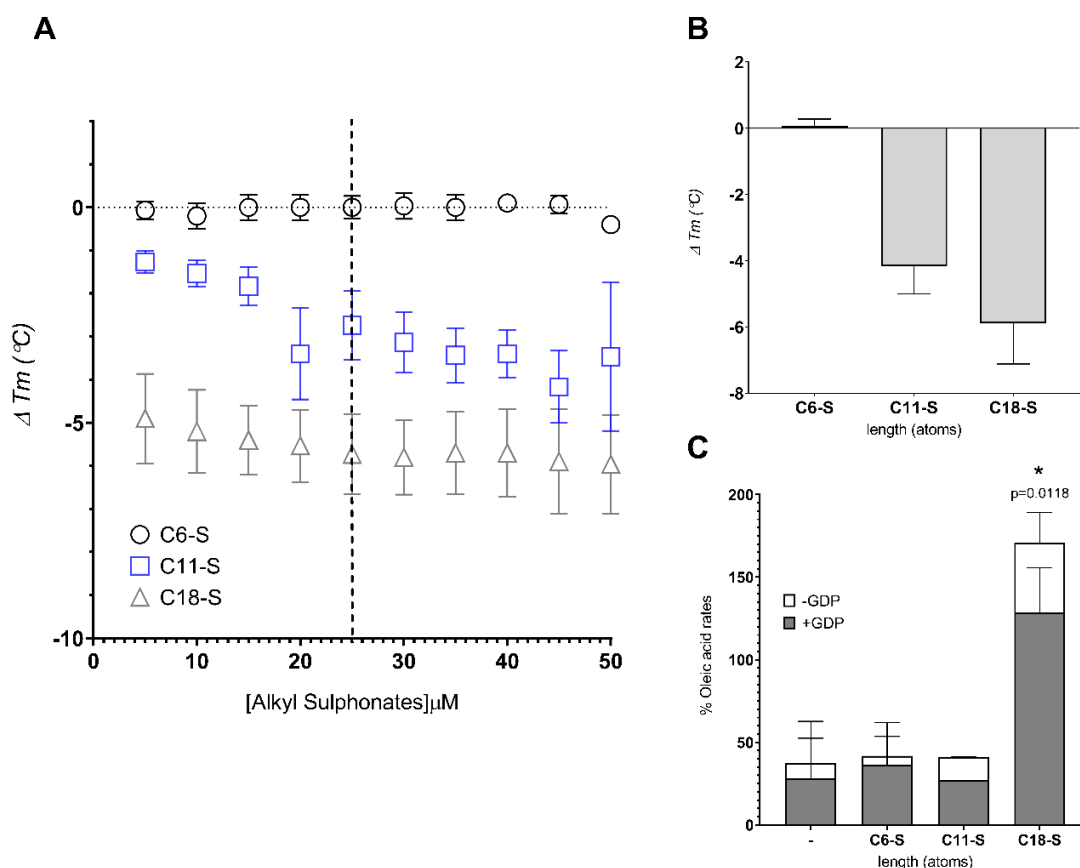


**Figure 3.4. Trends in UCP1 thermostability with alkyl sulphonate chain length. Panel A.** Titre of increasing concentration of hexanesulphonate (C6-S), undecanesulphonate (C11-S) and octadecanesulphonate (C18-S), comparing  $\Delta T_m$  trends in the range 0 – 50  $\mu\text{M}$ . Note, C18-S was added with 1.6 mM methyl- $\beta$ -cyclodextrins ( $m\beta\text{CD}$ ), see also chapter 2, section 2.4. **Panel B.**  $\Delta T_m$  of hexanesulphonate (C6-S), undecanesulphonate (C11-S) and octadecanesulphonate (C18-S), at 25  $\mu\text{M}$ ; **Panel C.** Anion transport rates normalized to oleic acid, after addition of 100  $\mu\text{M}$  of alkyl sulphonates compared to no addition control. Values expressed as averages  $\pm$ SD, statistical analysis performed by one-way ANOVA (\* $p < 0.05$ , \*\* $p < 0.02$ , \*\*\* $p < 0.001$ ).

Three alkyl sulphonates with varying alkyl chain lengths, hexanesulphonate (C6-S), undecanesulphonate (C11-S), and octadecanesulphonate (C18-S) were selected for testing. Examining the effect of these species on UCP1 thermostability, they showed trends in melting temperature similar to those seen with the linear fatty acid

activators, with only octanesulphonate (C18-S) presenting a decrease in  $T_m$  with a distinct plateau (see panel A figure 3.4). These results indicate that transport substrates interact with UCP1 in a similar specific manner as fatty acids, and thus fatty acid activators potentially interact as transport substrates in the UCP1 mechanism of proton leak. The decrease in thermal stability, exemplified by the  $\Delta T_m$ , correlated to the length of acyl chain, as evidenced in panel B of figure 3.4. The shortest chain molecule barely caused any changes in melting temperature, whereas increasing destabilization of UCP1 was seen with the longer 11 and 18 carbon alkyl sulphonates. Alkyl sulphonates cannot move directly across the membrane due to the charge they possess and thus require to be transported by UCP1. Panel C of figure 3.4 shows the result of an anion transport assay with native UCP1 reconstituted in liposomes, tracking anion movement, with the potassium sensitive fluorophore PBFI. It is notable how only the longest chain alkyl sulphonate, octadecanesulphonate (C18-S) was transported by UCP1 ( $p=0.0118$ ). Undecanesulphonate (C11-S) did not seem to be transported, however this molecule is a harsh ionic detergent (it closely resembles SDS). This same effect is also seen in the thermostability assay, where at high concentration it is much more damaging to UCP1 integrity than C6-S or C18-S. In the anion transport assay, the membrane polarity differs compared to the proton transport assay, with the liposome positively charged inside and negatively outside ([219] see Methods section 2.7 for detail), in order to allow for anion uptake into the liposomes. This setup is documented to generate lower GDP inhibition [107], increasing the difficulty to clarify UCP1-specific activity from non-specific effects (e.g. apparent transport from lysed liposomes).

### **3.3.2. UCP1 ligands exploration – thermostability based screen**

The detection of a specific destabilisation of UCP1 by activator-like molecules provided an opportunity to use thermostability analysis to identify novel UCP1 ligands in screens. Compounds were chosen, by their association with brown fat and UCP1 (e.g. TUG-891 [237]) or their relevance to mitochondrial metabolism, and screened in the thermostability assay for ligand interactions with UCP1 (figure 3.5). The compounds were loosely grouped into three categories of molecules: metabolites, fatty acids/lipids, and drugs.

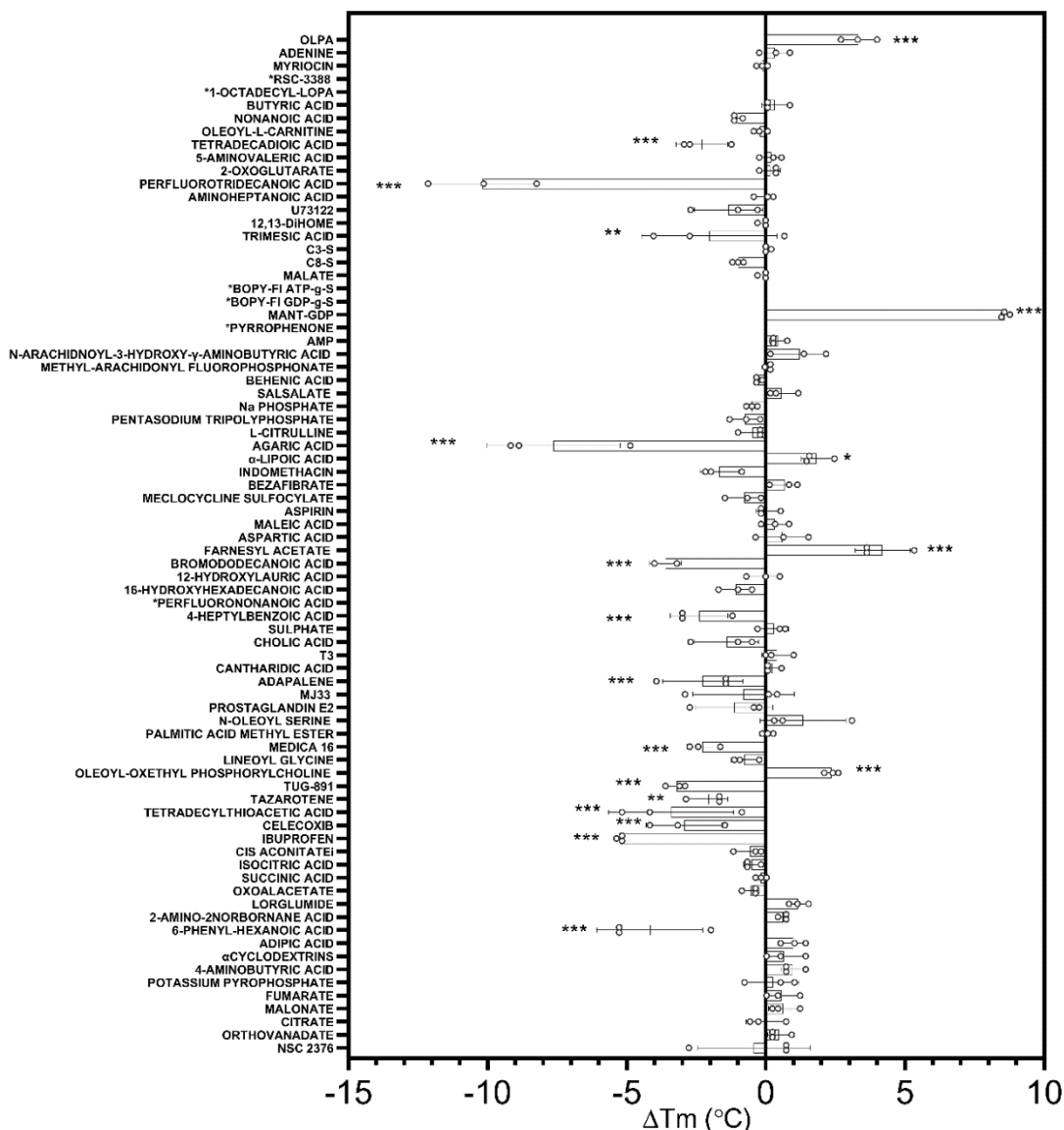


**Figure 3.5. UCP1 thermostability screen for detection of interacting ligands.** Assays performed at pH 7.5 in 0.1%12MNG. Changes in  $T_m$  ( $\Delta T_m$ ) of the 78 molecules tested. Values expressed as averages  $\pm$ SD,  $n=3$ , statistical analysis performed by one-way ANOVA (\* $p < 0.05$ , \*\* $p < 0.02$ , \*\*\* $p < 0.001$ ).

Figure 3.5 shows the results of the thermostability screen measured as changes in  $\Delta T_m$ , for each of the 78 molecules tested. Of the total compounds selected, some had to be excluded because they interfered with the thiol-sensitive dye, either absorbing in overlapping wavelengths or presenting exposed thiols (such as CoA for example), (the full list is reported in table A1 of the appendix).

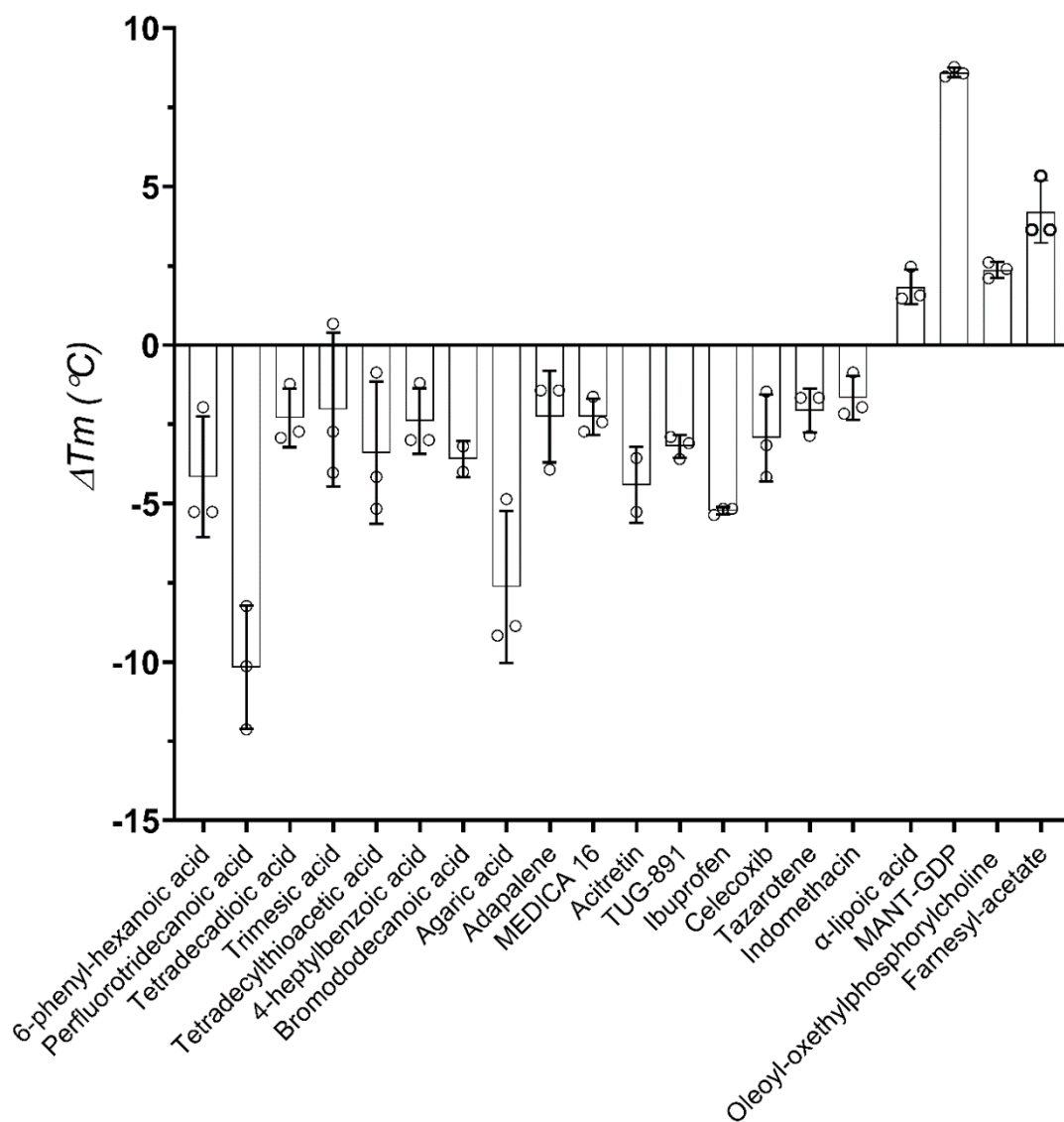


**Figure 3.6. Thermostability ligand screen – ligands inducing significant changes in melting temperature.** The 20 ligands that significantly changed the melting temperature identified in the screen. Data from figure 3.5. Values expressed as averages  $\pm$ SD, n=3.

The screen identified a total of 20 molecules which caused significant changes in  $T_m$  in either direction (shown in figure 3.6): 7 were drugs, 11 were fatty acid/lipids, and the remaining two belonged to the metabolite group.

Among them, 16 decreased UCP1 stability, and 4 increased it (figure 3.6). The biggest decrease was seen for perfluorotridecanoic acid ( $\Delta T_m -10.2 \pm 1.9$  °C) a low  $pK_a$  fluorinated fatty acid, while the smallest with trimesic acid ( $\Delta T_m -2.0 \pm 2.4$  °C), a benzene derivative with three carboxylates. The smallest positive  $T_m$  increase was instead observed with  $\alpha$ -lipoic acid ( $\Delta T_m +1.8 \pm 0.5$  °C), an important cofactor of alpha-keto acid dehydrogenases, and the highest positive  $\Delta T_m$  was registered

for MANT-GDP ( $\Delta T_m +8.6 \pm 0.6$  °C), an analogue of the purine nucleotide GDP with the MANT fluorophore group bound to the ribose. Based on the results of the screen, notable molecules were chosen for further testing in proton flux assays. Molecules belonging to the same class were either excluded if a representative molecule had already been tested (e.g. retinoids), or if it was a known effector (such as MANT-GDP) or a single representative molecule was chosen.

### **3.3.3. UCP1 activators - transport assays**

The thermostability assay was complemented by measuring proton uptake by UCP1 in phosphatidyl choline liposomes in response to the addition of the identified ligands (figure 3.7). Among the ligands that decreased the  $T_m$  not all were activators of proton transport. Statistical analysis identified 5 compounds that activated rates significantly higher than the endogenous rates of the control: tetradecylthioacetic acid, followed by ibuprofen, bromododecanoic acid, TUG-891 and 4-heptyl-benzoic acid. Importantly, the activated rates were 60-70% sensitive to GDP, confirming that they were mediated by UCP1 [113]. Another molecule, TUG-770, examined in subsequent experiments, showed similar trends in thermostability and activated UCP1-mediated proton transport (see appendix figure A4). Note, the effects of these novel activators of UCP1 mediated proton transport were not tested in empty liposomes (without UCP1). Hence, some of the GDP-insensitive effects of these molecules on proton flux could potentially be UCP1-independent.

To better understand how the decrease in UCP1  $T_m$  relates to protein function for the sub-set of molecules that did not activate proton leak, anion transport assays were carried out to see if these compounds were at least transported by UCP1 (panel B of figure 3.7). 4-heptyl-benzoic acid, which was shown to be both an activator and substrate by Jezek et al. [235]), was included as a control. The inclusion of 4-heptyl-benzoic acid clarified the difference between GDP inhibited rates in the two assays. Among the other molecules tested only perfluorotridecanoic acid appeared to be a possible transport substrate, along with the positive control, oleic acid, although neither molecule was highlighted in the statistical analysis because of the high standard deviation. As such, no robust conclusions could be derived from the data.

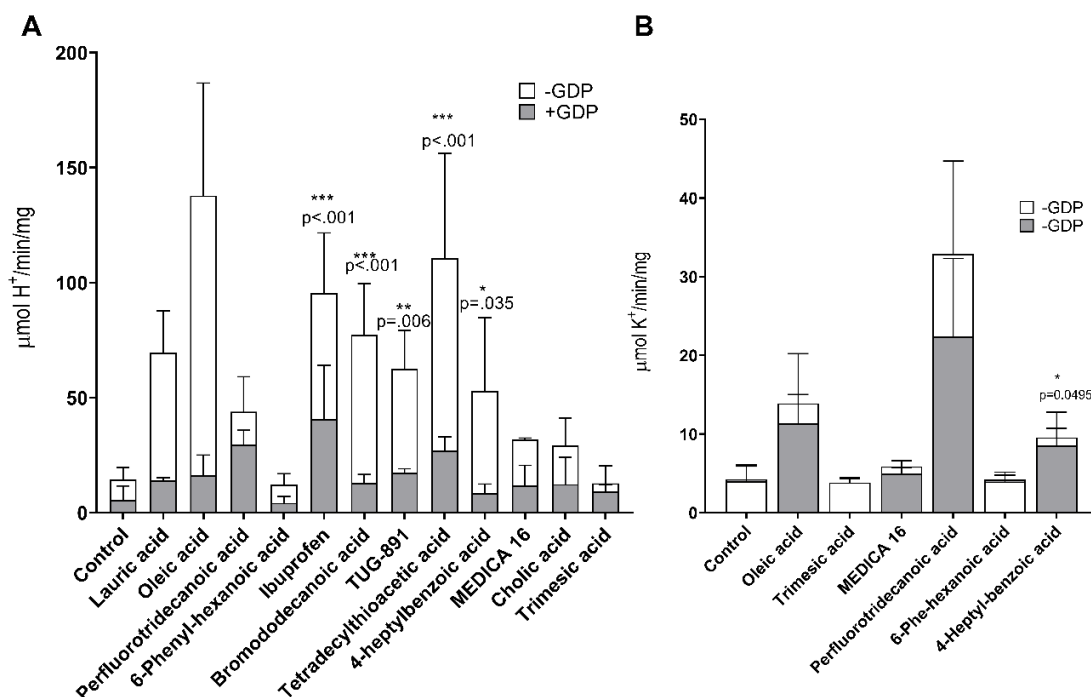


**Figure 3.7. The activation of UCP1 in proteoliposomes by novel ligands. Panel A.** Proton transport assay +/-GDP (1 mM) of molecules decreasing T<sub>m</sub> (100 μM); **Panel B.** Anion transport assays of molecules decreasing T<sub>m</sub> (100 μM) but not inducing proton transport to a statistically significant degree. Values expressed as averages of three to six independent experiments ±SD, statistical analysis performed by one-way ANOVA (\*p<0.05, \*\*p<0.02, \*\*\*p<0.001).

From the combination of the two assays, it appears that most ligands that decrease the T<sub>m</sub> to a statistically significant degree are activators and potentially transport substrates of UCP1. Though why medica-16, 6-phenyl hexanoic acid and trimesic acid did not appear to be transported is not clear. These compounds may have caused a decrease in T<sub>m</sub> of UCP1 for other reasons, e.g. non-specific denaturation. Hence, not all compounds causing a drop in UCP1 T<sub>m</sub> are activators of UCP1.

In addition to the molecules that destabilised UCP1, the molecules that increased the T<sub>m</sub> were tested in proton transport assays (figure 3.8). Because inhibitors have been shown to increase the T<sub>m</sub> (GDP for UCP1, CATR for AAC), all the molecules that induced significant positive changes of the T<sub>m</sub> were tested not only on their own to see if any induced proton conductance, but also in the presence of a potent activator, oleic acid, to determine if they were inhibitors similarly to purine nucleotides.

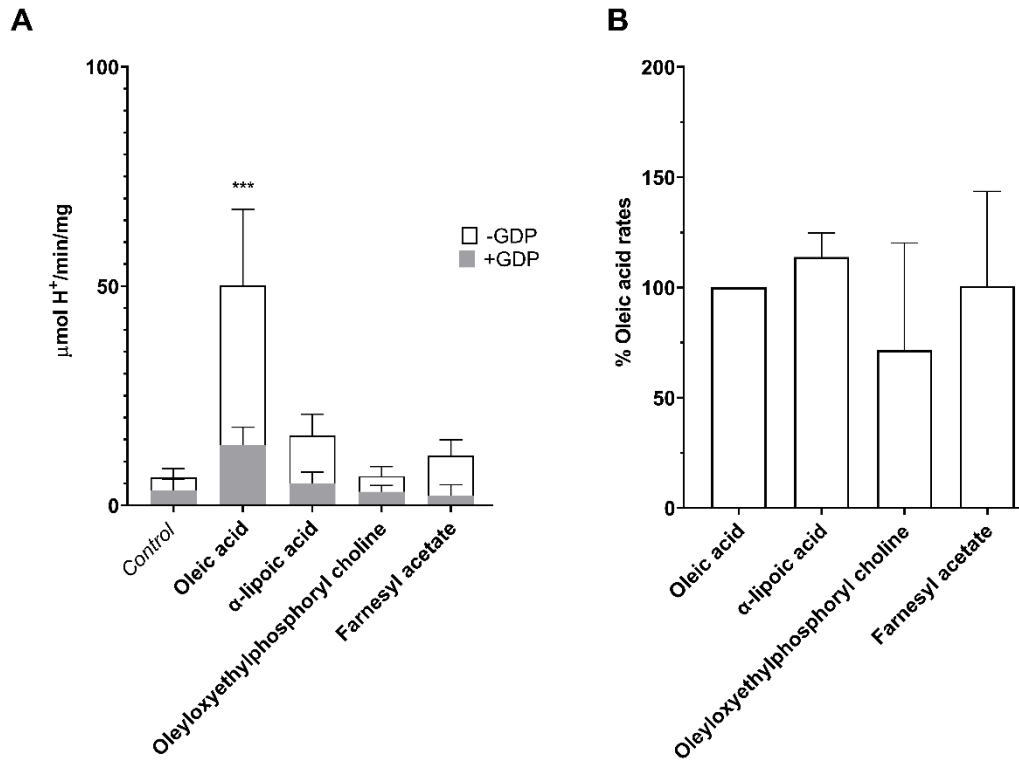


**Figure 3.8. Ligands increasing the melting temperature are non-inhibitors in flux assays. Panel A.** Proton transport assay +/-GDP (1 mM) of molecules increasing Tm (100 μM). **Panel B.** Proton transport assays with 100 μM ligands and 100 μM oleic acid, rates expressed as % oleic acid rates. Values in both panels expressed as averages of three to six independent experiments ±SD, statistical analysis performed by one-way ANOVA (\*p<0.05, \*\*p<0.02, \*\*\*p<0.001). Statistical analysis of data from panel B found no significant differences.

Flux assays showed that the none of the molecules increasing the Tm of UCP1 was an activator of proton transport (panel A, figure 3.8). Equally, at least at the concentration used in the assays of 100 μM, none of the molecules inhibited the activated rates with 100 μM oleic acid (panel B, figure 3.8). Though not exhaustive, these data show that, of the UCP1 ligands identified, activators are only found among those compounds that significantly decrease the Tm of UCP1.

### 3.3.4. Ibuprofen activates UCP1-dependent proton transport

The protein thermostability screen reported for ibuprofen a statistically significant change in Tm ( $\Delta T_m$  of  $-4.9 \pm 0.1$  °C). Proton transport assays with UCP1 reconstituted in liposomes then confirmed that ibuprofen is an activator of proton transport (see figure 3.7 panel A).

Ibuprofen was subjected to a more in-depth analysis, because of its relevance as a widely used commercial drug. Ibuprofen belongs to the group of Non-Steroidal Anti-Inflammatory Drugs (NSAIDs), and is commonly used as an analgesic, and antipyretic. The compound acts by inhibiting cyclooxygenase enzymes (COX2 in particular), similarly to aspirin and paracetamol [238]. Ibuprofen is commonly produced as a racemic mixture of *R* and *S* enantiomers, where the *S* version is the more active as an inflammation inhibitor. Once consumed ibuprofen is rapidly absorbed; the metabolism of ibuprofen is mainly due to cytochrome P450s [239, 240]. There are four main metabolites: 1-hydroxyibuprofen, 2-hydroxyibuprofen, 3-hydroxyibuprofen and carboxyibuprofen [241]. These metabolites were tested to see if they, like ibuprofen, could activate UCP1 proton transport (figure 3.9).

Of the variants, only the 2 hydroxylated form appeared to show slightly higher rates, however, none of the metabolites showed rates significantly different to the non-activated control. Hence, only the parent ibuprofen is an activator of UCP1. Independent laboratory tests with ibuprofen in a cell environment using HEK293 cells transfected with mouse UCP1 [242], confirmed that ibuprofen induced a UCP1-dependent increase in oxygen consumption, consistent with increased uncoupling, in a dose dependent manner (personal communication, Dr Susanne Keipert and Dr Martin Jastroch, University of Stockholm). Notably, the experiment was also repeated in cultured brown adipocytes, though no increase in uncoupling was observed.

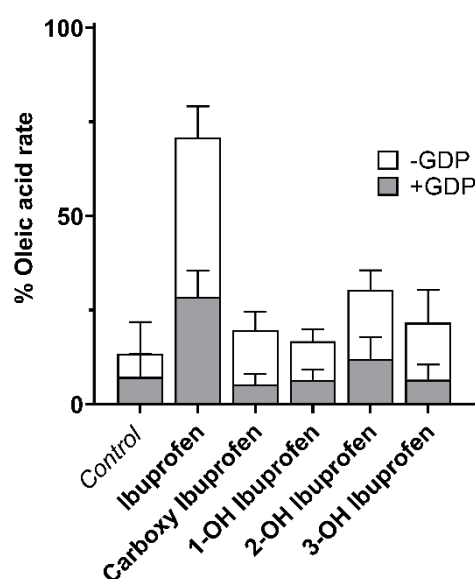


**Figure 3.9 Ibuprofen metabolites do not induce proton transport.** Proton transport assays with 100  $\mu\text{M}$  ibuprofen or ibuprofen metabolites. Rates shown as normalized % of activated rates (+oleic acid). Values expressed as averages of three independent experiments  $\pm$ SD. Statistical analysis performed by one-way ANOVA revealed no significant differences. Note, the ibuprofen data do not belong to the same experimental set and are taken from the data shown in figure 3.7 and transformed in % oleic acid rates to provide a comparison with the ibuprofen metabolite rates. Hence, ibuprofen was not included in the statistical analysis.

### 3.3.5 Oleoyl-CoA and UCP1

Acyl-CoA molecules are important for fatty acid catabolism and are produced in the cytosol in the first stages of shuttling fatty acid acyl groups into mitochondria, via the carnitine shuttle, for  $\beta$  oxidation [243]. In protein thermostability screen acyl-CoAs were shown to decrease the melting temperature. Initial measurement of palmitoyl-CoA had a  $\Delta T_m$  of  $-15.3 \pm 7.9$   $^{\circ}\text{C}$ , oleoyl-CoA of  $-7.4 \pm 1.8$   $^{\circ}\text{C}$ , and the short chain acetyl-CoA a  $\Delta T_m$  of  $-0.1 \pm 1.0$   $^{\circ}\text{C}$ , whilst CoA was also included in the screen but because of the exposed thiol it reacted directly with the CPM dye, producing a fluorescent signal outside the detection range, which could not be measured.

Because a destabilisation of UCP1 in protein thermostability assays is indicative of a potential transport substrate or activator of UCP1, the UCP1-oleoyl CoA interaction was selected for further investigation. Figure 3.10 A shows the  $T_m$  of native ovine UCP1 in the presence of 0 to 100  $\mu\text{M}$  of oleoyl CoA. Low micromolar concentrations of oleyl CoA caused an initial drop in  $T_m$  of  $\sim 5$   $^{\circ}\text{C}$ , similar to fatty acids. However, with increasing concentrations a pseudo-plateau occurred, where  $T_m$  values gradually increased, trending back toward a  $\Delta T_m$  of 0  $^{\circ}\text{C}$ . This effect is not unprecedented, as seen for the ADP/ATP carrier, where ADP transport substrate has a destabilising effect at low micromolar concentrations [169] but a stabilising one at higher concentrations in separate studies [216]. As can be seen in figure 3.10 panel B, when tested at double the previous maximum concentration, 200  $\mu\text{M}$ , oleoyl-CoA produced a positive shift in UCP1 stability. These results indicate that oleoyl-CoA is a specific ligand and could potentially be a physiological regulator of UCP1. Hence, the effect of oleoyl-CoA on GDP inhibition of UCP1 was tested. Figure 3.10 panel B shows the effects of the competition between 1 mM GDP

and increasing concentrations of oleoyl-CoA, where GDP was added first to the assay followed by oleoyl-CoA.

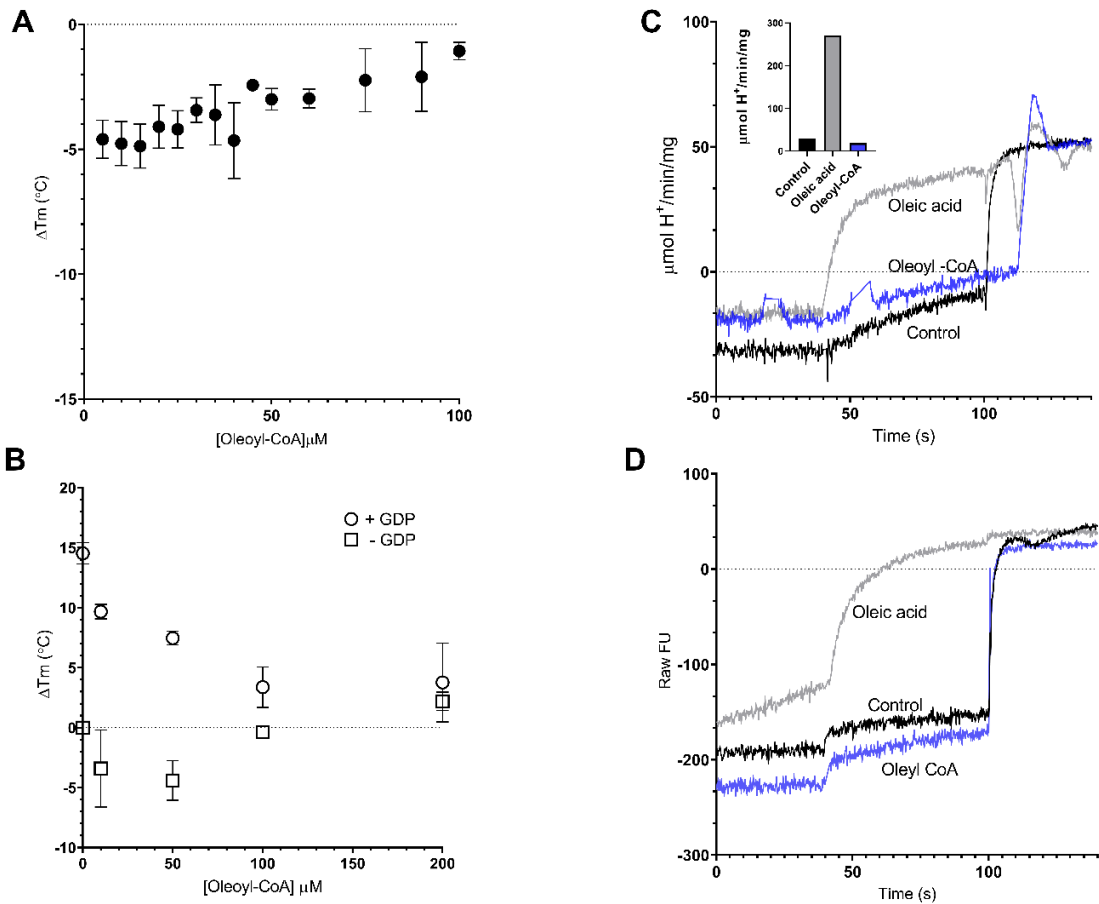


**Figure 3.10 Oleoyl CoA ligand interactions with UCP1. Panel A.**  $\Delta T_m$  trends from a titre of Oleoyl-CoA (0-100  $\mu\text{M}$ ) with native ovine UCP1. **Panel B.**  $\Delta T_m$  trends in the presence of oleoyl-CoA and 1 mM GDP (separate experiment, different from the experiment in panel A). Increasing concentrations of oleoyl-CoA reduce the positive  $\Delta T_m$  from GDP addition. **Panel C.** Proton transport flux assay with no addition (black) + oleic acid (grey) and + oleoyl CoA 100  $\mu\text{M}$  (blue) traces and relative rates,  $n=1$ . **Panel D.** Anion transport flux assay with 100  $\mu\text{M}$  oleoyl-CoA, raw fluorescence traces,  $n=1$ . Values in panels A and B are expressed as averages of three to four independent experiments  $\pm$ SD.

Strikingly, increasing concentrations of oleoyl-CoA diminished the strong stabilization effect of 1 mM GDP, bringing the  $\Delta T_m$  from  $\sim 15$  °C to  $\sim 4$  °C at 200  $\mu\text{M}$ , which correlated to  $\Delta T_m$  that occurred in the presence of oleoyl-CoA alone and complete absence of GDP. This result seemingly indicates competition between the two molecules, where low micromolar concentrations of oleoyl CoA can potently

displace GDP. The effect of oleoyl-CoA on UCP1 was also tested in one-off experiments with proton and anion transport assays. Panel C of figure 3.10 shows that the addition of oleoyl-CoA alone to UCP1 produced a rate much lower than the maximum activated rate from oleic acid, comparable to the no addition control rates, therefore oleoyl-CoA was unlikely to be an activator of proton leak. Panel D of figure 3.10 shows that anion transport rates (uncalibrated) were not induced by oleoyl CoA alone above no addition controls, suggesting oleoyl-CoA anions are not uniport transport substrates of UCP1. In conclusion, the data indicate that although oleoyl-CoA binds to UCP1 it is not transported by the protein but can potentially compete with GDP for binding.

### **3.4 Discussion**

The results presented in this chapter show that the thermostability assay is an efficient instrument for screening compounds for novel native UCP1 ligands and substrates. This method confirms its suitability to the study of membrane proteins and mitochondrial carriers, proving that shifts in protein stability can help distinguish molecules with potential to bind and activate native UCP1 from inhibitors and non-binders, when combined with the use of proton flux assays with liposomes containing reconstituted native UCP1. By monitoring changes in the thermostability of the carrier in relation to different activators and inhibitors, an indirect measurement of the folding state of the protein is also obtained, providing information on ligand binding as well as a quality control of the sample [169].

#### **3.4.1 Fatty acids as transport substrates of UCP1**

Ligand binding can be detected by a change in the melting temperature of the protein. Native UCP1 is destabilised in the presence of fatty acids, however the assay is run at physiological pH, at which fatty acids - particularly medium chain ones such as lauric acid - exhibit detergent behaviour that can damage UCP1 integrity.

An observed decrease of the  $T_m$  could thus in principle be caused either by substrate binding or protein denaturation. These possibilities were resolved by moving away from single point measurements and instead testing at variable concentrations, to show trends consistent with the specific binding of fatty acids,

distinct from more general detergent denaturation effects. The titres revealed a plateau in the drop in  $T_m$  indicative of the saturation of a specific binding event that occurred with known UCP1 activators, retinoids, but importantly matched the profile observed for confirmed substrates of UCP1, alkyl sulphonates. Thus, the results of this chapter support the mechanism models in which UCP1 activators act as transport substrates of the carrier and are transported across the membrane, consistent with the cycling and shuttling models over other proposed mechanisms (see [244] for a review of cycling model, [123] for a review of shuttling model, and section 1.3.2 of chapter 1 as well as [111] for a review of all UCP1 mechanism models).

### **3.4.2 Novel activators of UCP1**

By testing selected compounds in screens, novel activators were identified. It was also noted that activators are found exclusively among the ligands that cause a significant decrease in native UCP1 stability, confirming the link between decreases in stability and substrate binding, as only substrates can also be activators.

Five activators were identified: TUG-891, ibuprofen, the fatty acid tetradecylthioacetic acid (TTA), and two other fatty acid - like molecules, bromododecanoic acid, and 4-heptylbenzoic acid, which had previously already been indicated as UCP1 activators [235].

TUG-891, in particular, is a synthetic free fatty acid receptor 4 (GPR120) agonist and has been recently claimed to increase oxygen consumption and activate brown adipocytes by both GPR120 dependent routes and direct action on UCP1 [237]. Ibuprofen is widely used as an over-the-counter drug for the treatment of mild acute pain (fever, headache, dental pains). The observation that ibuprofen is a direct activator of UCP1 is thus particularly relevant for the development of future therapies focused on the direct activation of the uncoupling protein rather than adrenergic stimulation of the whole tissue. Interestingly, ibuprofen activated proton transport but none of its metabolites did.

### **3.4.3 Low structural specificity of UCP1 activators**

Symmetry analysis of the mitochondrial carrier family to which UCP1 belongs, and the crystal structures of the ADP/ATP carrier, its best characterized member, [135, 136] have shown the central importance of the conserved three-fold pseudo symmetry of carriers for their mechanism [133, 137, 138, 144]. Deviations from the

symmetry have been highlighted in the substrate binding sites, where the different carriers have adapted to the specific non-symmetrical nature of their substrate molecule(s). A high degree of structural variety was observed in the molecules identified as activators of native UCP1. Native UCP1 activators are relatively hydrophobic: the partition coefficient ( $\log P$ ) of the molecules identified ranged from 3 to 7. This is consistent with UCP1 activators partitioning into a hydrophobic environment before coming into contact with the protein. However, a molecule in order to be an activator of proton transport needed to have a protonatable group with the appropriate  $pK_a$ . This was a  $pK_a > 4$ . Many of the most potent activators have a  $pK_a$  around 4.5, including oleic acid and lauric acid. Further structural criteria also need to be met. However, comparison of the structures of activators shows few clear structural constraints. The low structural specificity required by native UCP1 in selecting activators, as well as the identification of ibuprofen as an activator, highlights the wide range of molecules, including commercially available drugs and drug-like compounds, worth exploring to find additional novel ligands and activators able to target the protein.

### **3.4. UCP1 and acyl-CoAs**

The thermostability experiments successfully identified acyl-CoA molecules as ligands of native UCP1. The effect of long-chain acyl-CoAs on UCP1 has been tested, but with mixed findings [246-251]. Palmitoyl-CoA was reported to inhibit the ADP/ATP carrier in isolated rat liver mitochondria [252]. Cannon et al. proposed palmitoyl-CoA as a regulator of nucleotide binding to brown adipose tissue as far back as the 1970's [253]. Woldegiorgis and collaborators showed that N-(3-iodo-4-azidophenyl propionamide) cysteinyl-5-(Z-thiopyridyl cysteine) CoA (ACTCoA) in the presence of CATR labels only UCP1, and in the presence of GDP only AAC, whilst without any inhibitors present both proteins are labelled. However, in the presence of 12.5  $\mu$ M palmitoyl-CoA neither is labelled. Palmitic acid in contrast does not have the same effect [250]. These results pointed at a competition between acyl-CoA and nucleotides in binding UCP1. In contrast, Jezek et al. found no effect of palmitoyl-CoA on GDP inhibition of proton transport with isolated BAT mitochondria in swelling studies [250]. Protein thermostability measurements at variable acyl-CoA concentrations in conjunction with GDP showed that oleoyl-CoA is a ligand competing with GDP for binding, whilst preliminary flux assays hinted that it is not

transported by UCP1. If long-chain acyl CoAs were competing with GDP not only *in vitro* but also *in vivo*, it might help explain the role of GDP and purine nucleotides in the regulation of UCP1 activity. GDP and purine nucleotides show high affinity with UCP1 in *in vitro* systems, with  $K_d$  values for purine nucleotide binding in the low micromolar to nanomolar range [168]. Neither isolated protein nor mitochondrial  $K_d$  values are high enough to explain why the protein can be active in the presence of millimolar concentrations of ADP/ATP, acyl-CoA could now explain this issue [48, 49, 168, 254]. 10  $\mu$ M of oleoyl-CoA were sufficient to start showing competition with GDP with a concentration 2 orders of magnitude greater (1 mM), providing a clue that GDP binding to UCP1 may not be so potent and that acyl-CoA could contribute to removing it.



## **4. Characterisation of the human, mouse, and ovine UCP1 isoforms**

### **4.1 Introduction**

A number of isoforms of UCP1 have been studied in research: most commonly rat and mouse, as well as hamster in the earlier experiments with isolated brown adipose tissue mitochondria [246]. More recently, the human UCP1 isoform has attracted interest for human biomedical studies, after the detection of UCP1 in healthy adult humans [20, 22, 255].

Mouse UCP1 (MmUCP1) is used in HEK cell expression systems (see for example [5, 242]) or studies with isolated mitochondria (e.g. [213]). It also has the advantage of being extremely similar to rat and hamster UCP1 (96.7 % sequence identity to rat UCP1, 92.8 % to hamster UCP1) and mouse brown adipose tissue (BAT) is a good model for human BAT and UCP1 function [256], despite differences in beige adipose cells [29]. The ovine UCP1 isoform (OaUCP1) was chosen as a control for the other two recombinant isoforms. Ovine UCP1 is the native isoform of UCP1 used for the experiments in chapter 1 [157]. Moreover, human UCP1 (HsUCP1) has been proposed in a recent paper to have unique functional properties, differing from mouse, rat, and other isoforms of UCP1 [213]. According to respirometry measurements in isolated yeast mitochondria, HsUCP1 did not exhibit basal proton transport activity (i.e., in the absence of fatty acids), in contrast with mouse and rat UCP1. However, all isoforms showed a similar response to the addition of fatty acids, increasing respiration, and were inhibited by GDP.

This chapter provides a direct comparison of the biochemical functions of three widely researched UCP1 isoforms: MmUCP1, OaUCP1, and HsUCP1. These isoforms were purified, and the functional characteristics were analysed by thermostability analysis and proton transport assay to clarify any isoform specific differences.

## 4.2 Aims

1. To characterise the basic functional properties of UCP1 isoforms that are currently most used in research (HsUCP1 and MmUCP1, as well as OaUCP1 which is specific to the Crichton lab).
2. To determine if HsUCP1 differs functionally from MmUCP1 and OaUCP1 isoforms, as claimed in a recent paper [213] .

## 4.3 Results

### 4.3.1 UCP1 isoforms expression in yeast

The human (HsUCP1), mouse (MmUCP1), and ovine (OaUCP1) isoforms were expressed in yeast cells (w303 strain). Typical yields of cells were ~100-150 g wet weight from 6 L of culture, which provided 400-800 mg of mitochondrial membranes following isolation. The yeast expressing human UCP1 provided the largest amount of mitochondrial membranes despite the lowest amount of material obtained from the 6 L cultures.

### 4.3.2 UCP1 isoforms purification

Each of the UCP1 isoforms were purified using hydroxyapatite (HA) and TPS chromatographies based on methods described in [157] (see Methods, section 2.5). Figure 4.1 shows the Coomassie stained gels and UCP1 and AAC by western analysis of samples at each stage of the purification procedure, to give a profile of the purification. Overall, it can be seen that each of the isoforms were successfully expressed and presented similar purification profiles, consistent with those of native UCP1 (an example is shown in appendix figure A5). Following solubilisation in 3 % Triton X-100 and passage through an hydroxyapatite column (HA-flowthrough), two bands were visible on the gels around the 30 kDa mark, the approximate size of mitochondrial carriers, and where UCP1 is expected to be seen. Successive immobilisation and purification by covalent chromatography with thiol reactive TPS resin (TPS elution 1 and elution 2 samples) retained both protein bands. Native UCP1 purifications showed one very prominent band at the 30 kDa mark in the TPS elution samples, and a very faint second higher band, consistent with the second

band being a contaminant or a UCP1 truncation in the yeast recombinant system. A 5 µg sample 'overload' was also added to each gel to help detect contaminants. Here, in addition to the two bands at ~ 30 kDa, all three isoforms showed a faint band at ~ 60 kDa (more evident in the human sample), which likely represents UCP1 dimers (see appendix figure A6 showing MmUCP1 anti-UCP1 blot with a dimer signal) [151].

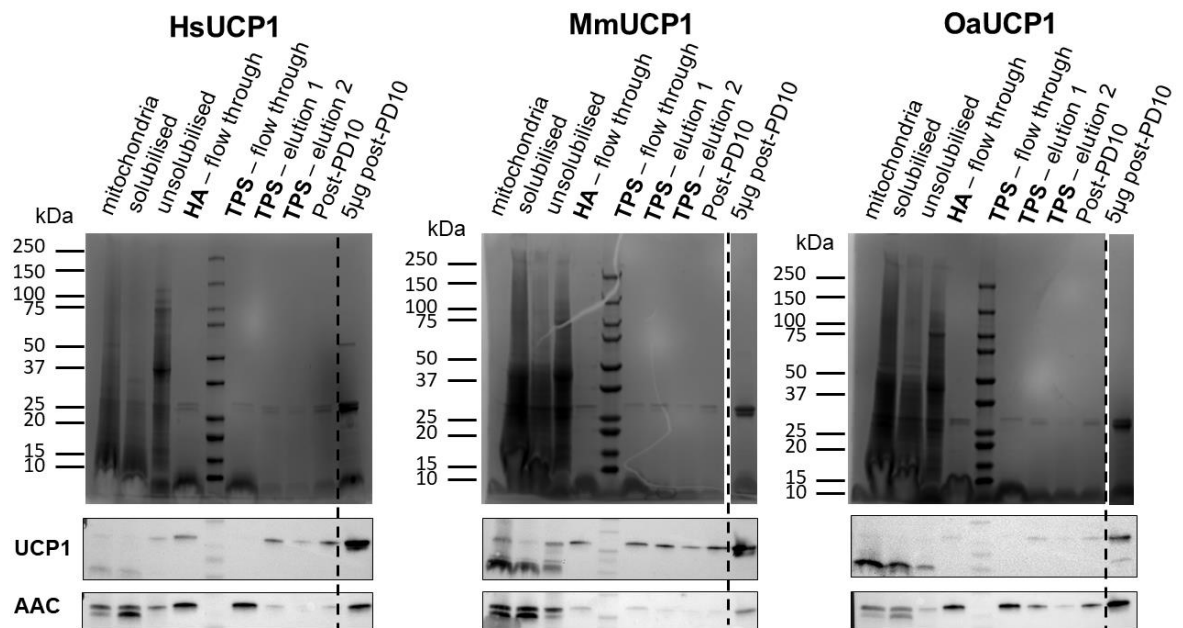


**Figure 4.1. Coomassie gels and western blots of purification profiles.** HA=Hydroxyapatite; TPS=Thiopropyl Sepharose; PD10=desalting column. **Upper panel.** Gels profiles stained with coomassie dye (Imperial Stain). Last lane of MmUCP1 and OaUCP1 gels belongs to the same gel but is edited to remove empty lanes in between for better comparison. **Lower panels.** Western blots of the same purification profiles with anti-UCP1 and anti-AAC antibodies, tracking the proteins through the purification.

Duplicate SDS gels of the purification profile were used for anti-UCP1 and anti-AAC western blot analysis, to ensure that UCP1 was present in the final samples, as well as to detect the presence of the ADP/ATP carrier, which is the most abundant carrier in mitochondria and a potential contaminant [153]. Western blots confirmed the presence of UCP1 in the final sample, with no indication of losses relative to the UCP1 present in the solubilised fraction, except for MmUCP1 specifically, where some protein seem lost in the TPS flowthrough fraction. Western blots highlighted the presence of AAC, which was detected in the final sample of all three isoforms, however, unlike UCP1, a large proportion of AAC was lost during the purification,

particularly in the TPS flowthrough fractions, resulting in an improved ratio of UCP1 to AAC in the final sample. In conclusion, the procedure obtained purified UCP1 alongside perhaps one unknown contaminant, which potentially accounts for up to ~ 50% of final purified sample. However, in the 5 µg load lanes, two bands can be seen in the UCP1 westerns. Hence, it is still likely both bands are UCP1.

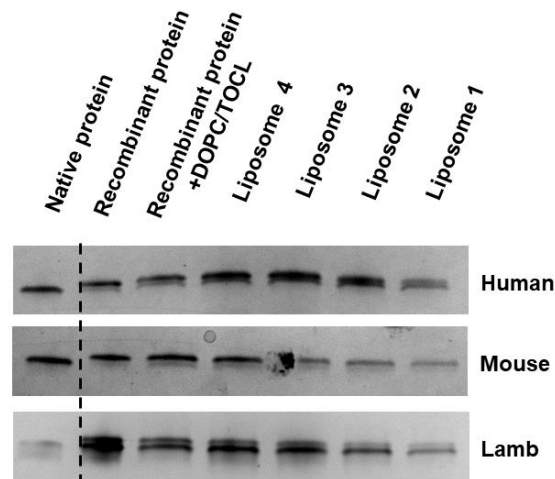


**Figure 4.2. Silver stain gels of UCP1 liposomes.** Silver stain gel of recombinant MmUCP1, HsUCP1 and OaUCP1 preparations following purification ( $\pm$  DOPC/TOCL lipids) and following reconstitution into liposomes (four separate samples were tested, as shown). The recombinant protein standard is supposed to be the equivalent of 100 % reconstitution for each gel, a native ovine UCP1 sample was also included for comparison (left lane). DOPC=1,2-Dioleoyl-sn-glycero-3-phosphocholine; TOCL=tetraoleoylcardiolipin.

With the detection of some possible contaminant protein, the downstream use of reconstitution of UCP1 into liposomes was explored as a potential purification process. In order to detect the low amounts of protein in liposome samples, SDS-gels were run, and the protein was detected by silver staining methods, rather than coomassie blue, to exploit its higher sensitivity. Figure 4.2 shows the resulting silver-stained gels. As expected, the control lane containing native UCP1 showed only one band (this is less defined in the OaUCP1 gel, but the native sample used was the same as for MmUCP1 and HsUCP1 gels). For all isoforms, the recombinant protein lanes showed double bands, with or without liposome reconstitution, matching those seen in the purification profiles (cf. figure 4.1), suggesting reconstitution is not a purifying step. Further attempts to identify this possible contaminant and distinguish between the two main bands appearing on the

purification profile gels were made by mass spectrometry. However, only UCP1 was identified in either band cut out from gels at each location. This result can be interpreted as both bands being UCP1, where the lower band is perhaps a truncated version of the carrier (figure 4.1).

The purification yielded ~ 200 to 450 µg of recombinant UCP1 per 100 mg of mitochondrial membranes, a much lower amount than the native protein, which averages around 1 mg of yield per 100 mg of membranes. Recombinant HsUCP1 had the highest yield ratio of protein per mg of membrane obtained.

### 4.3.3 UCP1 isoforms thermostability analysis

The folding and integrity of the purified isoforms was assessed by protein thermostability assay (see chapter 3 and Methods section for details). All isoforms showed a sigmoidal profile both with and without GDP that is indicative of a folded protein (figure 4.3). Moreover, the three isoforms presented similar melting temperatures,  $58.3 \pm 0.9$  °C HsUCP1,  $59.0 \pm 0.9$  °C MmUCP1, and  $61.3 \pm 1.0$  °C OaUCP1 (figure 4.4). HsUCP1 gave a lower signal amplitude than the other isoforms. MmUCP1 and OaUCP1 presented similar initial backgrounds, around 30 arbitrary fluorescent units.

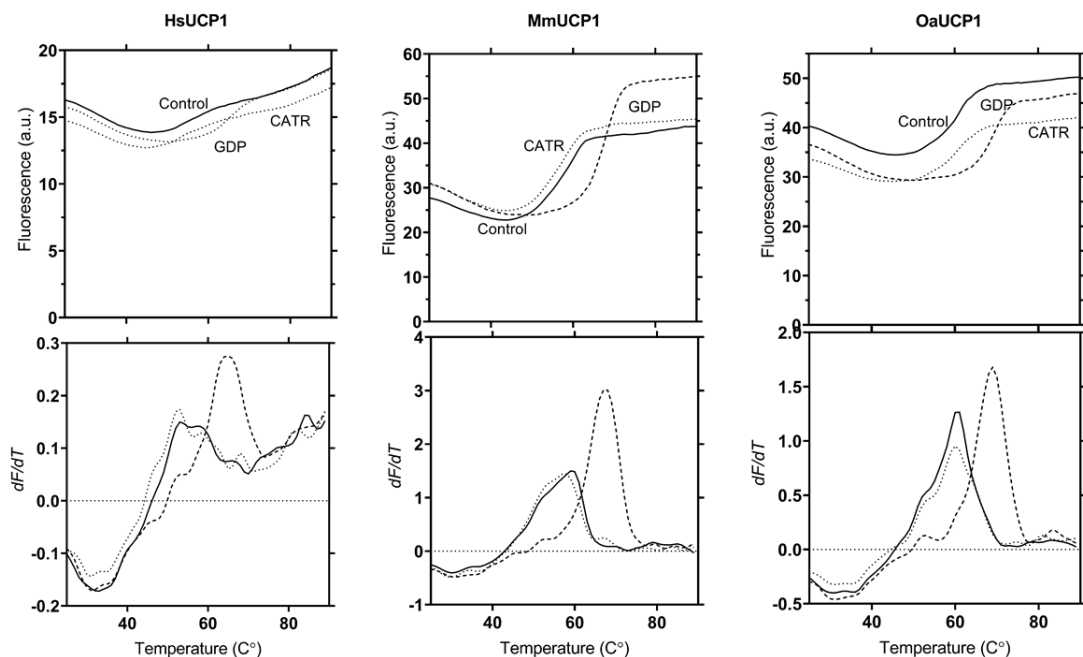


**Figure 4.3. The thermostability of recombinant UCP1 isoforms.** Assays were performed at pH 7.5 in 0.1 % 12MNG, 2 µg of protein per sample. **Upper panels** raw fluorescence traces of recombinant UCP1 with 40 µM CATR (dots) and 1 mM GDP (dashes). **Bottom**

panels corresponding derivative of the profiles in the upper panels, the peaks of which indicate the protein 'melt temperature' ( $T_m$ ).

Figure 4.4 also reports the melting temperatures of the recombinant UCP1 isoforms associated with GDP or CATR. All three protein unfolding profiles were responsive to GDP addition, which increased the stability of the proteins. GDP addition significantly increased the melting temperature for all recombinant isoforms, an important sign that the protein was folded and responsive to ligand binding: HsUCP1  $+7.8 \pm 2.4$  °C, MmUCP1  $+10.0 \pm 2.9$  °C, OaUCP1  $+10.9 \pm 3.6$  °C.

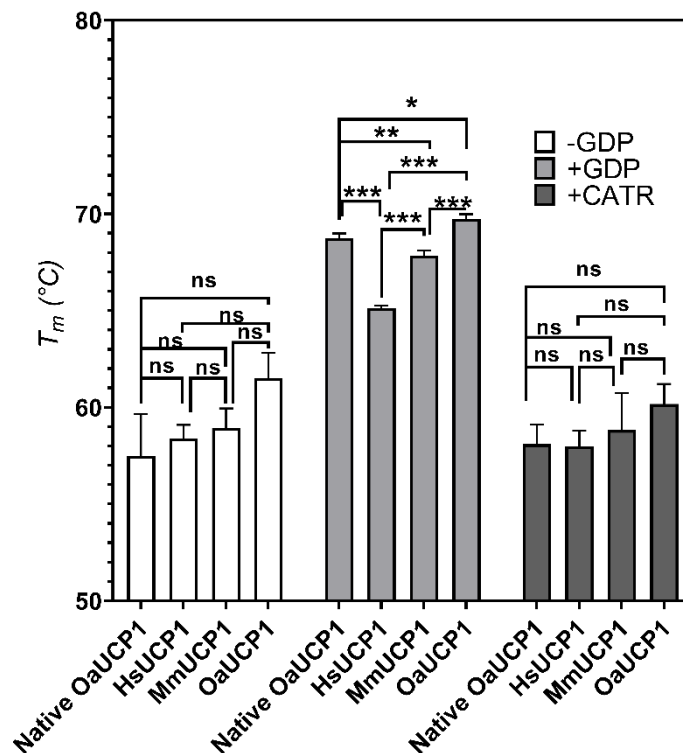


**Figure 4.4.  $T_m$  values of the recombinant UCP1s compared to native UCP1 upon GDP or CATR addition.** Assays performed at pH 7.5 in 0.1 % 12MNG. Values are averages  $\pm$ SD of three independent repeats, where a statistical analysis was performed by one-way ANOVA (ns = not significant, \* $p < 0.05$ , \*\* $p < 0.02$ , \*\*\* $p < 0.001$ ). There are no statistically significant differences between -GDP and +CATR groups, while +GDP rates are all significantly higher than the other two groups. There are also no significant differences within the -GDP and +CATR groups, while within the +GDP group each protein isoform is significantly different from the others.

There were no significant differences within the -GDP (no addition) group, whilst within the +GDP group native ovine UCP1 and recombinant protein isoforms had a +GDP T<sub>m</sub> significantly different from the others. HsUCP1 presented a lower T<sub>m</sub> value in the presence of GDP than both native ovine UCP1 and the other recombinant proteins, while also having a comparable no addition T<sub>m</sub>, showing to be less responsive to GDP addition.

The effect of the ADP/ATP carrier (AAC) inhibitor carboxyatractyloside (CATR) was also tested on the preparations, since western blots had shown the presence of AAC contamination in the final sample post-purification. The inhibitor is known to strongly increase the melting temperature of purified AAC in the thermostability tests (+ ~20 °C in 1 % DDM, pH 7.4) [169]. Addition of CATR did not produce appreciable changes in the protein unfolding profiles and melt temperatures compared to the no addition (-GDP) group, indicating that AAC was not present in a functional form in the final sample in sufficient quantities to influence the assay. In summary, all three recombinant isoforms could be purified in a folded state capable of binding GDP, where they represent the dominant functional species in each preparation.

#### **4.3.4 UCP1 isoforms reconstitution in proteoliposomes**

HsUCP1, MmUCP1 and OaUCP1 proteins were reconstituted into liposomes, similarly to native UCP1, where both protein species of ~30 kDa in the sample were reconstituted, as shown by silver-stained gels of figure 4.2.

The amount of UCP1 reconstituted into each liposome sample was determined by UCP1 quantification by Western blot analysis, where UCP1 signals were calibrated to UCP1 protein standards of known concentration (figure 4.5). Densitometry analysis of signal intensity allowed standard curves to be constructed and, through interpolation, the UCP1 protein present in the liposome samples was estimated. Panel B of figure 4.5 shows that HsUCP1 liposomes reconstituted on average 50 % of used UCP1, while MmUCP1 was reconstituted at 58.5 % and OaUCP1 at 50.5 %.

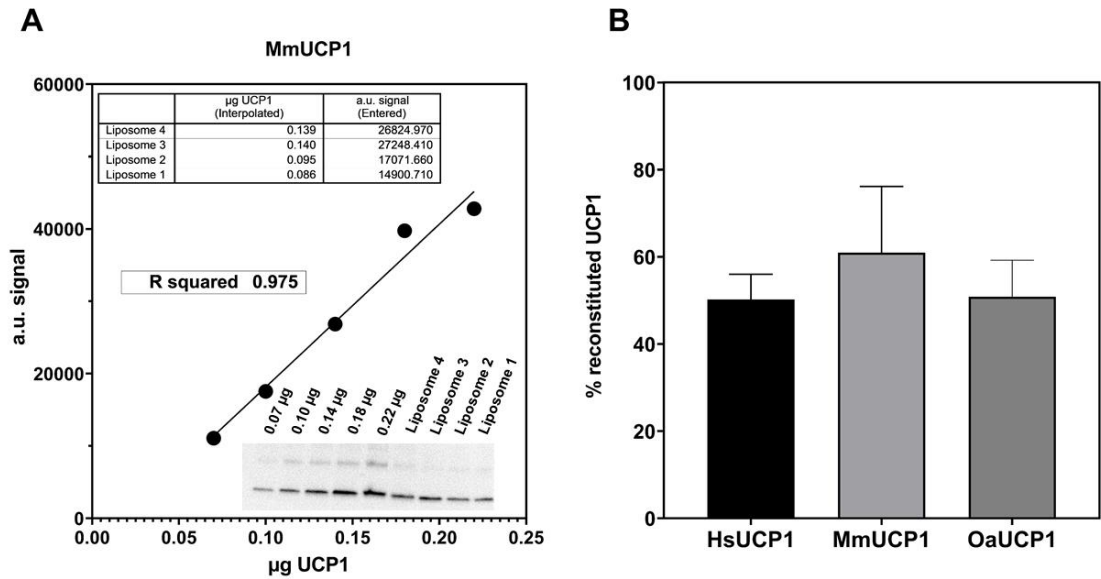


**Figure 4.5. Determination of UCP1 reconstituted in liposomes. Panel A.** Standard curve of increasing amounts of UCP1 used to determine the quantity of MmUCP1 reconstituted in each of the repeats by interpolation (ovine and human blots are shown in appendix figure A7). **Panel B.** % of UCP1 reconstituted in liposome for each isoform. Values expressed as averages  $\pm$ SD of four independent repeats.

In proton flux assays following reconstitution into liposomes, all three isoforms responded to oleic acid addition and catalysed proton transport that were sensitive to GDP (figure 4.6 A). The basal (“control”) rates did not present statistically significant differences among isoforms ( $p > 0.99$  HsUCP1 vs MmUCP1,  $p > 0.99$  HsUCP1 vs. OaUCP1, and  $p = 0.98$  MmUCP1 vs OaUCP1; significance tested by one-way ANOVA). However, the activated proton transport rates of the three isoforms were different. MmUCP1 had higher activated (+oleic acid) rates than the other two isoforms ( $p < 0.001$  vs HsUCP1 and OaUCP1, significance tested by one-way ANOVA). While OaUCP1 activated rates were lower than those of HsUCP1, despite having similar amounts of protein reconstituted, the difference is not statistically significant ( $p = 0.83$ ).

Activated rates of all three isoforms varied between experiments, giving a large standard deviation proportional to the size of the rate. Each rate value was also expressed relative to the fully activated rate obtained with the same sample to reduce the noise in the data (figure 4.6 panels B, C, and D). The basal proton rates (“control”), when expressed in such a way, appeared similar for the three isoforms,

amounting to between 15 to 20 % of the activated rates, and did not show a statistically significant difference between isoforms ( $p > 0.99$  HsUCP1 vs MmUCP1,  $p > 0.99$  HsUCP1 vs. OaUCP1, and  $p > 0.99$  MmUCP1 vs OaUCP1).

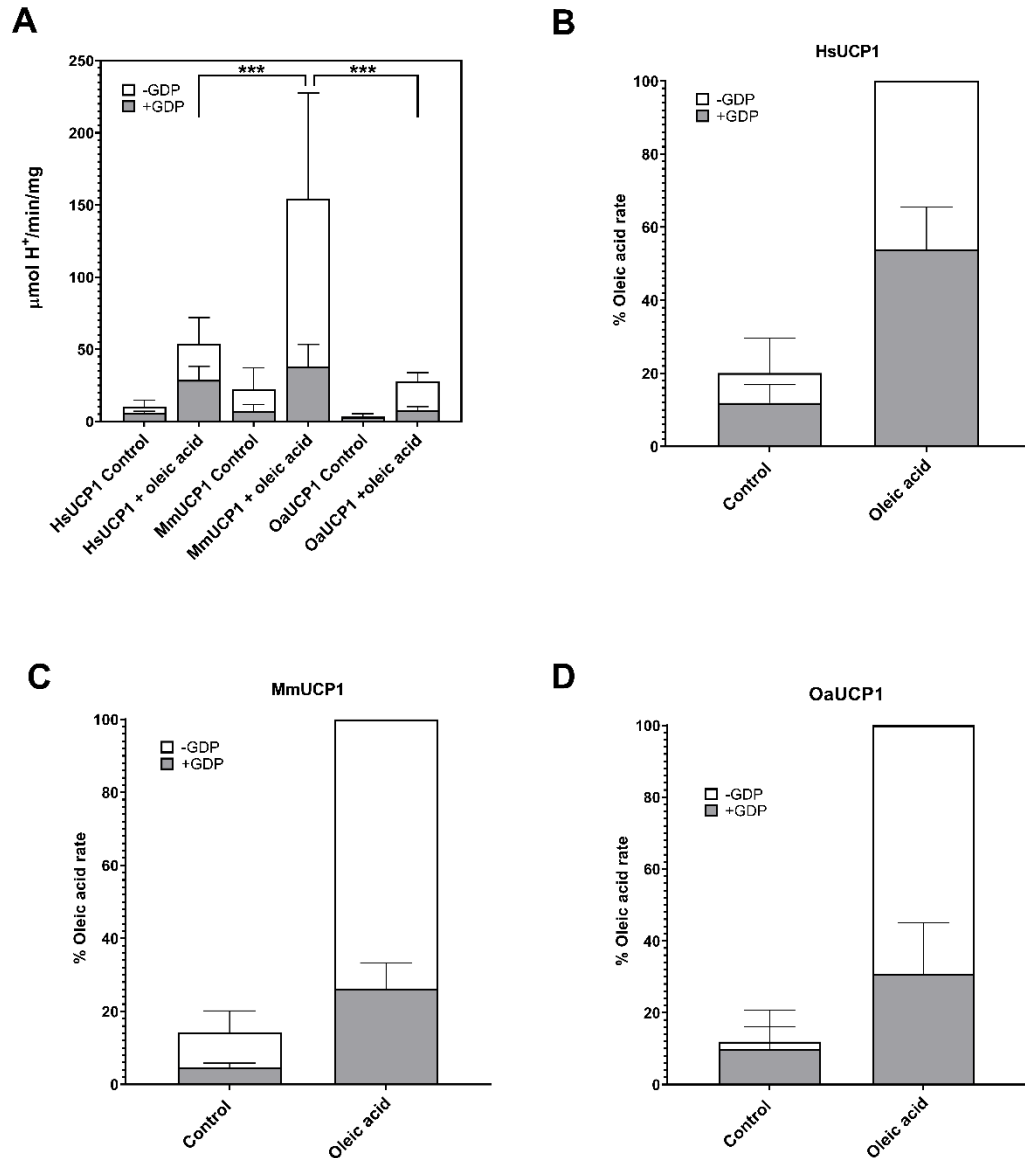


**Figure 4.6. Flux assays with recombinant UCP1 isoforms. Panel A.** Proton transport rates +/- 1 mM GDP and +/- 100 μM oleic acid of UCP1 recombinant isoforms. All values are expressed as averages ±SD of four independent repeats, where significance was tested by one-way ANOVA (\* $p < 0.05$ , \*\* $p < 0.02$ , \*\*\* $p < 0.001$ ). **Panel B-D:** Proton transport rates for recombinant HsUCP1 (B), MmUCP1 (C) and OaUCP1 (D) normalized to the equivalent fully activated “+oleic acid” rate for each protein. All values are expressed as averages ±SD of four independent repeats.

The GDP sensitivity of the oleic acid-activated proton transport rates was similar for OaUCP1 and MmUCP1 isoforms, ~ 66 % - 70 % inhibition by 1 mM GDP of the fully activated rate (figure 4.6 D and C), a value in line with what seen in proton transport assays with the native protein (see chapter 3) and consistent with the values reported in the literature for this type of transport assay [113, 257]. In contrast, the HsUCP1 isoform showed a significantly lower ~50 % inhibition of the activated rates by GDP ( $p = 0.004$  vs MmUCP1 and  $p = 0.027$  vs OaUCP1, significance tested by one-way ANOVA). Taking into consideration that HsUCP1 also had a lower response to GDP addition in the thermostability shift assay (figure 4.4), consistent with less tight binding, HsUCP1 might be less responsive to GDP, compared to MmUCP1 and OaUCP1, at least at pH 7.5 at which the experiments were performed.

Rodriguez-Sanchez et al. have reported that human UCP1 differs from mouse UCP1 [213]. According to the authors' respiratory analysis of UCP1 isoforms in isolated yeast mitochondria, whilst MmUCP1 had GDP-sensitive basal proton transport activity (i.e., in the absence of added fatty acids), HsUCP1 did not. Whereas both isoforms behaved similarly in the presence of added fatty acids, increasing respiration to similar degrees in a GDP-sensitive manner. Having isolated both MmUCP1 and HsUCP1 it was attempted to analyse the basal (control) proton transport rates to investigate such difference.

Recombinant MmUCP1 and HsUCP1 and OaUCP1 all presented basal proton rates in the *in vitro* liposome system. All isoforms showed similar basal rates that are ~20 % of the maximal rates (Figure 4.6 B-D). Neither the basal rates shown in figure 4.6 A or the basal rates normalized to oleic acid rates on the day (figure 4.6 B-D) of the three isoforms were significantly inhibited by GDP. These results contrast with the result by Rodriguez-Sanchez et al. Within the signal to noise of the experiment a difference between MmUCP1 and HsUCP1 basal proton rates was not seen, as both isoforms were observed to have basal proton rates of about 15 to 20 % the activated rates but did not show significant GDP inhibition.

To remove free fatty acids from UCP1, recombinant UCP1 isoforms were pretreated with 40 mM m $\beta$ CD. It is possible therefore that the lower endogenous GDP-sensitive activity here reflects more efficient removal of contaminating fatty acids from the

samples. Hence, the endogenous activity reported by Rodriguez-Sanchez et al. [213] in isolated yeast mitochondria seems unlikely to relate to an inherent proton leak activity in MmUCP1 that is absent in HsUCP1, as claimed. Instead, it could maybe relate to differing concentrations of, and/or differing isoform sensitivities to, endogenous fatty acids present in the isolated yeast mitochondria that were not effectively removed.

## **4.4 Discussion**

In this chapter it was shown that three isoforms of UCP1, human (HsUCP1), mouse (MmUCP1), and ovine (OaUCP1), could be expressed in a yeast recombinant system and purified (by the same method as native UCP1) to a sufficient degree to be biochemically characterised. All isoforms were found to be folded and responsive to nucleotides in thermostability shift assays. In summary, MmUCP1, HsUCP1 and OaUCP1 isoforms could be reconstituted into liposomes, showed a positive response to the addition of fatty acids and nucleotides, and thus were active. MmUCP1 presented higher activated rates, while HsUCP1 and OaUCP1 both showed lower rates, non-significantly different from each other.

### **4.4.1 Isoform purification and behaviour in the thermostability shift assay**

Although all isoforms were successfully expressed and could be purified, a double band was seen in gels of the final purified sample, with both bands roughly at the 30 kDa mark that would be expected for UCP1 and mitochondrial carriers. Could one of the bands be UCP1 and the other a small UCP1 truncation? A second band seemed not to be present in the UCP1 western blot of the purification fraction, except for the high load 5 µg lanes where the signal looks to be made up of two bands. Mass spectrometry did not find any contaminant, the only match for the fragments obtained was either the trypsin used in the preparation of the samples or UCP1 itself. Moreover, the three isoforms showed profiles consistent with folded UCP1 in the thermostability shift assays, but also presented differences, HsUCP1 had a lower signal. The starting background, or 'plateau', of a thermostability profile (at lower temperatures before the protein has unfolded) depends on the number of exposed cysteines to which CPM is bound and on the total amount of protein in the assay. It is not clear why HsUCP1 has a lower signal in thermostability profiles. The isoform has the same number of cysteine residues as OaUCP1 and activity in

liposomes suggests there is equivalent proton leak activity compared to the recombinant OaUCP1 protein. Hence, the CPM adduct signal may not be low due to less UCP1 protein present but is instead dampened for another reason. HsUCP1 also showed a reduced  $T_m$  change upon GDP addition in thermostability shift assays. In the thermostability assay HsUCP1 had the lowest +GDP absolute  $T_m$ , despite having a -GDP  $T_m$  comparable to MmUCP1, and the smallest relative increase of melting temperature ( $\Delta T_m$ :  $+7.8 \pm 2.4$  °C). UCP1 is known to vary the strength of GDP binding depending on pH. At lower pH GDP binds more tightly. This change correlates with a change in melting temperature of the protein, which increases at lower pH in the presence of GDP ([169] see also appendix figure A2). Furthermore, in proton transport assays an equal amount of GDP was less effective in inhibiting the activated rates of HsUCP1 compared to MmUCP1 and OaUCP1. In flux assays 1 mM GDP inhibited MmUCP1 and OaUCP1 rates by about 70 %, while HsUCP1 showed only about 50 % inhibition.

#### **4.4.2 UCP1 isoforms basal proton transport rates**

A basal (also called endogenous) rate of proton transport was seen in all samples of recombinant protein, regardless of the isoform considered, and was not significantly different between isoforms, in contrast to that reported by Rodriguez-Sanchez et al. [213]. The endogenous proton transport rates in liposomes assays are likely to be caused by residual fatty acids coming from the protein purification, and possibly also limited lipid breakdown from the lipid mixture added to form the liposomes. To limit these rates, which lower the resolution of the transport assay, liposomes were pre-treated in methyl-beta-cyclodextrins ( $m\beta CD$ ), cyclic sugar molecules that are able to absorb free fatty acids [115, 258]. In the native ovine UCP1 samples, treated with lower amount of  $m\beta CD$  (20 mM), a more prominent basal rate was observed, compared to the recombinant isoforms which were treated with a higher amount (40 mM). However basal rates are still observed in all three isoforms. Doubling the concentration of cyclodextrins did not completely remove endogenous fatty acids, showing how challenging it is to obtain a fatty acid-free sample. Hence, it is possible that observations of Rodriguez-Sanchez et al. [213] were equally caused by a failure in exhausting the endogenous fatty acids in the mitochondrial samples with BSA. Differences in UCP1 isoforms expression could have also contributed, if for instance HsUCP1 was less expressed than mouse

UCP1; Stuart et al. have reported that UCP1 overexpression in yeast can lead to experimental artifacts [181].

## 5. Homology modelling and systematic analysis of key structural features of UCP1

### 5.1 Introduction

As mentioned in chapter 1, the structures of the ADP/ATP carrier (AAC) [134-136, 259] obtained in the last 16 years have provided a model for the conformation of a mitochondrial carrier in two states, with the central cavity opened to the cytoplasm in the c-state and, more recently, to the mitochondrial matrix in the m-state, revealing the core metabolite transport mechanism. UCP1 is part of the mitochondrial carrier family. Bioinformatic studies and recent biochemical characterisations (see also chapter 3) have highlighted that UCP1 shares key carrier structural features important for the carrier transport mechanism, at least in the c-state, as well as more similarity to other mitochondrial carriers than previously thought [133, 136, 137, 141-143, 157, 169]. To date, an experimental structure of the uncoupling protein 1 has not yet been obtained. However, the similar size and amino acid sequence overlap in relatedness to AAC makes homology modelling to obtain structural models of UCP1, now in two mechanistically-relevant carrier states, a potentially useful avenue to explore structure-function relations.

There is a wealth of site-specific mutagenesis and functional studies on UCP1 that, at the time of first publishing, did not have the benefit of any carrier structural information to contextualise the findings [47, 153, 155, 156, 158, 212, 260-262]. These studies were successful in identifying residues that, for instance, are important for nucleotide binding, such as R84, R183 and R277 [158, 263], the pH dependency of nucleotide binding, such as E191 [153], or for full proton transport activity, such as D28, H146 and H148 [262] (human UCP1 amino acid residue numbering). The lack of a basic structural context meant that in most cases the function of these residues in the protein could not be easily determined.

The c-state and recently resolved m-state of AAC, which underpin the transport mechanism, provide therefore a timely opportunity to both explore the UCP1 m-state and reanalyse past information from UCP1 literature in the context of the new structural framework that has emerged.

## 5.2 Aims

In this chapter homology models of the uncoupling protein in both c and m-state were generated, to better understand and characterise the presence and location of conserved structural features and amino acid residues within the protein, and to re-examine models and hypothesis that have been proposed in the past without the benefit of a structural context. The aims are:

1. To determine if UCP1 conserves structural features compatible with a conventional carrier transport mechanism cycling between c- and m-states.
2. To retrospectively reanalyse the wealth of historic UCP1 mutagenesis and functional information with the benefit of the c-state and the new m-state structural framework.

## 5.3 Results

### 5.3.1 Creating homology models

The relevant available structures in the Protein Data Bank (PDB) with the highest degree of homology with UCP1 were selected. UCP1 is related to AAC [104, 264], its sequence identity, obtained with a BLAST protein to protein sequence alignment, is of about 27-29 % with any of the AAC isoforms that have been structurally solved. UCP1 was homology modelled in two states, c and m, using MODELLER [224], in UCSF Chimera [225].

The model building process was initially explored and defined using ovine UCP1 (OaUCP1). 100 models were initially generated in MODELLER for each state using as a template the structure from the thermophilic fungus *Thermothelomyces thermophila* - TtAAC (6GCI) for the m-state [136] and either the structure from bovine AAC - BtAAC1 (1OKC) [134] alone or BtAAC1 in combination with yeast structures - ScAAC2 (4C9G/J) and ScAAC3 (4C9J) [135] for the c-state, giving a total of 300 models (see table 5.1). The same process was repeated for the mouse

(MmUCP1) and human UCP1 (HsUCP1) isoforms, generating a total of 900 models in this first phase of model building.

**Table 5.1. Overview information of the creation and refinement process for generating UCP1 homology models**

<b>Isoform</b>	<b>Conformation state</b>	<b>Template</b>	<b>Modeller (number of models generated)</b>	<b>GalaxyRefine2 (number of models generated)</b>
<i>OaUCP1</i>	c	BtAAC1	100	60
	c	BtAAC1 +ScAAC2/3	100	20
	m	TtAAC	100	60
<i>MmUCP1</i>	c	BtAAC1	100	20
	c	BtAAC1 +ScAAC2/3	100	20
	m	TtAAC	100	20
<i>HsUCP1</i>	c	BtAAC1	100	20
	c	BtAAC1 +ScAAC2/3	100	20
	m	TtAAC	100	20

For *OaUCP1*, 6 of the models generated in MODELLER from BtAAC1 and 2 of the models generated from BtAAC1 + ScAAC2/3 for the c-state, and 6 from TtAAC were then selected for further refinement. Model selection was done in the following way: each set of 100 models was sorted by two parameters: estimated overlap and root mean square deviation (RMSD), both provide an indication of the deviation of the generated model atoms from the template structure. The estimated overlap consists of the fraction of C $\alpha$  atoms in the model within 3.5 Å from the template backbone when the two structures are superimposed, while the RMSD provides the average value, in Å, of the deviation between corresponding C $\alpha$  atoms. RMSD and overlap of the homology models tended to have a linear relationship with inverse

proportionality, where a higher overlap corresponded a lower RMSD. As shown in figure 5.1. the model in the top left corner is that with the highest fidelity to the AAC template. The model combining the best RMSD and overlap value (highlighted with an arrow in figure 5.1) was always selected for model refinement for a more objective approach. A second one was also picked from the top 10, but more subjectively based upon visual inspection and manual overlap with the template structure. In this approach, the correct orientation of the transmembrane helices and, in particular, the residues composing the matrix network for m-state models and the cytoplasmic network for m-state models were assessed, as these were judged fundamental structural features and their correct position corroborated the accuracy of the model produced. In the case of the OaUCP1 models the top six models and not just top two were selected for further model refinement.

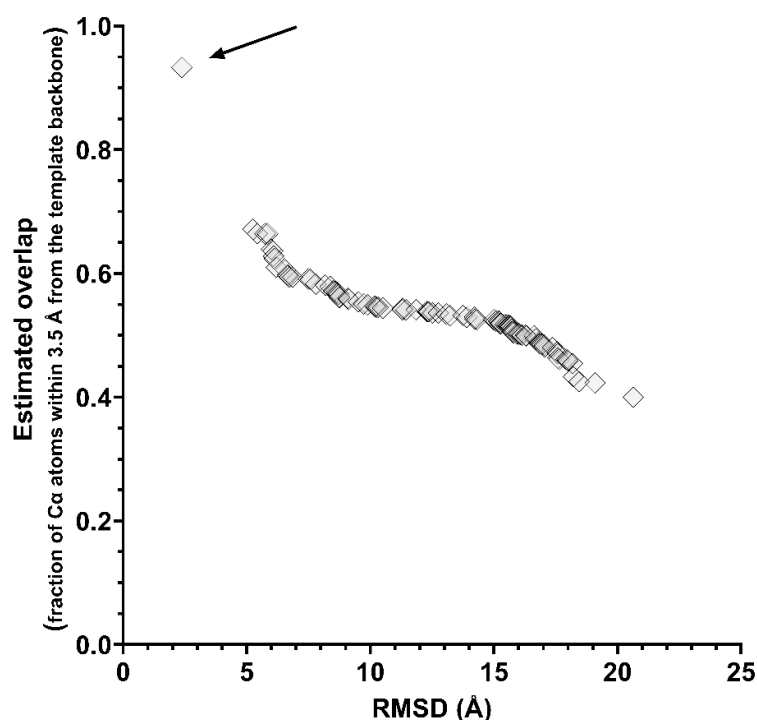


**Fig 5.1. Distribution of generated homology models for HsUCP1 c-state, according to RMSD and estimated overlap to the template AAC structure.** Example of inverse direct proportionality relationship between root mean squared deviation (RMSD) (in Å) on the x axis and estimated overlap (fraction of Cα atoms in the model within 3.5 Å from the AAC template backbone) on the y axis for homology models of c-state human UCP1. The model with the highest estimated overlap and the lowest root mean squared deviation (RMSD) is highlighted by an arrow.

### 5.3.2 Model refinement and quality control

The selected homology model was optimized with the GalaxyRefine2 programme available through the GalaxyWEB server, a repository of structural refinement tools developed by the Seok laboratory of the University of Seoul [226, 265]. GalaxyRefine2 generated 10 refined structures per each model submitted, scored by energy. The top scoring structure was then taken forward for manual inspection, focusing on the orientation of important residues (e.g. those corresponding to cytoplasmic and matrix gates) to determine if the helices were likely to be correctly modelled. In some instances, the models presented interruptions in the transmembrane alpha helices at points where the helices are known to have kinks from the AAC structures. These sections of a few residues were modelled manually with the “model/refine loop” instrument in UCSF Chimera to conserve an extra helical turn. Assessment by overlap of the generated structures with the AAC templates was continuous and used as the main instrument to identify any issues in the final homology models.

Before and after refinement, the models were evaluated with MolProbity [227] and QMEANbrane [228] online software packages. MolProbity was chosen as one of the consensus software packages used for quality assessment of experimentally determined structures which is summarized in the MolProbity score. The closer the score is to one, the better the quality of the model. Table 5.2 shows that all UCP1 models improved in quality after refinement with GalaxyRefine2, and that the AAC crystal structures used to generate the models also showed an improved MolProbity score after refinement.

**Table 5.2. Model refinement – MolProbity score**

<b>Model</b>	<b>MolProbity Score Pre-refinement</b>	<b>MolProbity Score Post-refinement</b>
<i>c-state OaUCP1</i>	<b>3.07</b>	<b>0.97</b>
<i>c-state MmUCP1</i>	<b>3.13</b>	<b>0.78</b>
<i>c-state HsUCP1</i>	<b>2.94</b>	<b>0.58</b>
<i>m-state OaUCP1</i>	<b>3.17</b>	<b>1.15</b>
<i>m-state MmUCP1</i>	<b>2.97</b>	<b>1.43</b>
<i>m-state HsUCP1</i>	<b>3.27</b>	<b>1.19</b>
<i>c-state BtAAC</i>	<b>2.23</b>	<b>0.50</b>

<i>m</i> -state TtAAC	1.48	0.59
-----------------------	------	------

QMEANbrane is a quality control software package for membrane protein structural analysis, part of Swiss-Model, the online homology modelling platform developed by the Centre for Molecular Life Sciences, University of Basel. The software estimates the local quality of membrane protein models through a score between 0 and 1 (where 1 is best and 0 is the worst) relying on comparison to a dataset of membrane proteins structures. The score is also visually transposed onto the models, using a colour spectrum going from orange (worst) to blue (best) as shown in panel A and C of figure 5.2. Plots in panel B (pre-refinement) and panel D (post refinement) give an example of the improvement of the Local Quality Estimate score for the *m*-state model of OaUCP1.

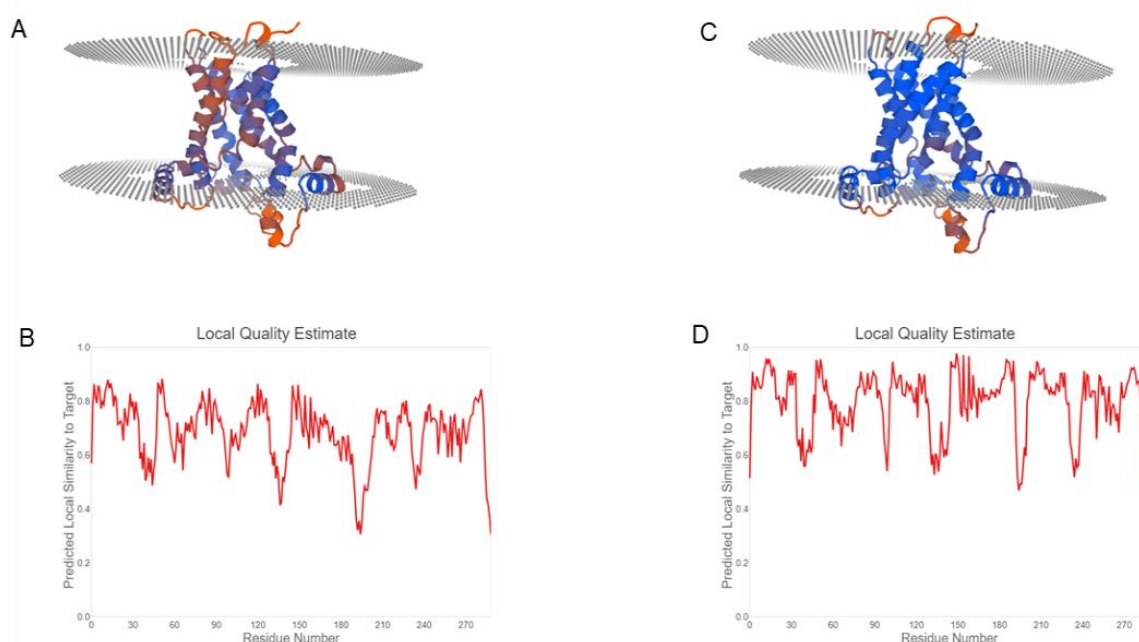


**Fig 5.2. Example of quality control with QMEANbrane with a OaUCP1 model.** (A) *m*-state OaUCP1 model as generated from MODELLER and (B) associated local quality estimate. (C) The same OaUCP1 model after optimization (energy minimization and bonds angles correction) with GalaxyRefine2 and (D) corresponding local quality estimate along the protein sequence.

Model refinement procedures generated 10 models from each of the models submitted for refinement. For OaUCP1, a further 60 models were generated from the BtAAC1 models, 20 from the BtAAC1 + ScAAC2/3 models and another 60 from TtAAC models, for a total of 140 models. After testing the models generated by combining BtAAC and ScAAC templates it was decided to limit the generation of homology models to the BtAAC1 template only. The models generated from BtAAC1 only presented better performance in modelling complete transmembrane alpha helices while the models from BtAAC1+ScAAC2/3 presented two to three interruptions of the helix in the membrane, often around the proline kinks. Through reasoning that UCP1 is likely to present complete transmembrane alpha helices, and conserves prolines kinks like AAC where in AAC the secondary structure is maintained, models without this issue were preferred, allowing for more effective refinement later. No additional issue was found in building m-state homology models, compared to c-state models, supporting the hypothesis that UCP1 can enter an m-state conformation. The definitive models chosen after evaluation were manually inspected a final time, where again the UCP1 models were superimposed with the template AAC structures to check for accurate folding of the helices and the correct orientation of cytosolic and matrix networks was verified.

### **5.3.3 Analysis by symmetry**

Mitochondrial carriers are formed of three repeat domains, exhibiting three-fold pseudosymmetry where each residue at a given position in a domain is related by symmetry to a residue at a similar position in each of the other two domains, which together form a symmetry-related 'triplet'. In previous works Kunji and Robinson have rationalised that because of the three-fold symmetrical structure, the mechanism of transport of mitochondrial carriers is likely to also follow a three-fold symmetrical process [137-139]. Accordingly, residues within a triplet that are more similar and symmetrical are therefore likely to relate to the mechanism of transport. Deviations from symmetry would instead represent adaptations in carriers to accommodate the non-symmetric nature of the various metabolite transport substrates. The analysis of triplet conservation and symmetry has helped identify key features of carriers, notably a common central substrate binding site across the family [137]. Based on the symmetric properties that UCP1 shares with AAC it was decided to organize a systematic analysis of symmetry-related triplets to determine

possible interactions between residues in the UCP1 models. Using a symmetry-based alignment of multiple mitochondrial carriers as a guide (see example, supplemental [136, 137]), each of the three domains of the UCP1 isoform sequences were aligned to identify symmetry-related triplets of residues, which were highlighted and ordered by triplet accordingly (see appendix figure A9). The alignment comprised the transmembrane helices and the matrix helices, which exhibit high symmetry and conservation in the proteins, unlike the more variable linker sections (between the first transmembrane helix and matrix helix of each domain), where alignments were extended only to where clear conservation across the domains could be observed. The homology models generated were then systematically analyzed triplet by triplet, assessing residue positions and potential for interaction partners. For each triplet, each residue was selected in turn on UCSF Chimera and systematically checked using the “*Find clash/contact*” tool set at the default settings (“Find atoms with VDW overlap  $\geq 0.1$ ”; Van der Waal overlap is defined as the sum of their radii minus the distance between them minus a further 0.4 Å to take into account possible H-bond pairs). In reviewing the results of the analysis particular relevance was given to contacts that had been evidenced between pairs of oppositely charged residues or residues with a similar polar/hydrophobic nature, in the search for relevant structural features in UCP1. An example of the annotated outcome is shown in table 5.3 for human UCP1, where the residues in the symmetry related triplet Q<sup>100</sup>-K<sup>199</sup>-K<sup>293</sup> are suitably positioned to form potential interactions with Y96, E290 and D97, respectively, in the m-state but not in the c-state, while T104 has potential to interact with Q100 in both states.

**Table 5.3. Example of amino acid residue interaction analysis in HsUCP1**

Residue	Interacting residues <i>c-state</i>	Interacting residues <i>m-state</i>
<b>Q 100</b>	thr104	thr104/tyr96
<b>K 199</b>	none	glu290
<b>K 293</b>	none	asp97

What follows is a report of results from the systematic analysis subdivided according to mitochondrial carrier features as described for the ADP/ATP carrier previously [135, 136], alongside the reevaluation of residues addressed in past literature relevant for each group of interactions identified. Residue numbering refers in all cases to the human UCP1 isoform, unless otherwise stated.

### 5.3.4 The common carrier substrate binding site in UCP1, the arginine triplet R<sup>84</sup>-R<sup>183</sup>-R<sup>277</sup>

Past bioinformatic analysis showed that UCP1 has three conserved symmetrically related arginine residues in the central cavity of the protein (triplet R<sup>84</sup>-R<sup>183</sup>-R<sup>277</sup> in HsUCP1), that correspond to those that form a common substrate binding site in the wider carrier family [137-139, 158, 261, 263]. Here, systematic analysis did not show likely contacts among the three arginines (or with other residues) with the exception of the m-state of HsUCP1, which indicated a possible contact between R183 and R277.

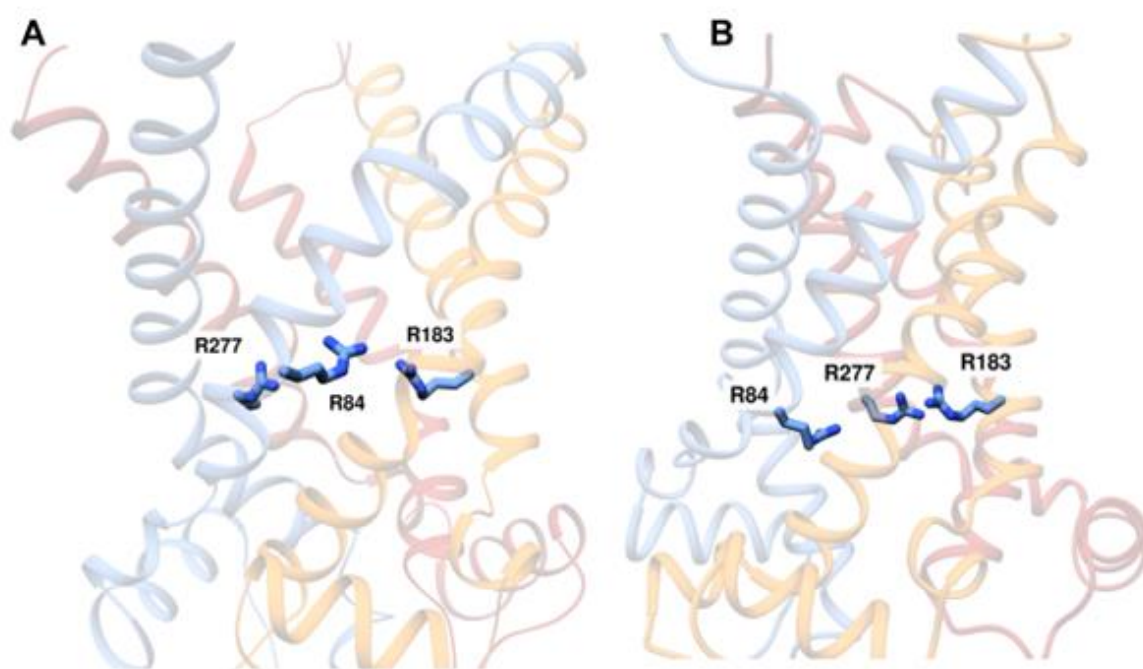


**Figure 5.3. Arginine triplet.** The arginine triplet R<sup>84</sup>-R<sup>183</sup>-R<sup>277</sup> (blue) believed to be the substrate binding site of UCP1, shown in the c-state (panel A) and m-state (panel B) models of HsUCP1 viewed from the membrane. Each domain has been coloured differently (cyan, orange and red) to help distinguish them and highlight the symmetry of UCP1 structure.

Past mutation experiments of the arginine triplet had highlighted the involvement of these residues in nucleotide binding: single mutations of each of the three arginines

showed compromised or abolished nucleotide binding, where fatty-acid activated proton transport still occurred but was not inhibited by purine nucleotides [158, 263]. As such, the three positively charged arginines are the likely interaction site for the binding of negatively charged phosphate groups of nucleotides, as discussed in [111, 157], see also chapter 1. Though it is not clear if they are where fatty acids interact with UCP1 - more severe double or triple arginine mutations may be required to rule out binding at this location [111]. The UCP1 models here showed the arginines to maintain a central position in the protein cavity in both the c and m-state, consistent with a function in binding ligands/substrates for transport. The presence of conserved residues in a carrier-like binding site, effectively modelled on AAC, is thus consistent with UCP1 utilising a conventional carrier mechanism.

### 5.3.5 UCP1 has the potential to form cytoplasm and matrix interaction networks

UCP1 had already been determined to have the potential to form networks of salt bridges and hydrogen bonds, similarly to AAC [111]. This analysis found that the UCP1 residues equivalent to those forming the matrix and cytoplasmic networks in AAC have similar charge properties and capacity to form similar networks of interactions in the models produced (see figure 5.4).

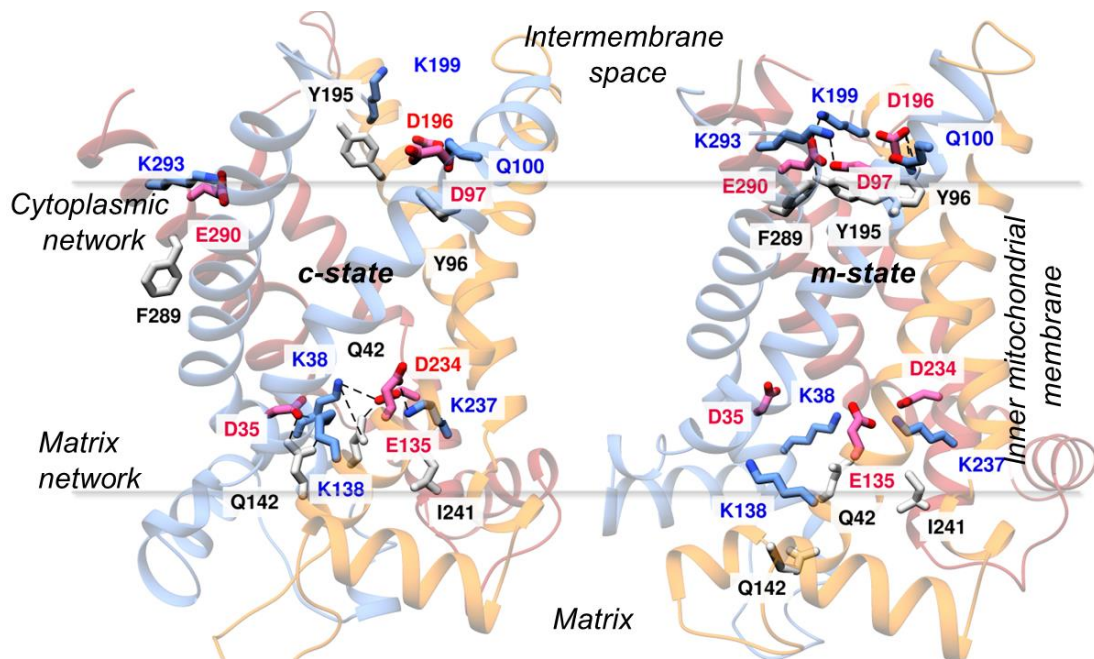


**Figure 5.4.** Models of Human UCP1 as seen from the membrane in a c-state (left) and m-state (right). Residues of the putative cytoplasmic and matrix salt bridge networks of

UCP1 (which form in the m- and c-state, respectively) are shown as sticks coloured in magenta and blue; residues part of the glutamine and tyrosine braces are coloured in white. Putative interactions between residues of the matrix and cytoplasmic salt bridge networks are shown as dashed black lines. Each domain has been coloured differently (cyan, orange and red) to help distinguish them and highlight the symmetry of UCP1 structure

Triplet sequence alignment (see appendix figure A8-9) to the ATP/ADP carrier and analysis of the UCP1 models clarified the UCP1 residues corresponding to the matrix and cytoplasmic interaction networks, which are composed of triplets of polar or positively charged and negatively charged residues. The triplets forming the matrix network in the c-state of HsUCP1 are K<sup>38</sup>-K<sup>138</sup>-K<sup>237</sup> and D<sup>35</sup>-E<sup>135</sup>-D<sup>234</sup>, whilst those forming the cytoplasmic network in the m-state of HsUCP1 are D<sup>97</sup>-D<sup>196</sup>-E<sup>290</sup> and Q<sup>100</sup>-K<sup>199</sup>-K<sup>293</sup>, as seen in figure 5.5.

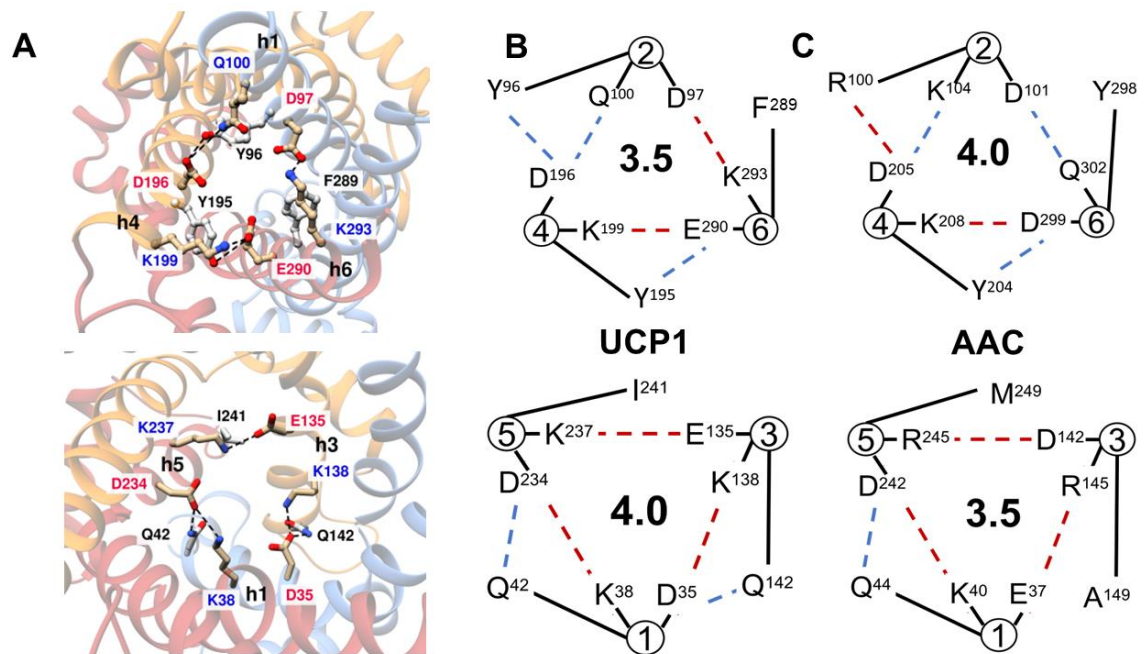


**Figure 5.5 Cytoplasmic and matrix gates of AAC and UCP1 with their relative network strength.** **Panel A.** View from the intermembrane space of the cytoplasmic interaction network (top) and matrix interaction network (bottom) of HsUCP1 in m and c-states, respectively. **Panel B.** Schematic representation of the same networks shown in panel A for HsUCP1; salt bridges are indicated in red and hydrogen bonds in blue. Circled numbers represent odd and even transmembrane helices; bold numbers indicate the relative network strength. **Panel C.** Schematic representation of TtAAC cytoplasmic (top) and matrix (bottom) networks; salt bridges are indicated in red and hydrogen bonds in blue. Circled

numbers represent odd and even transmembrane helices; bold numbers represent the relative network strength.

Panel B of figure 5.5 shows the cytoplasmic and matrix networks of HsUCP1, which are shared by all 3 UCP1 isoforms. Only position 241, which has potential to provide a supporting 'glutamine brace' in other carriers, is a non-conserved residue (isoleucine or valine but always non-polar and separate from the core network). Panel C shows the equivalent cytoplasmic and matrix network of AAC from the experimentally determined structures, for comparison. The cytoplasmic network of UCP1 has 2 salt bridges and 1 hydrogen bond as main components, complemented by 2 further hydrogen bonds provided by the tyrosine braces. The cytoplasmic network of AAC is similar but has only one salt bridge and two hydrogen bonds among its main residues, which are complemented by one extra hydrogen bond provided by its braces. All 3 UCP1 isoform have only 2 tyrosine braces, with the third residue being a non-polar residue, phenylalanine. In contrast the tyrosine braces of TtAAC include an arginine residue capable of forming a salt bridge, alongside two conventional tyrosine residues.

The matrix network of UCP1 has 3 salt bridges, with two hydrogen bonds from the glutamine braces. The matrix network of AAC also has 3 ionic interactions but with only 1 hydrogen bond added from the glutamine braces, as residues 149 and 249 are non-polar. Following the network analysis performed by the Kunji group initially in [137] and later in [135] and in [140] - where the importance of the nature of the interaction (ionic interactions or hydrogen bonds) of the networks for the stability of AAC was shown - the relative strength of the cytoplasmic and matrix networks of UCP1 was measured following the same principles. It has been proposed that the strength of the networks can be estimated by assigning an arbitrary value of either 1 (salt bridge) or 0.5 (hydrogen bond) to each interaction, allowing to compare the relative strengths of networks of different carriers. Both cytoplasmic and matrix networks of UCP1 are strong, with matrix ones being slightly stronger (matrix network value = 4, cytoplasmic network value = 3.5). Compared to AAC, UCP1 isoforms presented one more glutamine brace in the matrix network, for a relative strength of 4 against 3.5 of the AAC, however, the cytoplasmic network of TtAAC presented one more brace, an arginine residue, alongside two tyrosines, compared

to the only two tyrosines braces in UCP1. In this case then the situation is inverted with the AAC cytoplasmic network with a relative strength of 4 and UCP1 with 3.5.

This analysis confirms the presence of features with potential to form both matrix and cytoplasmic networks in UCP1, similar to AAC in both c-state and m-state, highlighting how UCP1 could enter both conformations for function. OaUCP1, MmUCP1 and HsUCP1 isoforms possess almost identical matrix and cytoplasm salt bridge networks, sharing the same residues. All three isoforms of UCP1 also have the same numbers of glutamine and tyrosine braces. These results indicated that the UCP1 models show similar network strengths to AAC and could potentially be equally able to assume both m and c conformations.

### **5.3.6. A novel structural feature: a secondary cytoplasmic network**

Analysis of the triplet alignment and of the models created from the novel m-state led to the identification of a possible second set of interactions forming a network on the cytoplasmic side of UCP1. Systematic analysis highlighted a triplet of positively charged and polar residues, which in HsUCP1 are Q<sup>16</sup>-K<sup>116</sup>-H<sup>215</sup>, which have potential to form contacts with negatively charged residues of another triplet, E<sup>101</sup>-E<sup>200</sup>-R<sup>294</sup> in an m-state conformation only (figure 5.6). The potential contacts were through Q16-E101 and K116-E200. Analysis of the m-state models confirmed that these interactions, absent in AAC structures, were possible in all three UCP1 isoforms by selecting appropriate rotamers for the residues involved. These interactions are intra-domain, between the first and second helices of the same domain and, being specific to the m-state, would potentially add to the primary inter-domain cytoplasmic salt-bridge network gate. The residues involved are conserved to different degrees across isoforms and other carriers: they are present in UCP2, UCP3 and the dicarboxylate carrier (DIC), but are less prominent in the carnitine carrier (CAC), and completely absent in AAC isoforms. Notably, only two of the three residue pairs that align between triplets can form ionic interactions, indicating a possible deviation from symmetry. The third position has a mismatch of an arginine (294) and histidine (215) residue, which may both be positively charged at neutral pH.

An examination of UCP1 mutagenesis studies by Echtay et al. [156, 212] revealed that H215, alongside two conserved aspartic acid residues, D210 and D211, which

are in close proximity in the UCP1 models (see figure 5.6; residues corresponding to H213, D208 and D209, respectively, OaUCP1 numbering; the ovine UCP1 model was chosen as it demonstrates a stronger secondary network), were, unlike other residues, found to specifically influence the pH dependent binding affinity for triphosphopurine nucleotides (TNPs) but not diphosphopurine nucleotides [156, 212]. Histidine 215 was hypothesized to protrude into a binding pocket for nucleotides when in neutral form, hindering the entrance of the  $\gamma$ -phosphate of TNPs only. When protonated in response to pH changes, H215 was suggested to interact with one of the negatively charged aspartic acid residues and be retracted from the binding site, allowing for binding of TNPs (see [155, 210] for details).

The novel intra-domain interactions that bridge neighbouring helices, seem to be present only in the m-state conformation. However, the limitation of the models (built on AAC, which lacks this secondary network feature) means that it cannot be completely excluded that the intradomain interactions could also be maintained in the c-state. If so, they may act to clamp the domains as rigid bodies in the mechanism of the protein. If they are not present in the c-state, however, this additional interaction network would add to the total bond energy of UCP1 in the m-state only.

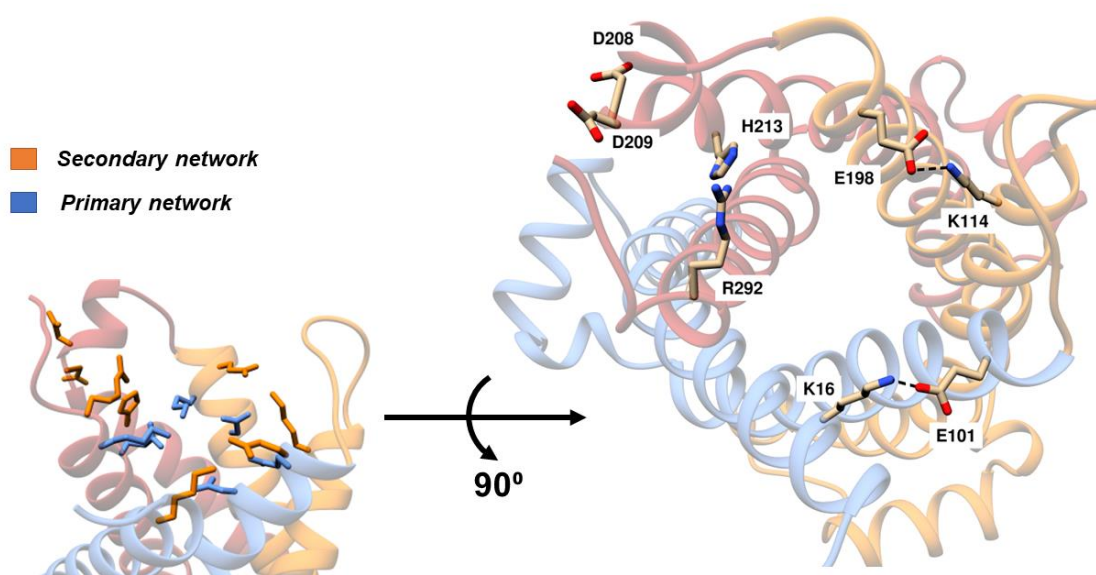


**Figure 5.6. The secondary cytoplasmic network.** Lateral view from the membrane and top view from the cytoplasm of OaUCP1 in the m-state, highlighting the relative position of the secondary network, above the primary cytoplasmic interaction network (lateral view

only), and the residues forming it. The position of two aspartic acid residues, D208 and D209, which, like H213, influence the binding of purine trinucleotides [156, 212] are also shown. (Note, the main text refers to HsUCP1 numbering: H215 in HsUCP1 corresponds to H213 in OaUCP1 (shown); D210 and D211 in HsUCP1 correspond to D208 and D209 in OaUCP1 and R294 in HsUCP1 corresponds to R292 in OaUCP1).

As such, UCP1 would be much more stable in its m-state with a total bonding score of 6 – 6.5 (including a further interaction between residues R92-E191 discussed in a later section), than its c-state with a bonding score of 4. In support of an m-state specific role, it is worth noting that where the estimated strength of the residues of the secondary salt bridge network change in, for example, UCP2/3 compared to UCP1 (a K-Q hydrogen bond changes to a K-E ionic interaction), there are compensatory changes in the primary cytoplasmic network (a K-D ionic interaction change to a Q-D hydrogen bond). As already mentioned, the third position of the triplet pair forming the secondary network gives a mismatch with H215 (which is either positively charged or neutral, depending on pH) aligned to R294 (which is positively charged), ruling out a full set of symmetry-related secondary cytoplasmic network interactions. However, the two highly conserved aspartic acid residues (D210 and D211), close to H215 at cytoplasmic end of the same helix, may potentially be able to ionically interact with R294 to provide the third network interaction in this case (see figure 5.6). When protonated at low pH, H215 may also interact with D210 or D211, as hypothesised in past mutagenesis studies (see above), though in this case they would prevent a D210 - or D211 - R294 helix-bridging interaction as the third network interaction.

**Table 5.4. Sequence alignment – secondary cytoplasmic network**

	H1 H2	H3 H4	H5 H6	H5/6
	+ -	+ -	+ -	-/*
HsUCP1	Q <i>E</i> *	<b>K</b> <b>E</b> **	H R	<b>D</b> **
MmUCP1	<b>K</b> <b>E</b> **	K G	H <b>K</b> **	<b>D</b> **
OaUCP1	<b>K</b> <b>E</b> **	<b>K</b> <b>E</b> **	H <b>R</b> **	<b>D</b> **
HsUCP2	K Q *	<b>R</b> <b>D</b> **	H R	<b>D</b> **
MmUCP2	K Q *	<b>R</b> <b>D</b> **	H R	<b>D</b> **
HsUCP3	K Q *	<b>R</b> <b>E</b> **	H R	N *
MmUCP3	K Q *	<b>R</b> <b>E</b> **	H R	N *
HsDIC1	<b>R</b> <b>D</b> **	K Q *	H K	N *
HsCAC	K Q *	L N	I <b>K</b>	<b>E</b> **
HsM2OM	<b>K</b> <b>E</b> **	K Q *	H K	N *
ScAAC2	D A	N P	S M	S
ScAAC3	N L	N P	S M	S
BtAAC1	D Q *	N P	H K	N *
TtAAC	D A	N P	N I	N

\*\* ionic interaction  
\* hydrogen bond

**bold** = residue involved in ionic interaction  
*italic* = residue involved in hydrogen bond

### 5.3.7 Residues in the central cavity: a hydrophobic triplet

The systematic analysis by symmetry highlighted the triplet F<sup>88</sup>- I<sup>185</sup>- W<sup>279</sup> (OaUCP1 residues and numbering; HsUCP1 has a Phe to Ser substitution) that is located in the central cavity, toward the cytosolic side of UCP1 (figure 5.7 panel A). The triplet is conserved in MmUCP1 and OaUCP1, and has one residue substitution in HsUCP1, and formed of strongly hydrophobic and aromatic residues that orientate into the central cavity, near to the common carrier substrate binding site. The analysis showed that possible contacts between the residues within the triplet were present in both states, although the residues appear to cluster slightly more closely in the m-state (figure 5.7 panel, panel B). The analysis also showed possible contacts of the triplet with other residues in the m-state, R92 and R173 and E191. R92 and E191 are above the hydrophobic triplet, toward the cytoplasmic side, and are part of the triplet, R<sup>92</sup>- E<sup>191</sup>- M<sup>285</sup> (HsUCP1 residue numbering).

The F<sup>88</sup>- I<sup>185</sup>- W<sup>279</sup> triplet (FIW - residue numbering referring to OaUCP1) is conserved in UCP1 isoforms, except for the phenylalanine to serine substitution in HsUCP1. It is also conserved, at least in its hydrophobic character in UCP2 and 3, where the isoleucine residue is substituted with valine, creating the FVW triplet. The residues of the FIW triplet correspond to a less hydrophobic triplet in AAC, formed by threonine, tyrosine, and alanine residues, while in isoforms of the carnitine/acyl-

carnitine carrier, a transporter of substrates with fatty acyl groups, the triplet of shorter amino acids VAA is conserved.

Past searches for a hydrophobic group of residues in UCP1 that may act to facilitate fatty acid tail binding (see chapter 3), including a comparative analysis of the carnitine-acylcarnitine carrier (CAC) that must also accommodate the binding and transport of an acyl chain moiety, did not identify an obvious hydrophobic region or set of residues [111]. However, the FIW conserved triplet, now observed here more prominently in the m-state, is a possible candidate site for this role in the central cavity of UCP1, where ionic interactions of the fatty acid carboxylate headgroup could also occur with the arginine triplet  $R^{84}$ - $R^{183}$ - $R^{277}$ .

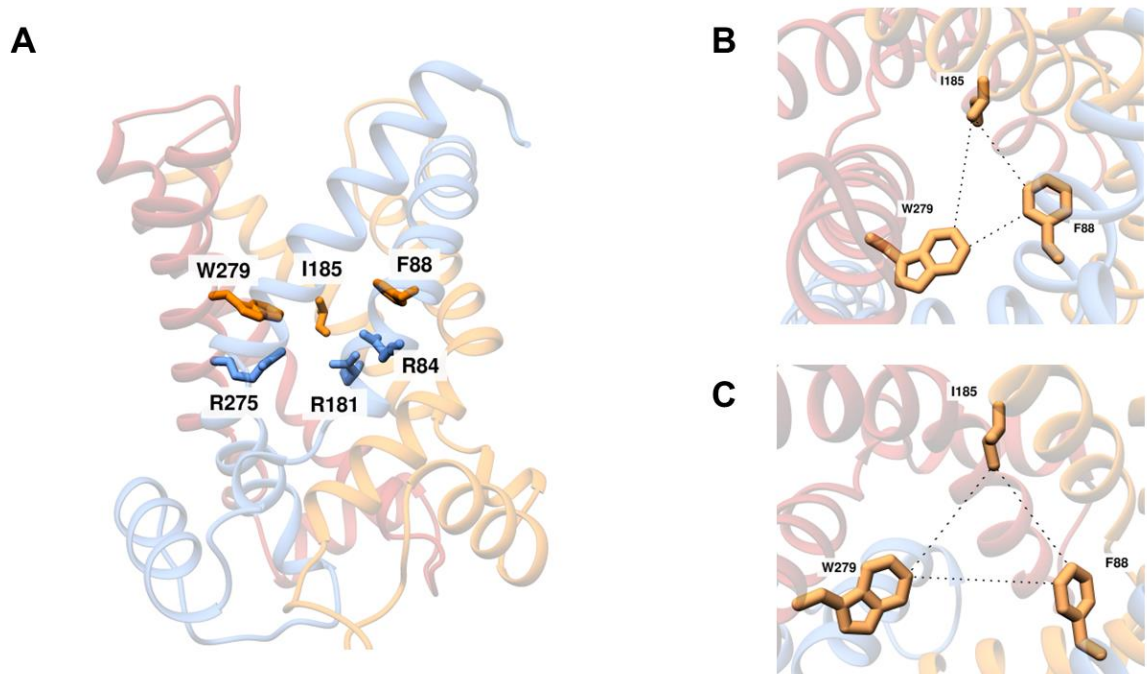


**Figure 5.7. FIW triplet and its position in OaUCP1. Panel A.** Lateral view OaUCP1 m-state showing arginine triplet (blue) and FIW triplet (orange) respective positions; the FIW triplet sits toward the cytoplasmic side in respect to the arginines (residue numbering of OaUCP1). **Panel B.** Top view OaUCP1 m-state from the cytoplasm, (residue numbering of OaUCP1). Shortest distances of approach between sidechains (dotted lines): W279 - F88 = 4.92 Å; F88 - I185 = 6.17 Å; I185 - W279 = 7.87 Å. **Panel C.** Top view OaUCP1 c-state from the cytoplasm, (residue numbering of OaUCP1). Shortest distances of approach between sidechains (dotted lines): W279 - F88 = 9.12 Å; F88 - I185 = 9.04 Å; I185 - W279 = 9.38 Å.

### 5.3.8 Residues in the central cavity: additional gating bonds relevant to nucleotide binding

Systematic analysis showed that the R<sup>92</sup>- E<sup>191</sup>- M<sup>285</sup> triplet (HsUCP1), which orient into the central cavity like the FIW triplet but lie further towards the cytosolic side of the protein (figure 5.8), have potential contacts almost only in the m-state. Analysis of the UCP1 models indicated that R92 and E191 potentially form a salt bridge interaction specifically in the m-state (figure 5.8 panel B). Hence, this interaction, like the novel secondary cytoplasmic network (section 5.3.5), may also add to the cytoplasmic network 'gate' strength, and help stabilise the m-state conformation. The triplet R<sup>92</sup>- E<sup>191</sup>- M<sup>285</sup>, (REM), appears highly conserved not only in UCP1 but also UCP2 and 3. This triplet corresponds to the triplet in the m-state structure TtAAC called by Ruprecht and colleagues the "ceiling of the substrate binding site" [136] which is conserved as N<sup>96</sup>-Y<sup>200</sup>-V<sup>294</sup> in AAC isoforms, and is positioned in the central cavity one helix turn below (toward the matrix side) of the residues of the 'hydrophobic plug' in the m-state (see chapter 1).

This potential interaction is of particular interest as R92 and E191 are two of several well conserved residues in UCP1 that have been the focus of past UCP1 mutagenesis studies. Both residues have been investigated by both Garlid [158, 261] and Klingenberg [263] [153, 154] for their possible role in proton transport, anion transport, and purine nucleotide binding. The results of their experiments identified E191 as the residue that predominates the strong pH dependency of nucleotide binding affinity in UCP1. The E191Q mutation showed a loss of pH dependency, with lowered nucleotide affinity at low pH but increased affinity at higher pH, towards 7.5. The mutation R92T also showed a loss of pH dependency, but with a loss of nucleotide affinity at all pH values tested, more similar to mutations of the central arginine triplet (R<sup>84</sup>-R<sup>183</sup>-R<sup>277</sup>) that abolished nucleotide binding [155, 263]. Klingenberg et al. [263] hypothesized that R92, which was noted to occur in an equivalent position of a different amino acid sequence repeat to E191, may form an ionic interaction with E191 when the glutamate residue is deprotonated and negatively charged at higher pH values. The bond formation was proposed to gate access of nucleotides to their binding pocket, where once opened, R92, but not E191, could also directly interact with the nucleotide phosphate moiety [155, 263].

The m-state UCP1 models here confirm that R92 is indeed in the right position to be the binding partner of E191, as suggested by Klingenberg [263]. However, with the structural context provided here, and in [111], the binding pocket can be rationalised to be primarily composed of the arginine triplet (R<sup>84</sup>-R<sup>183</sup>-R<sup>277</sup>), in the centre of the central cavity, that interact with the negatively charged nucleotide phosphates, along with R92. R92 and E191 are located above this region on the cytoplasmic side, where they are well placed to interact with one another and gate the access of nucleotides to the site from the cytoplasm (figure 5.8) Importantly, these structural observations reveal that residues potentially involved in closing the central cavity to the cytosol in the m-state are linked to influencing the pH sensitivity of nucleotide binding affinity. As well as E191 and R92, Klingenberg et al. [155] highlighted H215, D210 and D211 as residues that also influence the affinity of nucleotides in a pH-sensitive manner (in this case specifically nucleotide triphosphates), which are shown here (see section 5.3.6, and Discussion below) to potentially partake or influence the formation of the secondary cytoplasmic network. Hence, changes in nucleotide affinity may merely reflect the likelihood that UCP1 is in a c-state, with the central cavity open to the cytosol for nucleotide binding, over an m-state, which is dictated by the relative strength of bonding networks that support each state. This possibility would be consistent with the much higher affinity for purine nucleotides by UCP1 at low pH, where E191 becomes more likely to be protonated and unable to contribute to closing the cytosolic side of the protein in an m-state, hence potentially favouring a 'nucleotide binding site open' c-state conformation.

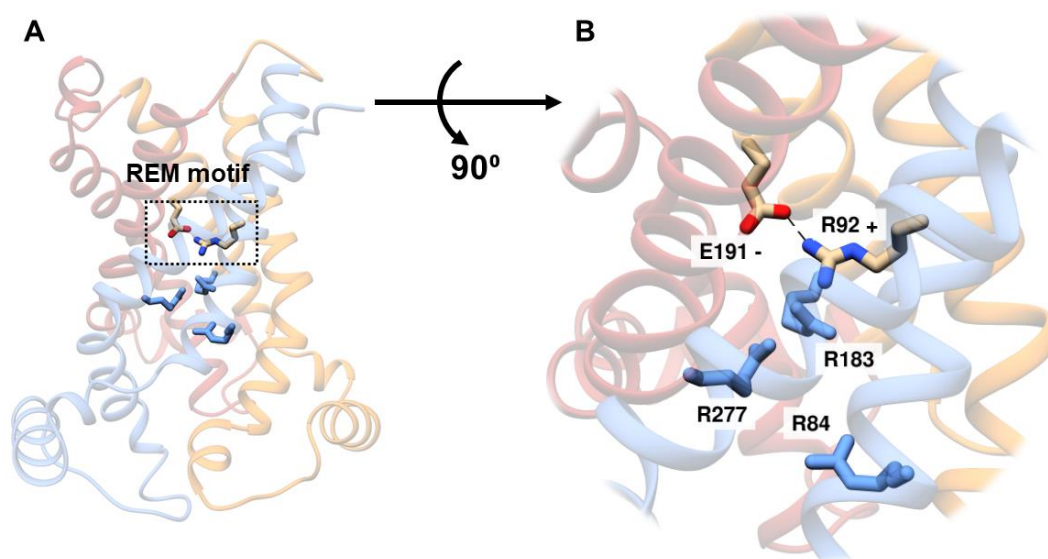


**Figure 5.8. The interaction between R92 and E191 in HsUCP1 (REM triplet).** **Panel A** The position of the REM triplet relative to the central arginine triplet (R<sup>84</sup>-R<sup>183</sup>-R<sup>277</sup>), in the m-state model of HsUCP1 viewed from the membrane; **Panel C**. Top view from the cytoplasm of the putative R92-E191 interaction; the arginine triplet is also highlighted in blue.

### 5.3.9 Other carrier structural features

Triplet alignment and systematic analysis showed that all three UCP1 isoforms conserved the key features of mitochondrial carriers, e.g. cardiolipin binding sites and ‘matrix tethers’ consistent with past analysis [111]. In addition, this analysis clarified the presence of other carrier structural features, such as a hydrophobic plug and small residue motifs at close packing helix interfaces (GxxxG and πxxxπ), which are particular to the m-state, as highlighted in the m-state structure of TtAAC [136]. Their presence in UCP1 further strengthens the case that the protein utilises an m-state conformation, as in AAC. Analysis of the homology models of c and m-states of the three isoforms provided very similar findings, as detailed in figure 5.9. All the conserved motifs and structural features were present and conserved in all three UCP1 isoforms, as outlined below.

Systematic analysis confirmed the presence and the relevance in the m-state of UCP1 of the hydrophobic plug: this structural feature formed by the triplet I<sup>93</sup>-L<sup>192</sup>-F<sup>286</sup> (human UCP1 residue numbering), which forms a “plug” of hydrophobic residues under the primary cytoplasmic network, toward the matrix side of UCP1

(figure 5.9 panel C). The analysis only indicated possible contacts in the m-state, specifically of the isoleucine and leucine residues with the phenylalanine residues, similar to the m-state of TtAAC (figure 5.9 panel C) , supporting UCP1 having an m-state conformation for function.

Cardiolipin binding sites, which are located at the matrix end of the even numbered alpha helices (figure 5.9 panels D and E), were identified as parts of two set of three triplets, the first set was identified as triplets (human UCP1 residue numbering): Y<sup>75</sup>-W<sup>174</sup>-F<sup>268</sup>, S<sup>76</sup>-K<sup>175</sup>-K<sup>269</sup>, and G<sup>77</sup>-G<sup>176</sup>-G<sup>270</sup>; the second set of triplets sits on the linker helices, just before the matrix helices, as these regions of the protein are less symmetric, obtaining a sequence alignment by triplets was more challenging, but enough symmetry is retained to identify the following three triplets (human UCP1 residue numbering): Y<sup>55</sup>-Y<sup>154</sup>-Y<sup>248</sup>, K<sup>56</sup>-T<sup>155</sup>-K(P/T)<sup>249</sup> and G<sup>57</sup>-G<sup>156</sup>-S<sup>250</sup>. The contacts highlighted by the analysis were with non-polar residues surrounding the cardiolipin binding features. It stands to reason that they were mainly due to imperfect orientations of the rotamers of the side chains.

The GxxxG feature is constituted by the residues of the triplet A<sup>20</sup>-G<sup>120</sup>-A<sup>219</sup> and A<sup>24</sup>-G<sup>124</sup>-G<sup>223</sup>, while the πxxxxπ feature by the triplets S<sup>90</sup>-C<sup>189</sup>-V<sup>283</sup> and G<sup>94</sup>-V<sup>193</sup>-V<sup>287</sup> (human UCP1 residue numbering). Both these features are only visible in the m-state (figure 5.9 panel G). Consistent with their function of facilitating the transition to an m-state by enabling the helices to rotate, the systematic analysis of the models did not show any possible contact in the c-state. The only possible contacts detected were in the m-state conformation with other non-polar residues of the neighbouring helices. This result also adds to the likelihood that UCP1 adopts an m-state conformation.

Systematic analysis also confirmed the presence of matrix tethers in the UCP1 models. Contact analysis of the mouse isoform models evidenced in the m-state contacts between residues R239 and E262, part of respectively the triplets R<sup>40</sup>-R<sup>140</sup>-R<sup>239</sup> and E<sup>69</sup>-E<sup>168</sup>-E<sup>262</sup> (human UCP1 residue numbering). No contacts were

observed in the c-state analysis. However, both the c and m-state models confirmed the presence of matrix tethers in both states (figure 5.9 panels H and I).

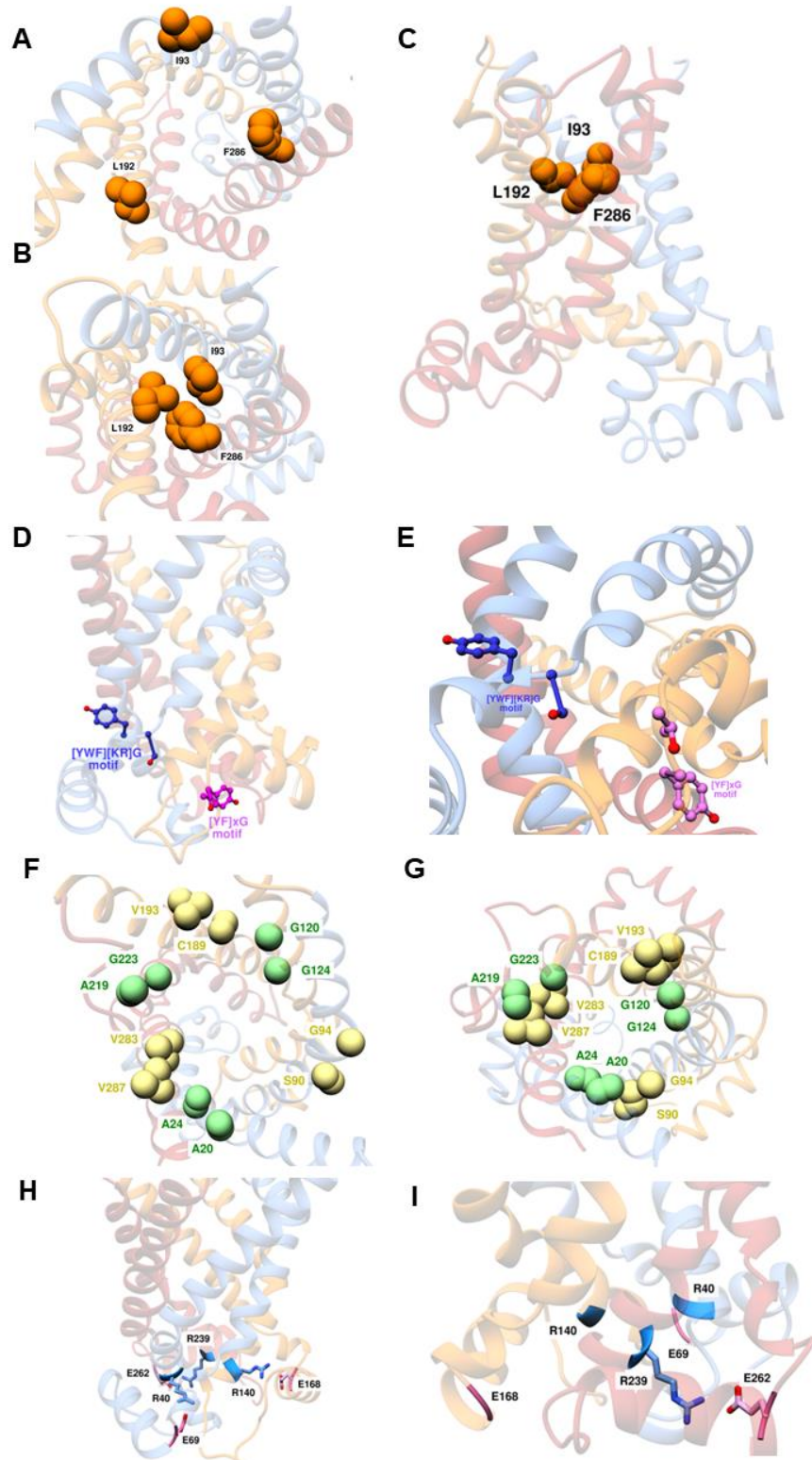


**Figure 5.9. Overview of carrier features possessed by UCP1, shown on HsUCP1 models. Panel A.** Top view of HsUCP1 hydrophobic plug residues (orange) as spheres of

their VDW radius in the c-state. **Panel B.** Top view of hydrophobic plug residues (orange) in the m-state. **Panel C.** Lateral view of the hydrophobic plug forming in an m-state conformation. **Panel D.** Lateral view of HsUCP1 (c-state), highlighting a cardiolipin binding site. **Panel E.** Zoomed in view showing the lateral chain of the residues of the [YWF][KR]G motif (light blue) and [YF]xG motif (purple). **Panel F.** HsUCP1 c-state position of GxxxG (green spheres) and πxxxπ (light yellow spheres) features at the interdomain interfaces. **Panel G.** HsUCP1 m-state position of GxxxG (green spheres) and πxxxπ (light yellow spheres) motifs at the interdomain interfaces. **Panel H.** Lateral view of HsUCP1 (c-state) evidencing the position of the arginine residues (light blue) and glutamates (magenta) at the interface between transmembrane helices and matrix helices. **Panel I.** Zoomed in view of the ionic interaction between K239 (light blue) and E262 (magenta), forming the matrix tethers.

### 5.3.10. Other notable UCP1 amino acid residues

As mentioned, many residues of UCP1 have been mutated in an effort to characterise the ligand binding sites and mechanism of the protein. However, without a solid structural context the results of these mutations were often difficult to interpret and are re-examined in this chapter. Among the residues that had been previously highlighted but without assigning a clear role in UCP1 function are D28 and Q85 [212]. Sequence alignment by triplets showed that they are respectively parts of the triplets: D<sup>28</sup>- V<sup>128</sup>- T<sup>227</sup> and Q<sup>85</sup>- S<sup>184</sup>- L<sup>278</sup> (human UCP1 residue numbering). Systematic analysis revealed possible contacts between these triplets. D28 was mutated by the Klingenberg group as one of the few negatively charged residues originally thought to be in the central region of the protein [212]. Neutralization of the residue affected proton transport. The residue later re-emerged in the analysis of UCP1 based on symmetry [111, 139, 266] as one of the few asymmetric residues in the central cavity, alongside Q85, and thus may represent a potential adaptation for the binding of a substrate. From the m-state models it can be noted that although in different triplets, D28 and Q85 can potentially interact via hydrogen bonding, at the inside of the internal cavity on neighbouring helices. They could form a polar hydrophilic niche just above the putative binding site of the arginine triplets, toward the cytoplasmic side of UCP1. Considering the position and the effect of neutralizing mutations on proton transport it cannot be ruled out that D28 could act as a partner for coordinating the proton of protonated fatty acids during proton transport, as proposed in [123, 266].

H146 and H148 (human UCP1 residue numbering) are two highly conserved residues in UCP1 that have been proposed to be important for proton transport [262]. However, sequence alignment by symmetric triplet and systematic analysis were not possible to be performed on the residues, as in all 6 models of the three UCP1 isoforms they are located in a loop region on the matrix side, which lacks symmetry, limiting what analysis can be performed. Past mutation of the residues strongly affected proton transport [262]. The two histidines are absent in marsupial UCPs, which have been postulated not to catalyse proton leak [1]. They are also not present in UCP2, a protein that although formally called a UCP has been questioned on its ability to uncouple, and may represent a conventional metabolite transporter [193]. Analysis of the homology models produced no new conclusions, the residues were not in proximity of structural features on the matrix side of the protein, such as matrix tethers. It cannot be excluded that the histidines, although not close to the central cavity of the protein, could have an important structural role in UCP1 activity, possibly exploiting the structural plasticity of the loop on which they are located.

Other residues that have been highlighted as important in UCP1 activity are cysteine C254 and the two lysines residues, K56 and K151 (human UCP1 residue numbering). K151 and K56 were excluded from the systematic triplet analysis because they are not part of triplets, being positioned in loop regions of the protein, which are not symmetrical. C254 however, is on a matrix helix, a symmetrical part of UCP1, and was identified as part of the triplet T<sup>61</sup>-A<sup>160</sup>-C<sup>254</sup> (human UCP1 residue numbering). Across the 3 isoforms were found 6 total contacts predominantly in the m-state and not with any other obvious structural features (C252-Y246 in the OaUCP1 m-state model, C254-V258 in the HsUCP1 m-state model, and C254-F240 in the MmUCP1 m-state model – residue numbering refers to each of the isoforms cited). While C254 has been proposed to act as a regulator of UCP1 activity through its reversible sulfenylation by Chouchani et al. [127], the two lysine residues have been hypothesized to influence UCP1 activity and general mitochondrial function when succinylated [267]. c- and m-state models showed that C254 is positioned in the middle of a matrix helix, pointing inward toward the matrix side of the protein. According to Chouchani et al. [127] sulfenylation of the thiol group would disrupt the interaction between the cardiolipin molecule and the cardiolipin binding site toward which C254 points in the fold of the protein. This interference would destabilize the

protein leading to UCP1 activation. The position on the models and sequence alignments do not provide information in favour of regulatory modifications to C254 and K56/K151 for UCP1 function; the residues are also found on other mitochondrial carriers (C254 and K151), and part of a shared conserved cardiolipin (K56) binding motif, and so would appear unlikely to facilitate a specialised UCP1 function like high proton leak activity to support thermogenesis. K151 is on a matrix loop, distant from any important regulatory structural motif currently identified/hypothesized for UCP1. C254 is buried in the interface between matrix and transmembrane helices in both states and would be potentially difficult to access for dynamic regulation (see figure 5.10). Furthermore, previous studies mutating all cysteine residues in UCP1 did not find changes in activity, suggesting cysteines, including C254, do not play a significant role in UCP1 function [128], but from the homology models further conclusions cannot be drawn.

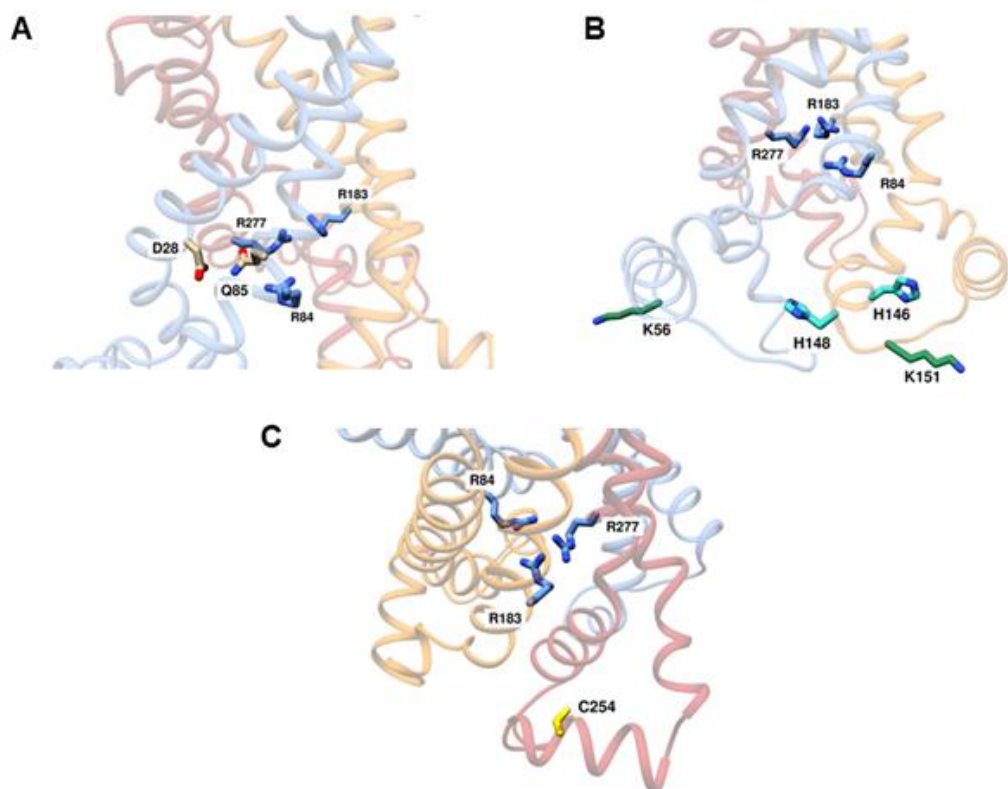


**Figure 5.10. Further important residues in UCP1, shown on HsUCP1 models. Panel A.** Zoomed in lateral view of HsUCP1 m-state homology model, D28 and Q85 next to the arginine triplet. **Panel B.** Zoomed in lateral view of HsUCP1 m-state homology model H146 and H148 and K56 and 151 are all located on matrix loops. **Panel C.** Zoomed in view from the matrix side of HsUCP1 m-state model, C254 on a matrix helix.

## 5.4 Discussion

In this chapter homology models of UCP1 in the c and m-state conformation were created. Creating models for an m-state conformation, based on the recent m-state structure of TtAAC, did not present more problems than generating models for the c-state for UCP1. Moreover, when the m-state models of the three UCP1 isoforms were examined for structural features through systematic analysis, the expected cytoplasmic network of ionic and hydrogen interactions were not only present, as had already been determined previously [111] by sequence analysis but were in the expected positions and orientations based on the AAC structures. The structural features of importance for transitioning to an m-state, such as the GxxxG and  $\pi$ xxx $\pi$  features which allow the tight packing of helices that enables the m-state, were also found mirroring their position in the m-state AAC structure, thus supporting the hypothesis that UCP1 can access c-state and m-state conformations just like AAC. The feasibility of building homology models of UCP1 in both the c and m-state also suggests that as other mitochondrial carriers it is likely to use an alternating access transport mechanism in its function.

### 5.4.1 Where do fatty acids bind on UCP1?

As discussed in chapter 1, UCP1 is proposed to transport fatty acids in its proton leak mechanism though how this may be achieved has not been clarified. Whilst no strong conclusions in favour of one of the models can be drawn from the homology models, no distinct region of polar residues on the outer hydrophobic surface of the protein were noted, suggesting the binding and transport of fatty acid polar head at the protein-membrane interface, as suggested by some [117] is unlikely to occur. As proposed in the more recent shuttling model [115] it appears more likely that fatty acids bind inside the cavity of UCP1. However, as noted by Kunji et al. [137], UCP1 is very symmetric compared to other carriers, without any obvious asymmetrical adaptations for substrates. Triplet alignment and systematic analysis of the m-state models, however, highlighted the existence of the F<sup>88</sup>-I<sup>185</sup>-W<sup>279</sup> triplet which forms a hydrophobic layer in the centre of the cavity in relative proximity to the region equivalent to the substrate binding site in other carriers. It could then be hypothesized that clustering of the F<sup>88</sup>-I<sup>185</sup>-W<sup>279</sup> triplet could provide the hydrophobic area to bind the hydrophobic portion of fatty acids and other activators

and ligands of UCP1. Results from chapter 3 highlight how little UCP1 displays specificity towards its ligands apart from requiring them to be of the correct size, hydrophobicity and amphipathic nature. The F<sup>88</sup>-I<sup>185</sup>-W<sup>279</sup> triplet symmetry and more obvious clustering in the m-state also explained why it was not highlighted in previous analysis focusing on asymmetric adaptation in the cavity.

#### **5.4.2 The secondary cytoplasmic network and nucleotide binding**

The identification of a novel 'secondary' cytoplasmic network with the additional m-state specific interaction of R92-E191, comprising residues historically connected in the literature with influencing nucleotide affinity [47, 153, 154], has provided new structural insights on how nucleotides may access and bind to UCP1. Evidence has shown that the arginine triplet likely provides the nucleotide binding site in the central cavity of the protein [158, 263]. E191 and R92 are shown in this chapter to be likely to form an ionic interaction in the m-state, contributing to the cytoplasmic network that closes the cavity to cytosolic nucleotides. The E191-R92 ionic interaction may form when E191 is deprotonated and so help promote gate formation at higher pH values towards a pH of 7, consistent with where UCP1 has a lower affinity for nucleotides [153, 154]. R92 likely also contributes in a more direct way to nucleotide binding in the c-state, as its loss severely decreases binding affinity, similarly to mutations of the arginines of the binding site. R92 is also aligned with the arginine triplet residues, sitting on the same helix as R84.

It is not unreasonable to think that R92 could then interact with one of the negative charges of the nucleotide, perhaps only temporarily, as it enters the central cavity and is oriented toward the positive charges of arginine triplet at the carrier substrate binding region.

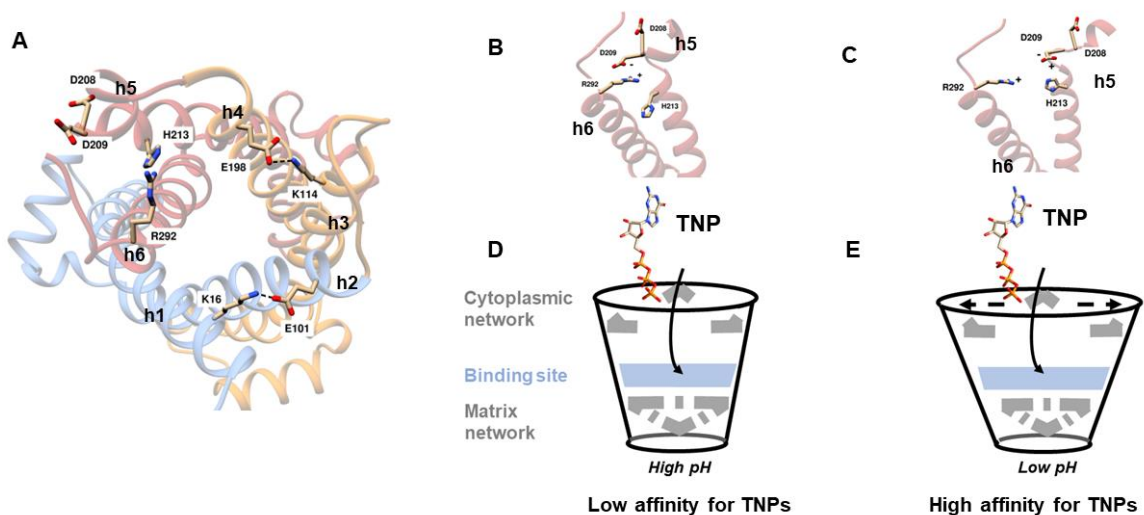


**Figure 5.11. A model for the regulation of binding of triphosphopurine nucleotides to UCP1, involving residues of the secondary cytoplasmic network, shown on an OaUCP1 model. Panel A.** View from the cytoplasm of OaUCP1 m-state, highlighted are the residues of the secondary cytoplasmic network and the helices of UCP1. Amino acid residue numbering in the legend and the figures refer to OaUCP1. **Panel B.** Zoomed in lateral view of helices 5 and 6 and their relative position to one another at high pH, corresponding to a tighter c-state conformation (panel D). **Panel C.** Zoomed in lateral view of helices 5 and 6 and their relative position at low pH, corresponding to a fully open c-state conformation (panel E) **Panel D.** In the c-state at high pH His 213 is in a neutral form, allowing the negatively charged D208 to interact with R292, preventing helices from moving apart and restricting the width of the central cavity for the bigger triphosphopurine nucleotides. **Panel E.** At low pH, H213 is charged and can form interactions with D208/209 on the same helix, preventing them from interacting with R292, and preserving a fully open aperture of the central cavity in the c-state.

As covered in section 5.3.6 and 5.3.8, changes in nucleotide affinity appear to correlate with changes in m-state cytoplasmic network in UCP1, and the likelihood of closing the central cavity to the cytosol. These observations provide a structural model for how UCP1 may alter its affinity for triphosphopurine nucleotides (TNPs) with pH. The protein binds triphosphopurine nucleotides with higher affinity than diphosphopurine nucleotides, where mutagenesis of H215 (residue numbering relative to the human isoform) has been shown to specifically influence the affinity of only the former [156]. The residue is protonated at  $\text{pH} < \sim 7$ , where it supports the increased affinity of the protein for TNPs. As shown in figure 5.11, H215 is positioned within the proposed secondary cytoplasmic network, close to the two aspartate

residues, D210 and D211 (residue numbering refers to the human isoform), which themselves may interact with R294 to form a network interaction. At high pH (>7), where H215 is uncharged, nucleotides may access the central cavity of UCP1 in a c-state conformation, where the unique asymmetric D210/D211 interaction with R294 prevents helix 5 and 6 from moving fully apart, limiting the access of bulkier triphosphopurine nucleotides but not to the smaller diphosphopurine ones to the arginine triplet binding site (figure 5.11, B and D). At low pH (<7), H215 will become protonated and can interact with D210/D211 to prevent the D210-R294 intra-domain interaction from forming, allowing helices 5 and 6 to move apart with the rest of the helices at the cytoplasmic side of the protein, and adopt a fully open conformation that does not restrict TNPs (figure 5.11, C and E). As well as altering access, the movement of helix 6, would also shift its corresponding arginine of R-triplet in the central cavity to alter nucleotide affinity at the binding site.

In conclusion, the homology models of UCP1 and their systematic analysis highlight that UCP1 can potentially utilise both c- and m-states in its function and contains a possible novel set of m-state specific interactions that stabilises the conformation. Furthermore, the structural correlations imply that changes in nucleotide affinity potentially relate to changes in m-state networks and the shift of UCP1 between m and c states.



## **6. Discussion and conclusion**

### **6.1 Key experimental findings**

#### **6.1.1 The regulatory ligands of native ovine UCP1**

Mitochondrial carriers are known to be challenging proteins to study, as they are unstable when purified, even in relatively mild detergents [169]. In the case of UCP1 the study of the interaction between the protein and fatty acid activators is further complicated by the nature of fatty acids as harsh ionic detergents at physiological pH, representing a possible source of damage to the integrity of UCP1. In chapter 3, a thermostability shift assay that can detect ligand interactions based on shifts in thermostability of a mitochondrial carrier was used. This analytical technique has been developed for use with membrane proteins and has been successfully employed to identify substrates and ligands with various mitochondrial carriers and transporters [140, 157, 215, 216, 268]. Chapter 3 showed that fatty acids have a UCP1 thermostability shift profile that is characteristic of transport substrates of the protein, such as anionic alkyl sulfonates, along with other activators of UCP1, such as retinoids. This characteristic profile features a plateau of the  $\Delta T_m$  with ligand concentration after an initial drop in stability; the plateau represents a specific interaction with the protein. Whilst the location of where fatty acids bind in UCP1 cannot be determined with certainty, based on the results presented in this thesis, fatty acids were shown to interact as transport substrates. Moreover, through the thermostability assay 20 small molecules, including putative activators, were identified based on negative thermostability shifts. When tested in flux assays with the reconstituted native UCP1 in liposomes, a subset of these molecules was observed to stimulate UCP1-mediated proton transport and were identified as activators. Among the novel activators were TUG-891, ibuprofen and tetradecylthioacetic acid. The screen performed with thermostability shift assays thus proved to be an effective technique to identify small molecules interacting with native UCP1.

#### **6.1.2 Characterisation of the human, mouse, and ovine UCP1 isoforms**

After characterising native ovine UCP1 ligands and activators, in chapter 4, the focus was shifted onto characterising UCP1 isoforms. UCP1 research has utilised

various analytical approaches, from studying the protein in isolated mitochondria, purified and reconstituted into liposome or in cells that express the protein (see [269] for an extensive review on methodologies to study UCP1). Of the four main mechanism models two were derived from isolated UCP1 studies (the cofactor and cycling models [113, 119, 270]) and two from isolated mitochondria – or mitoplasts - (the functional competition and shuttling models [112, 115]). The differences in these approaches to studying UCP1 function can generate contrasting results and highlight the importance of having robust verified information on the basic characteristics of the isoforms.

The recombinant isoforms of UCP1, human, mouse and ovine were compared and characterised in thermostability assay and proton transport assays. The recombinant proteins were successfully expressed in yeast and purified. In each case, the purified protein was folded and responded to GDP binding in all isoforms. The UCP1 proteins were also reconstituted into liposomes, where they proved to be functional and catalysed proton transport upon addition of oleic acid. The oleic acid rates were also responsive to GDP inhibition indicating that proton leak was due to the reconstituted UCP1 and not unspecific. Analysis of the isoforms in a controlled environment, indicated that, in general, they behaved in a similar manner, whilst it was not observed that rodent UCP1 had a different inherent leak activity in contrast to human UCP1, as previously claimed [213].

### **6.1.3 Homology modelling and systematic analysis of key structural features of UCP1**

In chapter 5, an analytical approach similar to those that have helped the structural and mechanistic understanding of transport by mitochondrial carriers [133, 136, 144] was applied to UCP1, expanding on previous work by Crichton et al. [111]. UCP1 homology models were created in both c and m-state conformations for each of the isoforms characterised in chapter 4. UCP1 homology models were analysed based on the pseudo-symmetrical properties of the tertiary structure of mitochondrial carriers. The main structural features shared by mitochondrial carriers that were clarified in the high-resolution structures of the ADP/ATP carrier, such as cytosolic and matrix salt bridge networks, cardiolipin binding sites, hydrophobic plug, GxxxG and  $\pi$ xxx $\pi$  motifs were all observed in the UCP1 models, indicating that UCP1 has the potential of assuming both a c-state and m-state conformation. Analysis of the

models by symmetry led to the identification of a second cytoplasmic salt bridge network, with residues creating intra-domain interactions, instead of the inter-domain interactions found in the primary cytoplasmic network. This second salt bridge network appeared to be m-state specific and absent in the ADP/ATP carrier. The additional energy provided by these interactions suggests that the UCP1 m-state is a much more stable conformation for the protein relative to the c-state, contrary to what was originally predicted previously based on relative c- and m-state network strengths [111, 133]. Re-interpreting the past mutation data available in the literature on UCP1, chapter 5 revealed a link between residues that likely stabilise one state over the other and changes in nucleotide affinity, which has provided a new structural interpretation for how nucleotides bind to UCP1, with a model to explain details in triphosphopurine nucleotides nucleotide binding in particular.

Homology models, however, have limitations. Models of UCP1 are based on AAC, which does not have the secondary network for example, so there may be unknown differences between AAC and UCP1 structures, and thus the homology models of UCP1 may have missed some structural feature. Furthermore, UCP1 models are based on AAC c and m-state models, where the carrier is bound to its specific inhibitors. The binding of an inhibitor puts the carrier in an energy minimum that blocks it from cycling through the conventional transport states, thus the inhibitor-bound state is technically an abortive state, different from a physiologically relevant one. UCP1 models share this limitation [133, 141, 144].

## **6.2 General discussion**

### **6.2.1. Acyl-CoAs interaction with UCP1**

In chapter 3, section 3.3.5 highlights a specific long-chain acyl-CoA interaction with UCP1. Acyl-CoAs are molecules involved in fatty acid catabolism [243]. There have been several studies that have sought to address a possible interaction between long chain acyl-CoAs and UCP1 (reviewed in [211]). Photoaffinity labelling of hamster brown fat mitochondria with a radioactive CoA derivative showed binding to both UCP1 and AAC, but pre-incubation with GDP led to the labelling of AAC only [250]. The long chain acyl-CoA palmitoyl CoA has been reported to inhibit the ADP/ATP carrier [247, 251]. Both Cannon et al. [253] and Strieleman et al. [247] reported that low micromolar concentrations of palmitoyl-CoA reversed GDP

inhibition in BAT mitochondria, hypothesising competition between palmitoyl-CoA and GDP [247, 253]. However, Locke et al. [246] reported that palmitoyl-CoA addition to isolated mitochondria only induced a slight depolarisation of the membrane, indicative of no-specific proton leak due to membrane damage. Moreover, Jezek et al. [249] reported that in swelling assays palmitoyl-CoA did not affect GDP inhibition of proton transport. Addition of palmitoyl-CoA did not cause changes in GDP  $IC_{50}$ , and the palmitoyl-CoA induced swelling observed in BAT mitochondria was also observed in liver mitochondria, where UCP1 is absent [249]. Thus, no clear interaction or regulatory role of palmitoyl-CoA with UCP1 has been established. The thermostability screen of acyl-CoA reported in chapter 3, showed that both palmitoyl-CoA and oleoyl-CoA decreased the  $T_m$  of UCP1, thus confirming that these species directly interact with the protein. A thermostability profile with oleoyl-CoA for a range of concentrations between 0-100  $\mu$ M showed that low micromolar concentration of the long chain acyl-CoA were sufficient to decrease the  $T_m$  of UCP1, and with increasing concentration, a pseudo-plateau was reached where the  $T_m$  gradually increased toward a  $\Delta T_m$  of 0  $^{\circ}$ C, consistent with a specific interaction. The UCP1 thermostability shift profile with oleoyl-CoA is similar to the behaviour of the ADP/ATP carrier with ADP substrate. Micromolar quantities of ADP have been shown to cause a decrease in  $T_m$  of AAC [169] while millimolar quantities have separately been shown to increase the  $T_m$  of AAC [216], comparable to the findings here with acyl-CoA on UCP1. This result would lead to hypothesise that oleoyl-CoA is transported by UCP1, as ADP is transported by AAC. However, a one-off anion transport assay showed that oleoyl-CoA is not imported as an anion. A similar trend in melting temperature was also observed with oleoyl lysophosphatidic acid (OLPA) (see appendix figure A3), an inhibitor of UCP1 [115]. Oleoyl lysophosphatidic acid decreased the  $T_m$  of UCP1 at low micromolar concentrations (<20  $\mu$ M), but gradually increased the  $T_m$  values toward a  $\Delta T_m$  above 0  $^{\circ}$ C with increasing concentrations of OLPA. Fedorenko et al. [115] observed in patch clamp experiments that low micromolar concentrations of long chain acyl-CoA (4  $\mu$ M of oleoyl-CoA) added from the cytosolic side, strongly inhibited UCP1 (92 % inhibition). They proposed that, given that acyl-CoA has a nucleotide moiety, the moiety would bind in the purine nucleotide binding site of UCP1, whilst the acyl chain in the hydrophobic pocket for the binding of fatty acids (these two binding sites would be either distinct or only partially overlapping) [123]. In chapter 3, oleoyl-CoA is also

shown to compete with GDP binding in ligand binding thermostability shift assays. The effects of oleoyl-CoA were quite potent, low micromolar concentrations were enough to prevent the strong increase in stability that otherwise occurs with 1 mM GDP. Levels of acyl-CoAs have been reported to substantially increase in BAT after activation of thermogenesis and consequently lipolysis (235 +/- 40 nmol/g protein in control hamster vs 648 +/- 105 nmol/g protein in cold acclimated hamsters) [248]. Long-chain acyl-CoAs, and among these palmitoyl-CoA and oleoyl CoA in particular, have been observed to increase four folds in concentrations, and constitute as much as 50 % of the total acyl-CoA pool in cold acclimated hamster BAT [248]. From the results of chapter 3, long-chain acyl-CoAs showed *in vitro* behaviour that would be consistent with a physiological mechanism to remove purine nucleotide inhibition from UCP1 at the onset of thermogenesis (in agreement to what was initially proposed by Cannon et al. [253]). In past studies with isolated mitochondria [112], fatty acids were proposed to be responsible for removing nucleotides from UCP1 by competition, though this claim was not consistent with findings gained across various experimental systems [107, 113].

### **6.2.2. UCP1 mechanism of transport: reconciling structural features and transport assay data**

Based on the homology model analysis in chapter 5, UCP1 possesses all the structural features required for a conventional carrier transport mechanism. In this strict exchange model of transport, the binding of a substrate in the central binding site of the carrier is required to shift the protein between states (c and m) to complete a transport cycle. Substrate binding through an 'induced fit' process [140, 142] provides sufficient energy to break the opposing salt bridge network to facilitate the translocation of the metabolite across the membrane. In the new conformation, the second interaction network on the original side of the membrane will have formed. Therefore, once the substrate is released, a second substrate must bind to provide the binding energy to break the second gating network, initiating transport of the second molecule in the opposite direction back across the membrane. Hence, the presence of two salt bridge networks gating a central binding site is consistent with a strict metabolite exchange process, as observed for example with the ADP/ATP carrier that carries out 1:1 ADP: ATP exchange in mitochondria [135, 136, 141, 144]. However, unidirectional transport (uniport), as experimentally observed for some

carriers (e.g. the phosphate carrier), has been proposed to occur if one of the two networks is particularly weak [137]. In this case, after transporting a substrate, the energy required to break the second 'weak' network does not require a counter substrate to bind, where the protein returns empty, giving a net overall metabolite transport in one direction only [133]. UCP1 was highlighted to possess two strong salt bridge networks, comparable to AAC, which are not likely to be disrupted in the absence of a substrate, and so, like AAC, UCP1 was predicted to be a strict exchange carrier [111]. The additional cytoplasmic network reported in chapter 5, which appears to be m-state specific, alongside salt bridging between R92 and E191, also observed in the m-state models only, if anything strengthens this prevision, as UCP1 would have salt bridge networks requiring even higher substrate binding energies to break than those of the ADP/ATP carrier. However, the results presented in chapter 3, showed that fatty acids behaved as substrates of UCP1 like alkyl sulphonates, which were transported by the protein through an apparent uniport process. However, oleoyl-CoA, also presented substrate-like behaviour in thermostability profile but was not transported. Hence one possibility is that oleoyl-CoA would require a counter substrate (maybe a fatty acid) to be transported. This hypothesis was not tested in the anion transport experiment presented in chapter 3, as oleic acid and oleoyl-CoA were added to separate traces and would then constitute a possibility for future studies. Past transport data, both in mitoplast and with the isolated protein, reported a uniport process as well [107, 115, 235]. Fatty acid transport by UCP1 is described by the cycling model [117, 119] of UCP1 proton leak, where UCP1 operates as a uniporter [117, 119, 123]. However, for long chain fatty acids, the shuttling model [123] proposes that these species remain bound to UCP1 and are transported in both direction to chaperone only protons across the membrane, which would fit a strict exchange carrier transport mechanism.

Notably, the cycling and shuttling models make different hypothesis on the binding of fatty acids. The cycling model [118, 271, 272] states that fatty acids bind to UCP1 only from the matrix side, and thus the protein is active only in one direction. According to the model, UCP1 acts to export fatty acid anions from the matrix, while protonated fatty acids are able to independently flip-flop across the membrane and release proton into the matrix. In contrast, the shuttling model [115] states that long chain fatty acids bind from the cytosolic side into the central cavity of UCP1 and

remain bound during the transport in either direction. However, as has been argued [117], it is unclear why protonated fatty acids would use the pathway through UCP1 aqueous cavity to enter the mitochondrial matrix, when they can easily and rapidly flip directly across a lipid bilayer independently of UCP1 [117, 121, 244, 273].

### **6.2.3 Novel UCP1 activators and possible translational avenues**

The thermostability assay screen employed in chapter 3 proved to be a potent means for screening for novel substrates and activators of UCP1. As highlighted in chapter 1 the properties of brown adipose tissue have generated much research into ways to stimulate the growth of the tissue and induce thermogenesis for therapeutic purposes. Considerable research has thus been produced trying to exploit pathways that can proliferate brown fat (e.g.  $\beta$ -adrenergic activation) and induce the browning of white fat [8, 83]. However, unless physiologically stimulated, e.g. by cold exposure, brown fat may not be present in an activated state. The direct targeting of UCP1 for activation may circumvent this issue. In a small screen, the studies in chapter 3 identified ibuprofen, a well-used licensed drug, as an activating ligand of UCP1. Drug repurposing has assumed increasing importance in recent years, and offers a faster and more cost-effective approach to identify novel safety-assessed treatments, compared to *de novo* drug discovery [274]. Using the same combination of thermostability shift screening and liposome proton transport assay it would be possible to test a library of drugs chosen systematically, based on the characteristics determined for the activators of UCP1 reported both in this thesis, such as TUG-891 and ibuprofen, and the wider literature, such as many retinoids. Testing molecules with high  $\log P$  (hydrophobicity) and a carboxylate with a sufficiently high  $pK_a$  ( $>4$ ) to allow protonation at physiologically relevant pH could lead to the identification of other novel activators among small drug and drug-like molecules.

### **6.2.4 Homology models and AlphaFold models of UCP1**

Recently a new computational method for the *de novo* modelling of protein 3D structures has been developed, AlphaFold [275, 276]. The latest version, AlphaFold2, was found to be the most precise *de novo* modelling software in the latest CASP (Critical Assessment of Structure Prediction), a biyearly community experiment where participants submit computed structures for a group of modelling targets, and are then independently assessed. AlphaFold2-generated models had

the top results, with a RMSD (Root Mean Square Deviation) of about 1.5 Å to the target structure [275]. UCP1 models for the three isoforms analysed in this thesis are present in the database of AlphaFold. However, as of the month of June 2022, the UCP1 models available in the AlphaFold database are in the c-state only. The AlphaFold models seem to only differ slightly in the kink of the helices, and when they are superimposed and aligned, the RMSD of the AlphaFold models with the homology models generated for chapter 5 is relatively low, between 1.5 and 2 Å for all three isoforms (1.64 Å for HsUCP1, 1.71 Å for MmUCP1 and 1.74 Å for OaUCP1). For comparison, when modelling the same target protein in the latest CASP, CASP14, AlphaFold2 models presented a RMSD of about 2 Å with the models generated by the best other softwares for *de novo* protein prediction [275]. Moreover, when inspected in UCSF Chimera, important features in this conformation, such as the matrix salt bridge network, alongside the glutamine braces, appear to be modelled similarly to the chapter 5 homology models. Another important structural feature, the putative substrate binding site of UCP1 (the arginine triplet R<sup>84</sup>-R<sup>183</sup>-R<sup>277</sup>) is also modelled as in the chapter 5 models, with the lateral chains of the three residues pointing inward inside the protein cavity. Assessing the quality of the AlphaFold models with MolProbity, as done for the models generated for chapter 5, reveals that the AlphaFold models are also of good quality (0.62 for HsUCP1, 1.06 for MmUCP1, and 2.34 for OaUCP1). In conclusion the AlphaFold models seem to have modelled reasonably the key carrier features of the c-state of UCP1, in a similar manner to the homology models presented in chapter 5, but, crucially, do not include the m-state conformation of UCP1.

## 7. References

1. Hughes, D.A., M. Jastroch, M. Stoneking, and M. Klingenspor, *Molecular evolution of UCP1 and the evolutionary history of mammalian non-shivering thermogenesis*. BMC Evol Biol, 2009. **9**: p. 4.
2. Cannon, B. and J. Nedergaard, *Brown adipose tissue: function and physiological significance*. Physiol Rev, 2004. **84**(1): p. 277-359.
3. Golozoubova, V., E. Hohtola, A. Matthias, A. Jacobsson, B. Cannon, and J. Nedergaard, *Only UCP1 can mediate adaptive nonshivering thermogenesis in the cold*. Faseb j, 2001. **15**(11): p. 2048-50.
4. Nedergaard, J., V. Golozoubova, A. Matthias, A. Asadi, A. Jacobsson, and B. Cannon, *UCP1: the only protein able to mediate adaptive non-shivering thermogenesis and metabolic inefficiency*. Biochim Biophys Acta, 2001. **1504**(1): p. 82-106.
5. Jastroch, M., V. Hirschberg, and M. Klingenspor, *Functional characterization of UCP1 in mammalian HEK293 cells excludes mitochondrial uncoupling artefacts and reveals no contribution to basal proton leak*. Biochim Biophys Acta, 2012. **1817**(9): p. 1660-70.
6. Shabalina, I.G., M. Ost, N. Petrovic, M. Vrbacky, J. Nedergaard, and B. Cannon, *Uncoupling protein-1 is not leaky*. Biochim Biophys Acta, 2010. **1797**(6-7): p. 773-84.
7. Trayhurn, P., *Origins and early development of the concept that brown adipose tissue thermogenesis is linked to energy balance and obesity*. Biochimie, 2017. **134**: p. 62-70.
8. Vargas-Castillo, A., R. Fuentes-Romero, L.A. Rodriguez-Lopez, N. Torres, and A.R. Tovar, *Understanding the Biology of Thermogenic Fat: Is Browning A New Approach to the Treatment of Obesity?* Arch Med Res, 2017. **48**(5): p. 401-413.
9. Cannon, B. and J. Nedergaard, *Developmental biology: Neither fat nor flesh*. Nature, 2008. **454**(7207): p. 947-948.
10. Smith, R.E. and R.J. Hock, *Brown fat: thermogenic effector of arousal in hibernators*. Science, 1963. **140**(3563): p. 199-200.
11. Smalley, R.L. and R.L. Dryer, *Brown fat: thermogenic effect during arousal from hibernation in the bat*. Science, 1963. **140**(3573): p. 1333-4.
12. Oelkrug, R., E.T. Polymeropoulos, and M. Jastroch, *Brown adipose tissue: physiological function and evolutionary significance*. J Comp Physiol B, 2015. **185**(6): p. 587-606.
13. Cannon, B. and O. Lindberg, *Mitochondria from brown adipose tissue: isolation and properties*. Methods in enzymology, 1979. **55**: p. 65-78.
14. Symonds, M.E., M. Pope, and H. Budge, *The Ontogeny of Brown Adipose Tissue*. Annu Rev Nutr, 2015. **35**: p. 295-320.
15. Jastroch, M., R. Oelkrug, and S. Keipert, *Insights into brown adipose tissue evolution and function from non-model organisms*. J Exp Biol, 2018. **221**(Pt Suppl 1).
16. Bal, N.C., S. Singh, F.C.G. Reis, S.K. Maurya, S. Pani, L.A. Rowland, and M. Periasamy, *Both brown adipose tissue and skeletal muscle thermogenesis processes are activated during mild to severe cold adaptation in mice*. J Biol Chem, 2017. **292**(40): p. 16616-16625.
17. Sacks, H. and M.E. Symonds, *Anatomical locations of human brown adipose tissue: functional relevance and implications in obesity and type 2 diabetes*. Diabetes, 2013. **62**(6): p. 1783-90.
18. Heaton, J.M., *The distribution of brown adipose tissue in the human*. J Anat, 1972. **112**(Pt 1): p. 35-9.
19. Nedergaard, J., T. Bengtsson, and B. Cannon, *Unexpected evidence for active brown adipose tissue in adult humans*. Am J Physiol Endocrinol Metab, 2007. **293**(2): p. E444-52.
20. Cypess, A.M., S. Lehman, G. Williams, I. Tal, D. Rodman, A.B. Goldfine, F.C. Kuo, E.L. Palmer, Y.H. Tseng, A. Doria, G.M. Kolodny, and C.R. Kahn, *Identification and importance of brown adipose tissue in adult humans*. N Engl J Med, 2009. **360**(15): p. 1509-17.

21. van Marken Lichtenbelt, W.D., J.W. Vanhomerig, N.M. Smulders, J.M. Drossaerts, G.J. Kemerink, N.D. Bouvy, P. Schrauwen, and G.J. Teule, *Cold-activated brown adipose tissue in healthy men*. *N Engl J Med*, 2009. **360**(15): p. 1500-8.
22. Virtanen, K.A., M.E. Lidell, J. Orava, M. Heglind, R. Westergren, T. Niemi, M. Taittonen, J. Laine, N.J. Savisto, S. Enerback, and P. Nuutila, *Functional brown adipose tissue in healthy adults*. *N Engl J Med*, 2009. **360**(15): p. 1518-25.
23. Hess, S., B.A. Blomberg, H.J. Zhu, P.F. Hoiland-Carlsen, and A. Alavi, *The pivotal role of FDG-PET/CT in modern medicine*. *Acad Radiol*, 2014. **21**(2): p. 232-49.
24. Leitner, B.P., S. Huang, R.J. Brychta, C.J. Duckworth, A.S. Baskin, S. McGehee, I. Tal, W. Dieckmann, G. Gupta, G.M. Kolodny, K. Pacak, P. Herscovitch, A.M. Cypess, and K.Y. Chen, *Mapping of human brown adipose tissue in lean and obese young men*. *Proc Natl Acad Sci U S A*, 2017. **114**(32): p. 8649-8654.
25. Cypess, A.M., A.P. White, C. Vernochet, T.J. Schulz, R. Xue, C.A. Sass, T.L. Huang, C. Roberts-Toler, L.S. Weiner, C. Sze, A.T. Chacko, L.N. Deschamps, L.M. Herder, N. Truchan, A.L. Glasgow, A.R. Holman, A. Gavrilu, P.O. Hasselgren, M.A. Mori, M. Molla, and Y.H. Tseng, *Anatomical localization, gene expression profiling and functional characterization of adult human neck brown fat*. *Nat Med*, 2013. **19**(5): p. 635-9.
26. Symonds, M.E., *Adipose tissue biology*. 2017: New York : Springer, 2017.
27. Cannon, B. and J. Nedergaard, *Cell biology: Neither brown nor white*. *Nature*, 2012. **488**(7411): p. 286-7.
28. Lidell, M.E., M.J. Betz, and S. Enerback, *Two types of brown adipose tissue in humans*. *Adipocyte*, 2014. **3**(1): p. 63-6.
29. Wu, J., P. Bostrom, L.M. Sparks, L. Ye, J.H. Choi, A.H. Giang, M. Khandekar, K.A. Virtanen, P. Nuutila, G. Schaart, K. Huang, H. Tu, W.D. van Marken Lichtenbelt, J. Hoeks, S. Enerback, P. Schrauwen, and B.M. Spiegelman, *Beige adipocytes are a distinct type of thermogenic fat cell in mouse and human*. *Cell*, 2012. **150**(2): p. 366-76.
30. Lidell, M.E., M.J. Betz, O. Dahlqvist Leinhard, M. Heglind, L. Elander, M. Slawik, T. Mussack, D. Nilsson, T. Romu, P. Nuutila, K.A. Virtanen, F. Beuschlein, A. Persson, M. Borga, and S. Enerback, *Evidence for two types of brown adipose tissue in humans*. *Nat Med*, 2013. **19**(5): p. 631-4.
31. Cannon, B., J.M.A. de Jong, A.W. Fischer, J. Nedergaard, and N. Petrovic, *Human brown adipose tissue: Classical brown rather than brite/beige?* *Exp Physiol*, 2020. **105**(8): p. 1191-1200.
32. Symonds, M.E., P. Aldiss, M. Pope, and H. Budge, *Recent advances in our understanding of brown and beige adipose tissue: the good fat that keeps you healthy*. *F1000Res*, 2018. **7**.
33. Timmons, J.A., K. Wennmalm, O. Larsson, T.B. Walden, T. Lassmann, N. Petrovic, D.L. Hamilton, R.E. Gimeno, C. Wahlestedt, K. Baar, J. Nedergaard, and B. Cannon, *Myogenic gene expression signature establishes that brown and white adipocytes originate from distinct cell lineages*. *Proc Natl Acad Sci U S A*, 2007. **104**(11): p. 4401-6.
34. Seale, P., B. Bjork, W. Yang, S. Kajimura, S. Chin, S. Kuang, A. Scime, S. Devarakonda, H.M. Conroe, H. Erdjument-Bromage, P. Tempst, M.A. Rudnicki, D.R. Beier, and B.M. Spiegelman, *PRDM16 controls a brown fat/skeletal muscle switch*. *Nature*, 2008. **454**(7207): p. 961-7.
35. Rosenwald, M. and C. Wolfrum, *The origin and definition of brite versus white and classical brown adipocytes*. *Adipocyte*, 2014. **3**(1): p. 4-9.
36. Lee, Y.H., A.P. Petkova, E.P. Mottillo, and J.G. Granneman, *In vivo identification of bipotential adipocyte progenitors recruited by beta3-adrenoceptor activation and high-fat feeding*. *Cell Metab*, 2012. **15**(4): p. 480-91.
37. Nedergaard, J. and B. Cannon, *The changed metabolic world with human brown adipose tissue: therapeutic visions*. *Cell Metab*, 2010. **11**(4): p. 268-72.
38. Cannon, B., J. Nedergaard, J.M. Lundberg, T. Hökfelt, L. Terenius, and M. Goldstein, *'Neuropeptide tyrosine' (NPY) is co-stored with noradrenaline in vascular but not in*

- parenchymal sympathetic nerves of brown adipose tissue*. *Exp Cell Res*, 1986. **164**(2): p. 546-50.
39. Ikeda, K., P. Maretich, and S. Kajimura, *The Common and Distinct Features of Brown and Beige Adipocytes*. *Trends Endocrinol Metab*, 2018. **29**(3): p. 191-200.
  40. Collins, S. and R.S. Surwit, *The beta-adrenergic receptors and the control of adipose tissue metabolism and thermogenesis*. *Recent Prog Horm Res*, 2001. **56**: p. 309-28.
  41. Blondin, D.P., S. Nielsen, E.N. Kuipers, M.C. Severinsen, V.H. Jensen, S. Miard, N.Z. Jespersen, S. Kooijman, M.R. Boon, M. Fortin, S. Phoenix, F. Frisch, B. Guérin, E. Turcotte É, F. Haman, D. Richard, F. Picard, P.C.N. Rensen, C. Scheele, and A.C. Carpentier, *Human Brown Adipocyte Thermogenesis Is Driven by  $\beta$ 2-AR Stimulation*. *Cell Metab*, 2020. **32**(2): p. 287-300.e7.
  42. Cannon, B. and J. Nedergaard, *Studies of Thermogenesis and Mitochondrial Function in Adipose Tissues*, in *Adipose Tissue Protocols*, K. Yang, Editor. 2008, Humana Press: Totowa, NJ. p. 109-121.
  43. Shih, M.F. and P.V. Taberner, *Selective activation of brown adipocyte hormone-sensitive lipase and cAMP production in the mouse by beta 3-adrenoceptor agonists*. *Biochem Pharmacol*, 1995. **50**(5): p. 601-8.
  44. Schreiber, R., C. Diwoky, G. Schoiswohl, U. Feiler, N. Wongsiriroj, M. Abdellatif, D. Kolb, J. Hoeks, E.E. Kershaw, S. Sedej, P. Schrauwen, G. Haemmerle, and R. Zechner, *Cold-Induced Thermogenesis Depends on ATGL-Mediated Lipolysis in Cardiac Muscle, but Not Brown Adipose Tissue*. *Cell Metab*, 2017. **26**(5): p. 753-763 e7.
  45. Chaudhry, A. and J.G. Granneman, *Differential regulation of functional responses by beta-adrenergic receptor subtypes in brown adipocytes*. *Am J Physiol*, 1999. **277**(1 Pt 2): p. R147-53.
  46. Klingenspor, M., *Cold-induced recruitment of brown adipose tissue thermogenesis*. *Exp Physiol*, 2003. **88**(1): p. 141-8.
  47. Klingenberg, M., K.S. Echtay, M. Bienengraeber, E. Winkler, and S.G. Huang, *Structure-function relationship in UCP1*. *Int J Obes Relat Metab Disord*, 1999. **23 Suppl 6**: p. S24-9.
  48. Lin, C.S. and M. Klingenberg, *Characteristics of the isolated purine nucleotide binding protein from brown fat mitochondria*. *Biochemistry*, 1982. **21**(12): p. 2950-6.
  49. Bast-Habersbrunner, A. and T. Fromme, *Purine Nucleotides in the Regulation of Brown Adipose Tissue Activity*. *Frontiers in Endocrinology*, 2020. **11**(118).
  50. Kalinovich, A.V., J.M. de Jong, B. Cannon, and J. Nedergaard, *UCP1 in adipose tissues: two steps to full browning*. *Biochimie*, 2017. **134**: p. 127-137.
  51. Puigserver, P., D. Herron, M. Gianotti, A. Palou, B. Cannon, and J. Nedergaard, *Induction and degradation of the uncoupling protein thermogenin in brown adipocytes in vitro and in vivo. Evidence for a rapidly degradable pool*. *Biochem J*, 1992. **284 ( Pt 2)**(Pt 2): p. 393-8.
  52. Cao, W., K.W. Daniel, J. Robidoux, P. Puigserver, A.V. Medvedev, X. Bai, L.M. Floering, B.M. Spiegelman, and S. Collins, *p38 mitogen-activated protein kinase is the central regulator of cyclic AMP-dependent transcription of the brown fat uncoupling protein 1 gene*. *Mol Cell Biol*, 2004. **24**(7): p. 3057-67.
  53. Kozak, U.C., J. Kopecky, J. Teisinger, S. Enerback, B. Boyer, and L.P. Kozak, *An upstream enhancer regulating brown-fat-specific expression of the mitochondrial uncoupling protein gene*. *Mol Cell Biol*, 1994. **14**(1): p. 59-67.
  54. Villarroya, F., M. Peyrou, and M. Giralt, *Transcriptional regulation of the uncoupling protein-1 gene*. *Biochimie*, 2017. **134**: p. 86-92.
  55. Collins, S., E. Yehuda-Shnaidman, and H. Wang, *Positive and negative control of Ucp1 gene transcription and the role of beta-adrenergic signaling networks*. *Int J Obes (Lond)*, 2010. **34 Suppl 1**: p. S28-33.
  56. Lanni, A., M. Moreno, A. Lombardi, and F. Goglia, *Thyroid hormone and uncoupling proteins*. *FEBS Lett*, 2003. **543**(1-3): p. 5-10.

57. Silva, J.E., *The thermogenic effect of thyroid hormone and its clinical implications*. Ann Intern Med, 2003. **139**(3): p. 205-13.
58. Roesler, A. and L. Kazak, *UCP1-independent thermogenesis*. The Biochemical journal, 2020. **477**(3): p. 709-725.
59. Kazak, L., E.T. Chouchani, M.P. Jedrychowski, B.K. Erickson, K. Shinoda, P. Cohen, R. Vetrivelan, G.Z. Lu, D. Laznik-Bogoslavski, S.C. Hasenfuss, S. Kajimura, S.P. Gygi, and B.M. Spiegelman, *A creatine-driven substrate cycle enhances energy expenditure and thermogenesis in beige fat*. Cell, 2015. **163**(3): p. 643-55.
60. Wyss, M. and R. Kaddurah-Daouk, *Creatine and creatinine metabolism*. Physiol Rev, 2000. **80**(3): p. 1107-213.
61. Mottillo, E.P., P. Balasubramanian, Y.-H. Lee, C. Weng, E.E. Kershaw, and J.G. Granneman, *Coupling of lipolysis and de novo lipogenesis in brown, beige, and white adipose tissues during chronic  $\beta_2$ -adrenergic receptor activation*. Journal of Lipid Research, 2014. **55**(11): p. 2276-2286.
62. Bartelt, A., O.T. Bruns, R. Reimer, H. Hohenberg, H. Ittrich, K. Peldschus, M.G. Kaul, U.I. Tromsdorf, H. Weller, C. Waurisch, A. Eychmuller, P.L. Gordts, F. Rinninger, K. Bruegelmann, B. Freund, P. Nielsen, M. Merkel, and J. Heeren, *Brown adipose tissue activity controls triglyceride clearance*. Nat Med, 2011. **17**(2): p. 200-5.
63. Braun, K., J. Oeckl, J. Westermeier, Y. Li, and M. Klingenspor, *Non-adrenergic control of lipolysis and thermogenesis in adipose tissues*. J Exp Biol, 2018. **221**(Pt Suppl 1).
64. Yu, X.X., D.A. Lewin, W. Forrest, and S.H. Adams, *Cold elicits the simultaneous induction of fatty acid synthesis and  $\beta$ -oxidation in murine brown adipose tissue: prediction from differential gene expression and confirmation in vivo*. The FASEB Journal, 2002. **16**(2): p. 155-168.
65. Ikeda, K., Q. Kang, T. Yoneshiro, J.P. Camporez, H. Maki, M. Homma, K. Shinoda, Y. Chen, X. Lu, P. Maretich, K. Tajima, K.M. Ajuwon, T. Soga, and S. Kajimura, *UCP1-independent signaling involving SERCA2b-mediated calcium cycling regulates beige fat thermogenesis and systemic glucose homeostasis*. Nat Med, 2017. **23**(12): p. 1454-1465.
66. Periasamy, M., S.K. Maurya, S.K. Sahoo, S. Singh, F.C.G. Reis, and N.C. Bal, *Role of SERCA Pump in Muscle Thermogenesis and Metabolism*, in *Comprehensive Physiology*. p. 879-890.
67. Jastroch, M., A.S. Divakaruni, S. Mookerjee, J.R. Treberg, and M.D. Brand, *Mitochondrial proton and electron leaks*. Essays Biochem, 2010. **47**: p. 53-67.
68. Divakaruni, A.S. and M.D. Brand, *The regulation and physiology of mitochondrial proton leak*. Physiology (Bethesda), 2011. **26**(3): p. 192-205.
69. Bertholet, A.M., E.T. Chouchani, L. Kazak, A. Angelin, A. Fedorenko, J.Z. Long, S. Vidoni, R. Garrity, J. Cho, N. Terada, D.C. Wallace, B.M. Spiegelman, and Y. Kirichok, *H(+) transport is an integral function of the mitochondrial ADP/ATP carrier*. Nature, 2019. **571**(7766): p. 515-520.
70. Brand, M.D., J.L. Pakay, A. Ocloo, J. Kokoszka, D.C. Wallace, P.S. Brookes, and E.J. Cornwall, *The basal proton conductance of mitochondria depends on adenine nucleotide translocase content*. Biochem J, 2005. **392**(Pt 2): p. 353-62.
71. Harper, J.A., K. Dickinson, and M.D. Brand, *Mitochondrial uncoupling as a target for drug development for the treatment of obesity*. Obes Rev, 2001. **2**(4): p. 255-65.
72. Grundlingh, J., P.I. Dargan, M. El-Zanfaly, and D.M. Wood, *2,4-dinitrophenol (DNP): a weight loss agent with significant acute toxicity and risk of death*. J Med Toxicol, 2011. **7**(3): p. 205-12.
73. Lizcano, F., *The Beige Adipocyte as a Therapy for Metabolic Diseases*. International journal of molecular sciences, 2019. **20**(20): p. 5058.
74. Chouchani, E.T., L. Kazak, and B.M. Spiegelman, *New Advances in Adaptive Thermogenesis: UCP1 and Beyond*. Cell Metab, 2018.

75. Rothwell, N.J. and M.J. Stock, *A role for brown adipose tissue in diet-induced thermogenesis*. Nature, 1979. **281**(5726): p. 31-5.
76. Feldmann, H.M., V. Golozoubova, B. Cannon, and J. Nedergaard, *UCP1 ablation induces obesity and abolishes diet-induced thermogenesis in mice exempt from thermal stress by living at thermoneutrality*. Cell Metab, 2009. **9**(2): p. 203-9.
77. Kopecky, J., G. Clarke, S. Enerback, B. Spiegelman, and L.P. Kozak, *Expression of the mitochondrial uncoupling protein gene from the aP2 gene promoter prevents genetic obesity*. J Clin Invest, 1995. **96**(6): p. 2914-23.
78. Lidell, M.E., M.J. Betz, and S. Enerback, *Brown adipose tissue and its therapeutic potential*. J Intern Med, 2014. **276**(4): p. 364-77.
79. Geerling, J.J., M.R. Boon, G.C. van der Zon, S.A. van den Berg, A.M. van den Hoek, M. Lombes, H.M. Princen, L.M. Havekes, P.C. Rensen, and B. Guigas, *Metformin lowers plasma triglycerides by promoting VLDL-triglyceride clearance by brown adipose tissue in mice*. Diabetes, 2014. **63**(3): p. 880-91.
80. Chondronikola, M., E. Volpi, E. Børsheim, C. Porter, P. Annamalai, S. Enerbäck, M.E. Lidell, M.K. Saraf, S.M. Labbe, N.M. Hurren, C. Yfanti, T. Chao, C.R. Andersen, F. Cesani, H. Hawkins, and L.S. Sidossis, *Brown adipose tissue improves whole-body glucose homeostasis and insulin sensitivity in humans*. Diabetes, 2014. **63**(12): p. 4089-99.
81. Nedergaard, J., T. Bengtsson, and B. Cannon, *New powers of brown fat: fighting the metabolic syndrome*. Cell Metab, 2011. **13**(3): p. 238-40.
82. Pico, C., M.L. Bonet, and A. Palou, *Stimulation of uncoupling protein synthesis in white adipose tissue of mice treated with the beta 3-adrenergic agonist CGP-12177*. Cell Mol Life Sci, 1998. **54**(2): p. 191-5.
83. Bonet, M.L., P. Oliver, and A. Palou, *Pharmacological and nutritional agents promoting browning of white adipose tissue*. Biochim Biophys Acta, 2013. **1831**(5): p. 969-85.
84. Himms-Hagen, J., A. Melnyk, M.C. Zingaretti, E. Ceresi, G. Barbatelli, and S. Cinti, *Multilocular fat cells in WAT of CL-316243-treated rats derive directly from white adipocytes*. Am J Physiol Cell Physiol, 2000. **279**(3): p. C670-81.
85. Jockers, R., T. Issad, V. Zilberfarb, P. de Coppet, S. Marullo, and A.D. Strosberg, *Desensitization of the beta-adrenergic response in human brown adipocytes*. Endocrinology, 1998. **139**(6): p. 2676-84.
86. Cypess, A.M., L.S. Weiner, C. Roberts-Toler, E. Franquet Elia, S.H. Kessler, P.A. Kahn, J. English, K. Chatman, S.A. Trauger, A. Doria, and G.M. Kolodny, *Activation of human brown adipose tissue by a beta3-adrenergic receptor agonist*. Cell Metab, 2015. **21**(1): p. 33-8.
87. Lee, P., S. Smith, J. Linderman, A.B. Courville, R.J. Brychta, W. Dieckmann, C.D. Werner, K.Y. Chen, and F.S. Celi, *Temperature-acclimated brown adipose tissue modulates insulin sensitivity in humans*. Diabetes, 2014. **63**(11): p. 3686-98.
88. Hanssen, M.J., J. Hoeks, B. Brans, A.A. van der Lans, G. Schaart, J.J. van den Driessche, J.A. Jörgensen, M.V. Boekschoten, M.K. Hesselink, B. Havekes, S. Kersten, F.M. Mottaghy, W.D. van Marken Lichtenbelt, and P. Schrauwen, *Short-term cold acclimation improves insulin sensitivity in patients with type 2 diabetes mellitus*. Nat Med, 2015. **21**(8): p. 863-5.
89. Hanssen, M.J., A.A. van der Lans, B. Brans, J. Hoeks, K.M. Jardon, G. Schaart, F.M. Mottaghy, P. Schrauwen, and W.D. van Marken Lichtenbelt, *Short-term Cold Acclimation Recruits Brown Adipose Tissue in Obese Humans*. Diabetes, 2016. **65**(5): p. 1179-89.
90. Ricquier, D., *UCP1, the mitochondrial uncoupling protein of brown adipocyte: A personal contribution and a historical perspective*. Biochimie, 2017. **134**: p. 3-8.
91. Nicholls, D.G., *The hunt for the molecular mechanism of brown fat thermogenesis*. Biochimie, 2017. **134**: p. 9-18.
92. Nicholls, D.G. and E. Rial, *A history of the first uncoupling protein, UCP1*. J Bioenerg Biomembr, 1999. **31**(5): p. 399-406.

93. Lindberg, O., J. de Pierre, E. Rylander, and B.A. Afzelius, *Studies of the mitochondrial energy-transfer system of brown adipose tissue*. J Cell Biol, 1967. **34**(1): p. 293-310.
94. Nicholls, D.G. and O. Lindberg, *Brown-adipose-tissue mitochondria. The influence of albumin and nucleotides on passive ion permeabilities*. Eur J Biochem, 1973. **37**(3): p. 523-30.
95. Ricquier, D. and J.C. Kader, *Mitochondrial protein alteration in active brown fat: a sodium dodecyl sulfate-polyacrylamide gel electrophoretic study*. Biochem Biophys Res Commun, 1976. **73**(3): p. 577-83.
96. Heaton, G.M., R.J. Wagenvoort, A. Kemp, Jr., and D.G. Nicholls, *Brown-adipose-tissue mitochondria: photoaffinity labelling of the regulatory site of energy dissipation*. Eur J Biochem, 1978. **82**(2): p. 515-21.
97. Ricquier, D., C. Gervais, J.C. Kader, and P. Hemon, *Partial purification by guanosine-5'-diphosphate-agarose affinity chromatography of the 32,000 molecular weight polypeptide from mitochondria of brown adipose tissue*. FEBS Lett, 1979. **101**(1): p. 35-8.
98. Lin, C.S. and M. Klingenberg, *Isolation of the uncoupling protein from brown adipose tissue mitochondria*. FEBS Lett, 1980. **113**(2): p. 299-303.
99. Riccio, P., H. Aquila, and M. Klingenberg, *Purification of the carboxy-atractylate binding protein from mitochondria*. FEBS Lett, 1975. **56**(1): p. 133-8.
100. Ricquier, D., J.P. Barlet, J.M. Garel, M. Combes-George, and M.P. Dubois, *An immunological study of the uncoupling protein of brown adipose tissue mitochondria*. Biochem J, 1983. **210**(3): p. 859-66.
101. Bouillaud, F., D. Ricquier, J. Thibault, and J. Weissenbach, *Molecular approach to thermogenesis in brown adipose tissue: cDNA cloning of the mitochondrial uncoupling protein*. Proc Natl Acad Sci U S A, 1985. **82**(2): p. 445-8.
102. Bouillaud, F., S. Raimbault, and D. Ricquier, *The gene for rat uncoupling protein: complete sequence, structure of primary transcript and evolutionary relationship between exons*. Biochem Biophys Res Commun, 1988. **157**(2): p. 783-92.
103. Cassard, A.M., F. Bouillaud, M.G. Mattei, E. Hentz, S. Raimbault, M. Thomas, and D. Ricquier, *Human uncoupling protein gene: structure, comparison with rat gene, and assignment to the long arm of chromosome 4*. J Cell Biochem, 1990. **43**(3): p. 255-64.
104. Aquila, H., T.A. Link, and M. Klingenberg, *The uncoupling protein from brown fat mitochondria is related to the mitochondrial ADP/ATP carrier. Analysis of sequence homologies and of folding of the protein in the membrane*. Embo j, 1985. **4**(9): p. 2369-76.
105. Klingenberg, M. and E. Winkler, *The reconstituted isolated uncoupling protein is a membrane potential driven H<sup>+</sup> translocator*. Embo j, 1985. **4**(12): p. 3087-92.
106. Jezek, P., Z. Drahota, and K. Ring, *The activating effect of fatty acid on the mitochondrial uncoupling protein reconstituted in liposomes*. J Lipid Mediat, 1990. **2**(2): p. 85-94.
107. Jezek, P., D.E. Orosz, M. Modriansky, and K.D. Garlid, *Transport of anions and protons by the mitochondrial uncoupling protein and its regulation by nucleotides and fatty acids. A new look at old hypotheses*. J Biol Chem, 1994. **269**(42): p. 26184-90.
108. Rousset, S., M.-C. Alves-Guerra, J. Mozo, B. Miroux, A.-M. Cassard-Doulcier, F. Bouillaud, and D. Ricquier, *The Biology of Mitochondrial Uncoupling Proteins*. Diabetes, 2004. **53**(suppl 1): p. S130-S135.
109. Echtay, K.S., E. Winkler, and M. Klingenberg, *Coenzyme Q is an obligatory cofactor for uncoupling protein function*. Nature, 2000. **408**(6812): p. 609.
110. Echtay, K.S., D. Rousset, J. St-Pierre, M.B. Jekabsons, S. Cadenas, J.A. Stuart, J.A. Harper, S.J. Roebuck, A. Morrison, S. Pickering, J.C. Clapham, and M.D. Brand, *Superoxide activates mitochondrial uncoupling proteins*. Nature, 2002. **415**(6867): p. 96-9.
111. Crichton, P.G., Y. Lee, and E.R. Kunji, *The molecular features of uncoupling protein 1 support a conventional mitochondrial carrier-like mechanism*. Biochimie, 2017. **134**: p. 35-50.

112. Shabalina, I.G., A. Jacobsson, B. Cannon, and J. Nedergaard, *Native UCP1 displays simple competitive kinetics between the regulators purine nucleotides and fatty acids*. J Biol Chem, 2004. **279**(37): p. 38236-48.
113. Winkler, E. and M. Klingenberg, *Effect of fatty acids on H<sup>+</sup> transport activity of the reconstituted uncoupling protein*. J Biol Chem, 1994. **269**(4): p. 2508-15.
114. Garlid, K.D., M. Jabůrek, and P. Ježek, *The mechanism of proton transport mediated by mitochondrial uncoupling proteins*. FEBS letters, 1998. **438**(1-2): p. 10-14.
115. Fedorenko, A., P.V. Lishko, and Y. Kirichok, *Mechanism of fatty-acid-dependent UCP1 uncoupling in brown fat mitochondria*. Cell, 2012. **151**(2): p. 400-413.
116. Winkler, E. and M. Klingenberg, *An improved procedure for reconstitution of the uncoupling protein and in-depth analysis of H<sup>+</sup>/OH<sup>-</sup> transport*. European Journal of Biochemistry, 1992. **207**(1): p. 135-145.
117. Jezek, P., M. Jaburek, and K.D. Garlid, *Channel character of uncoupling protein-mediated transport*. FEBS Lett, 2010. **584**(10): p. 2135-41.
118. Skulachev, V.P., *Fatty acid circuit as a physiological mechanism of uncoupling of oxidative phosphorylation*. FEBS Lett, 1991. **294**(3): p. 158-62.
119. Garlid, K.D., D.E. Orosz, M. Modriansky, S. Vassanelli, and P. Jezek, *On the mechanism of fatty acid-induced proton transport by mitochondrial uncoupling protein*. J Biol Chem, 1996. **271**(5): p. 2615-20.
120. Wei, C. and A. Pohorille, *Flip-flop of oleic acid in a phospholipid membrane: rate and mechanism*. J Phys Chem B, 2014. **118**(45): p. 12919-26.
121. Hamilton, J.A., *Transport of fatty acids across membranes by the diffusion mechanism*. Prostaglandins, Leukotrienes and Essential Fatty Acids, 1999. **60**(5): p. 291-297.
122. Garlid, K.D., M. Jaburek, and P. Jezek, *Mechanism of uncoupling protein action*. Biochem Soc Trans, 2001. **29**(Pt 6): p. 803-6.
123. Bertholet, A.M. and Y. Kirichok, *UCP1: A transporter for H<sup>+</sup> and fatty acid anions*. Biochimie, 2017. **134**: p. 28-34.
124. Echtay, K.S., T.C. Esteves, J.L. Pakay, M.B. Jekabsons, A.J. Lambert, M. Portero-Otín, R. Pamplona, A.J. Vidal-Puig, S. Wang, S.J. Roebuck, and M.D. Brand, *A signalling role for 4-hydroxy-2-nonenal in regulation of mitochondrial uncoupling*. Embo j, 2003. **22**(16): p. 4103-10.
125. Echtay, K.S., J.L. Pakay, T.C. Esteves, and M.D. Brand, *Hydroxynonenal and uncoupling proteins: a model for protection against oxidative damage*. Biofactors, 2005. **24**(1-4): p. 119-30.
126. Shabalina, I.G., N. Petrovic, T.V. Kramarova, J. Hoeks, B. Cannon, and J. Nedergaard, *UCP1 and defense against oxidative stress. 4-Hydroxy-2-nonenal effects on brown fat mitochondria are uncoupling protein 1-independent*. J Biol Chem, 2006. **281**(20): p. 13882-93.
127. Chouchani, E.T., L. Kazak, M.P. Jedrychowski, G.Z. Lu, B.K. Erickson, J. Szpyt, K.A. Pierce, D. Laznik-Bogoslavski, R. Vetrivelan, C.B. Clish, A.J. Robinson, S.P. Gygi, and B.M. Spiegelman, *Mitochondrial ROS regulate thermogenic energy expenditure and sulfenylation of UCP1*. Nature, 2016. **532**: p. 112.
128. Arechaga, I., S. Raimbault, S. Prieto, C. Levi-Meyrueis, P. Zaragoza, B. Miroux, D. Ricquier, F. Bouillaud, and E. Rial, *Cysteine residues are not essential for uncoupling protein function*. Biochemical Journal, 1993. **296**(3): p. 693-700.
129. Bamber, L., M. Harding, M. Monne, D.J. Slotboom, and E.R. Kunji, *The yeast mitochondrial ADP/ATP carrier functions as a monomer in mitochondrial membranes*. Proc Natl Acad Sci U S A, 2007. **104**(26): p. 10830-4.
130. Aquila, H., T.A. Link, and M. Klingenberg, *Solute carriers involved in energy transfer of mitochondria form a homologous protein family*. FEBS Lett, 1987. **212**(1): p. 1-9.

131. Kunji, E.R., *The role and structure of mitochondrial carriers*. FEBS Lett, 2004. **564**(3): p. 239-44.
132. Palmieri, F., *The mitochondrial transporter family SLC25: identification, properties and physiopathology*. Mol Aspects Med, 2013. **34**(2-3): p. 465-84.
133. Ruprecht, J.J. and E.R.S. Kunji, *The SLC25 Mitochondrial Carrier Family: Structure and Mechanism*. Trends in Biochemical Sciences, 2019.
134. Pebay-Peyroula, E., C. Dahout-Gonzalez, R. Kahn, V. Trezeguet, G.J. Lauquin, and G. Brandolin, *Structure of mitochondrial ADP/ATP carrier in complex with carboxyatractyloside*. Nature, 2003. **426**(6962): p. 39-44.
135. Ruprecht, J.J., A.M. Hellawell, M. Harding, P.G. Crichton, A.J. McCoy, and E.R. Kunji, *Structures of yeast mitochondrial ADP/ATP carriers support a domain-based alternating-access transport mechanism*. Proc Natl Acad Sci U S A, 2014. **111**(4): p. E426-34.
136. Ruprecht, J.J., M.S. King, T. Zogg, A.A. Aleksandrova, E. Pardon, P.G. Crichton, J. Steyaert, and E.R.S. Kunji, *The Molecular Mechanism of Transport by the Mitochondrial ADP/ATP Carrier*. Cell, 2019.
137. Robinson, A.J., C. Overy, and E.R. Kunji, *The mechanism of transport by mitochondrial carriers based on analysis of symmetry*. Proc Natl Acad Sci U S A, 2008. **105**(46): p. 17766-71.
138. Kunji, E.R. and A.J. Robinson, *The conserved substrate binding site of mitochondrial carriers*. Biochim Biophys Acta, 2006. **1757**(9-10): p. 1237-48.
139. Robinson, A.J. and E.R. Kunji, *Mitochondrial carriers in the cytoplasmic state have a common substrate binding site*. Proc Natl Acad Sci U S A, 2006. **103**(8): p. 2617-22.
140. King, M.S., M. Kerr, P.G. Crichton, R. Springett, and E.R.S. Kunji, *Formation of a cytoplasmic salt bridge network in the matrix state is a fundamental step in the transport mechanism of the mitochondrial ADP/ATP carrier*. Biochim Biophys Acta, 2016. **1857**(1): p. 14-22.
141. Springett, R., M.S. King, P.G. Crichton, and E.R.S. Kunji, *Modelling the free energy profile of the mitochondrial ADP/ATP carrier*. Biochimica et biophysica acta. Bioenergetics, 2017. **1858**(11): p. 906-914.
142. Klingenberg, M., *Ligand-protein interaction in biomembrane carriers. The induced transition fit of transport catalysis*. Biochemistry, 2005. **44**(24): p. 8563-8570.
143. Jardetzky, O., *Simple Allosteric Model for Membrane Pumps*. Nature, 1966. **211**(5052): p. 969-970.
144. Ruprecht, J.J. and E.R.S. Kunji, *Structural changes in the transport cycle of the mitochondrial ADP/ATP carrier*. Current Opinion in Structural Biology, 2019. **57**: p. 135-144.
145. Javadpour, M.M., M. Eilers, M. Groesbeek, and S.O. Smith, *Helix packing in polytopic membrane proteins: role of glycine in transmembrane helix association*. Biophys J, 1999. **77**(3): p. 1609-18.
146. Lin, C.S., H. Hackenberg, and E.M. Klingenberg, *The uncoupling protein from brown adipose tissue mitochondria is a dimer. A hydrodynamic study*. FEBS Letters, 1980. **113**(2): p. 304-306.
147. Klingenberg, M. and M. Appel, *The uncoupling protein dimer can form a disulfide cross-link between the mobile C-terminal SH groups*. Eur J Biochem, 1989. **180**(1): p. 123-31.
148. Nury, H., C. Dahout-Gonzalez, V. Trézéguet, G. Lauquin, G. Brandolin, and E. Pebay-Peyroula, *Structural basis for lipid-mediated interactions between mitochondrial ADP/ATP carrier monomers*. FEBS Lett, 2005. **579**(27): p. 6031-6.
149. Bamber, L., M. Harding, P.J. Butler, and E.R. Kunji, *Yeast mitochondrial ADP/ATP carriers are monomeric in detergents*. Proc Natl Acad Sci U S A, 2006. **103**(44): p. 16224-9.
150. Crichton, P.G., M. Harding, J.J. Ruprecht, Y. Lee, and E.R. Kunji, *Lipid, detergent, and Coomassie Blue G-250 affect the migration of small membrane proteins in blue native gels: mitochondrial carriers migrate as monomers not dimers*. J Biol Chem, 2013. **288**(30): p. 22163-73.

151. Kunji, E.R. and P.G. Crichton, *Mitochondrial carriers function as monomers*. Biochim Biophys Acta, 2010. **1797**(6-7): p. 817-31.
152. Klingenberg, M., *Nucleotide binding to uncoupling protein. Mechanism of control by protonation*. Biochemistry, 1988. **27**(2): p. 781-91.
153. Echtay, K.S., M. Bienengraeber, and M. Klingenberg, *Mutagenesis of the uncoupling protein of brown adipose tissue. Neutralization Of E190 largely abolishes pH control of nucleotide binding*. Biochemistry, 1997. **36**(27): p. 8253-60.
154. Winkler, E., E. Wachter, and M. Klingenberg, *Identification of the pH sensor for nucleotide binding in the uncoupling protein from brown adipose tissue*. Biochemistry, 1997. **36**(1): p. 148-55.
155. Klingenberg, M. and K.S. Echtay, *Uncoupling proteins: the issues from a biochemist point of view*. Biochim Biophys Acta, 2001. **1504**(1): p. 128-43.
156. Echtay, K.S., M. Bienengraeber, E. Winkler, and M. Klingenberg, *In the uncoupling protein (UCP-1) His-214 is involved in the regulation of purine nucleoside triphosphate but not diphosphate binding*. J Biol Chem, 1998. **273**(38): p. 24368-74.
157. Lee, Y., C. Willers, E.R. Kunji, and P.G. Crichton, *Uncoupling protein 1 binds one nucleotide per monomer and is stabilized by tightly bound cardiolipin*. Proceedings of the National Academy of Sciences, 2015. **112**(22): p. 6973-6978.
158. Modrianský, M., D.L. Murdza-Inglis, H.V. Patel, K.B. Freeman, and K.D. Garlid, *Identification by site-directed mutagenesis of three arginines in uncoupling protein that are essential for nucleotide binding and inhibition*. J Biol Chem, 1997. **272**(40): p. 24759-62.
159. Acoba, M.G., N. Senoo, and S.M. Claypool, *Phospholipid ebb and flow makes mitochondria go*. J Cell Biol, 2020. **219**(8).
160. Santiago, E., N. López-Moratalla, and J.F. Segovia, *Correlation between losses of mitochondrial ATPase activity and cardiolipin degradation*. Biochem Biophys Res Commun, 1973. **53**(2): p. 439-45.
161. Zhou, M., N. Morgner, N.P. Barrera, A. Politis, S.C. Isaacson, D. Matak-Vinković, T. Murata, R.A. Bernal, D. Stock, and C.V. Robinson, *Mass spectrometry of intact V-type ATPases reveals bound lipids and the effects of nucleotide binding*. Science, 2011. **334**(6054): p. 380-385.
162. Mehdipour, A.R. and G. Hummer, *Cardiolipin puts the seal on ATP synthase*. Proc Natl Acad Sci U S A, 2016. **113**(31): p. 8568-70.
163. Fry, M. and D.E. Green, *Cardiolipin requirement for electron transfer in complex I and III of the mitochondrial respiratory chain*. J Biol Chem, 1981. **256**(4): p. 1874-80.
164. Robinson, N.C., *Functional binding of cardiolipin to cytochrome c oxidase*. J Bioenerg Biomembr, 1993. **25**(2): p. 153-63.
165. Claypool, S.M., *Cardiolipin, a critical determinant of mitochondrial carrier protein assembly and function*. Biochim Biophys Acta, 2009. **1788**(10): p. 2059-68.
166. Beyer, K. and M. Klingenberg, *ADP/ATP carrier protein from beef heart mitochondria has high amounts of tightly bound cardiolipin, as revealed by 31P nuclear magnetic resonance*. Biochemistry, 1985. **24**(15): p. 3821-6.
167. Hoffmann, B., A. Stockl, M. Schlame, K. Beyer, and M. Klingenberg, *The reconstituted ADP/ATP carrier activity has an absolute requirement for cardiolipin as shown in cysteine mutants*. J Biol Chem, 1994. **269**(3): p. 1940-4.
168. Klingenberg, M., *Cardiolipin and mitochondrial carriers*. Biochim Biophys Acta, 2009. **1788**(10): p. 2048-58.
169. Crichton, P.G., Y. Lee, J.J. Ruprecht, E. Cerson, C. Thangaratnarajah, M.S. King, and E.R. Kunji, *Trends in thermostability provide information on the nature of substrate, inhibitor, and lipid interactions with mitochondrial carriers*. Journal of Biological Chemistry, 2015. **290**(13): p. 8206-8217.

170. Chakrabartty, A., J.A. Schellman, and R.L. Baldwin, *Large differences in the helix propensities of alanine and glycine*. *Nature*, 1991. **351**(6327): p. 586-8.
171. O'Neil, K.T. and W.F. DeGrado, *A thermodynamic scale for the helix-forming tendencies of the commonly occurring amino acids*. *Science*, 1990. **250**(4981): p. 646-51.
172. Bouillaud, F., E. Couplan, C. Pecqueur, and D. Ricquier, *Homologues of the uncoupling protein from brown adipose tissue (UCP1): UCP2, UCP3, BMCP1 and UCP4*. *Biochimica et Biophysica Acta (BBA) - Bioenergetics*, 2001. **1504**(1): p. 107-119.
173. Fleury, C., M. Neverova, S. Collins, S. Raimbault, O. Champigny, C. Levi-Meyrueis, F. Bouillaud, M.F. Seldin, R.S. Surwit, D. Ricquier, and C.H. Warden, *Uncoupling protein-2: a novel gene linked to obesity and hyperinsulinemia*. *Nat Genet*, 1997. **15**(3): p. 269-72.
174. Gimeno, R.E., M. Dembski, X. Weng, N. Deng, A.W. Shyjan, C.J. Gimeno, F. Iris, S.J. Ellis, E.A. Woolf, and L.A. Tartaglia, *Cloning and characterization of an uncoupling protein homolog: a potential molecular mediator of human thermogenesis*. *Diabetes*, 1997. **46**(5): p. 900-6.
175. Pecqueur, C., M.C. Alves-Guerra, C. Gelly, C. Levi-Meyrueis, E. Couplan, S. Collins, D. Ricquier, F. Bouillaud, and B. Miroux, *Uncoupling protein 2, in vivo distribution, induction upon oxidative stress, and evidence for translational regulation*. *J Biol Chem*, 2001. **276**(12): p. 8705-12.
176. Alves-Guerra, M.C., S. Rousset, C. Pecqueur, Z. Mallat, J. Blanc, A. Tedgui, F. Bouillaud, A.M. Cassard-Doulcier, D. Ricquier, and B. Miroux, *Bone marrow transplantation reveals the in vivo expression of the mitochondrial uncoupling protein 2 in immune and nonimmune cells during inflammation*. *J Biol Chem*, 2003. **278**(43): p. 42307-12.
177. Rousset, S., J. Mozo, G. Dujardin, Y. Emre, S. Masscheleyn, D. Ricquier, and A.M. Cassard-Doulcier, *UCP2 is a mitochondrial transporter with an unusual very short half-life*. *FEBS Lett*, 2007. **581**(3): p. 479-82.
178. Fink, B.D., Y.S. Hong, M.M. Mathahs, T.D. Scholz, J.S. Dillon, and W.I. Sivitz, *UCP2-dependent proton leak in isolated mammalian mitochondria*. *J Biol Chem*, 2002. **277**(6): p. 3918-25.
179. Zácckova, M. and P. Jezek, *Reconstitution of novel mitochondrial uncoupling proteins UCP2 and UCP3*. *Biosci Rep*, 2002. **22**(1): p. 33-46.
180. Jabůrek, M., M. Varecha, R.E. Gimeno, M. Dembski, P. Jezek, M. Zhang, P. Burn, L.A. Tartaglia, and K.D. Garlid, *Transport function and regulation of mitochondrial uncoupling proteins 2 and 3*. *J Biol Chem*, 1999. **274**(37): p. 26003-7.
181. Stuart, J.A., J.A. Harper, K.M. Brindle, M.B. Jekabsons, and M.D. Brand, *A mitochondrial uncoupling artifact can be caused by expression of uncoupling protein 1 in yeast*. *Biochem J*, 2001. **356**(Pt 3): p. 779-89.
182. Stuart, J.A., J.A. Harper, K.M. Brindle, M.B. Jekabsons, and M.D. Brand, *Physiological levels of mammalian uncoupling protein 2 do not uncouple yeast mitochondria*. *J Biol Chem*, 2001. **276**(21): p. 18633-9.
183. Couplan, E., M. del Mar Gonzalez-Barroso, M.C. Alves-Guerra, D. Ricquier, M. Goubern, and F. Bouillaud, *No evidence for a basal, retinoic, or superoxide-induced uncoupling activity of the uncoupling protein 2 present in spleen or lung mitochondria*. *J Biol Chem*, 2002. **277**(29): p. 26268-75.
184. Bouillaud, F., *UCP2, not a physiologically relevant uncoupler but a glucose sparing switch impacting ROS production and glucose sensing*. *Biochim Biophys Acta*, 2009. **1787**(5): p. 377-83.
185. Jekabsons, M.B., K.S. Echtay, I. Arechaga, and M.D. Brand, *Molecular properties of purified human uncoupling protein 2 refolded from bacterial inclusion bodies*. *J Bioenerg Biomembr*, 2003. **35**(5): p. 409-18.
186. Jekabsons, M.B., K.S. Echtay, and M.D. Brand, *Nucleotide binding to human uncoupling protein-2 refolded from bacterial inclusion bodies*. *Biochem J*, 2002. **366**(Pt 2): p. 565-71.

187. Jaburek, M. and K.D. Garlid, *Reconstitution of recombinant uncoupling proteins: UCP1, -2, and -3 have similar affinities for ATP and are unaffected by coenzyme Q10*. J Biol Chem, 2003. **278**(28): p. 25825-31.
188. Berardi, M.J., W.M. Shih, S.C. Harrison, and J.J. Chou, *Mitochondrial uncoupling protein 2 structure determined by NMR molecular fragment searching*. Nature, 2011. **476**(7358): p. 109-13.
189. Berardi, M.J. and J.J. Chou, *Fatty acid flippase activity of UCP2 is essential for its proton transport in mitochondria*. Cell Metab, 2014. **20**(3): p. 541-52.
190. Zoonens, M., J. Comer, S. Masscheleyn, E. Pebay-Peyroula, C. Chipot, B. Miroux, and F. Dehez, *Dangerous liaisons between detergents and membrane proteins. The case of mitochondrial uncoupling protein 2*. J Am Chem Soc, 2013. **135**(40): p. 15174-82.
191. Chipot, C., F. Dehez, J.R. Schnell, N. Zitzmann, E. Pebay-Peyroula, L.J. Catoire, B. Miroux, E.R.S. Kunji, G. Veglia, T.A. Cross, and P. Schanda, *Perturbations of Native Membrane Protein Structure in Alkyl Phosphocholine Detergents: A Critical Assessment of NMR and Biophysical Studies*. Chem Rev, 2018. **118**(7): p. 3559-3607.
192. Kurauskas, V., A. Hessel, P. Ma, P. Lunetti, K. Weinhäupl, L. Imbert, B. Brutscher, M.S. King, R. Sounier, V. Dolce, E.R.S. Kunji, L. Capobianco, C. Chipot, F. Dehez, B. Bersch, and P. Schanda, *How Detergent Impacts Membrane Proteins: Atomic-Level Views of Mitochondrial Carriers in Dodecylphosphocholine*. The Journal of Physical Chemistry Letters, 2018. **9**(5): p. 933-938.
193. Vozza, A., G. Parisi, F. De Leonardis, F.M. Lasorsa, A. Castegna, D. Amorese, R. Marmo, V.M. Calcagnile, L. Palmieri, and D. Ricquier, *UCP2 transports C4 metabolites out of mitochondria, regulating glucose and glutamine oxidation*. Proceedings of the National Academy of Sciences, 2014. **111**(3): p. 960-965.
194. Hermes, G., D. Nagy, M. Waterson, A. Zsarnovszky, L. Varela, M. Hajos, and T.L. Horvath, *Role of mitochondrial uncoupling protein-2 (UCP2) in higher brain functions, neuronal plasticity and network oscillation*. Molecular Metabolism, 2016. **5**(6): p. 415-421.
195. Gaudry, M.J. and M. Jastroch, *Molecular evolution of uncoupling proteins and implications for brain function*. Neurosci Lett, 2018. **696**: p. 140-145.
196. Boss, O., S. Samec, A. Paoloni-Giacobino, C. Rossier, A. Dulloo, J. Seydoux, P. Muzzin, and J.P. Giacobino, *Uncoupling protein-3: a new member of the mitochondrial carrier family with tissue-specific expression*. FEBS Lett, 1997. **408**(1): p. 39-42.
197. Gong, D.W., Y. He, M. Karas, and M. Reitman, *Uncoupling protein-3 is a mediator of thermogenesis regulated by thyroid hormone, beta3-adrenergic agonists, and leptin*. J Biol Chem, 1997. **272**(39): p. 24129-32.
198. Vidal-Puig, A., G. Solanes, D. Grujic, J.S. Flier, and B.B. Lowell, *UCP3: an uncoupling protein homologue expressed preferentially and abundantly in skeletal muscle and brown adipose tissue*. Biochem Biophys Res Commun, 1997. **235**(1): p. 79-82.
199. Azzu, V., S.A. Mookerjee, and M.D. Brand, *Rapid turnover of mitochondrial uncoupling protein 3*. Biochem J, 2010. **426**(1): p. 13-7.
200. MacLellan, J.D., M.F. Gerrits, A. Gowing, P.J.S. Smith, M.B. Wheeler, and M.-E. Harper, *Physiological Increases in Uncoupling Protein 3 Augment Fatty Acid Oxidation and Decrease Reactive Oxygen Species Production Without Uncoupling Respiration in Muscle Cells*. Diabetes, 2005. **54**(8): p. 2343-2350.
201. Mozo, J., G. Ferry, A. Studeny, C. Pecqueur, M. Rodriguez, J.A. Boutin, and F. Bouillaud, *Expression of UCP3 in CHO cells does not cause uncoupling, but controls mitochondrial activity in the presence of glucose*. Biochem J, 2006. **393**(Pt 1): p. 431-9.
202. Samec, S., J. Seydoux, and A.G. Dulloo, *Role of UCP homologues in skeletal muscles and brown adipose tissue: mediators of thermogenesis or regulators of lipids as fuel substrate?* The FASEB Journal, 1998. **12**(9): p. 715-724.

203. Schrauwen, P., J. Hoeks, G. Schaart, E. Kornips, B. Binas, G.J. Van De Vusse, M. Van Bilsen, J.J. Luiken, S.L. Coort, J.F. Glatz, W.H. Saris, and M.K. Hesselink, *Uncoupling protein 3 as a mitochondrial fatty acid anion exporter*. *Faseb j*, 2003. **17**(15): p. 2272-4.
204. Seifert, E.L., V. Bézaire, C. Estey, and M.E. Harper, *Essential role for uncoupling protein-3 in mitochondrial adaptation to fasting but not in fatty acid oxidation or fatty acid anion export*. *J Biol Chem*, 2008. **283**(37): p. 25124-25131.
205. Mao, W., X.X. Yu, A. Zhong, W. Li, J. Brush, S.W. Sherwood, S.H. Adams, and G. Pan, *UCP4, a novel brain-specific mitochondrial protein that reduces membrane potential in mammalian cells*. *FEBS Lett*, 1999. **443**(3): p. 326-30.
206. Sanchis, D., C. Fleury, N. Chomiki, M. Goubern, Q. Huang, M. Neverova, F. Grégoire, J. Easlick, S. Raimbault, C. Lévi-Meyrueis, B. Miroux, S. Collins, M. Seldin, D. Richard, C. Warden, F. Bouillaud, and D. Ricquier, *BMCP1, a novel mitochondrial carrier with high expression in the central nervous system of humans and rodents, and respiration uncoupling activity in recombinant yeast*. *J Biol Chem*, 1998. **273**(51): p. 34611-5.
207. Kondou, S., S. Hidaka, H. Yoshimatsu, Y. Tsuruta, E. Itateyama, and T. Sakata, *Molecular cloning of rat brain mitochondrial carrier protein-1 cDNA and its up-regulation during postnatal development*. *Biochim Biophys Acta*, 2000. **1457**(3): p. 182-9.
208. Borecký, J., I.G. Maia, and P. Arruda, *Mitochondrial uncoupling proteins in mammals and plants*. *Biosci Rep*, 2001. **21**(2): p. 201-12.
209. Hoang, T., M.D. Smith, and M. Jelokhani-Niaraki, *Toward Understanding the Mechanism of Ion Transport Activity of Neuronal Uncoupling Proteins UCP2, UCP4, and UCP5*. *Biochemistry*, 2012. **51**(19): p. 4004-4014.
210. Klingenberg, M., *UCP1 - A sophisticated energy valve*. *Biochimie*, 2017. **134**: p. 19-27.
211. Nicholls, D.G., *Mitochondrial proton leaks and uncoupling proteins*. *Biochim Biophys Acta Bioenerg*, 2021. **1862**(7): p. 148428.
212. Echtay, K.S., E. Winkler, M. Bienengraeber, and M. Klingenberg, *Site-directed mutagenesis identifies residues in uncoupling protein (UCP1) involved in three different functions*. *Biochemistry*, 2000. **39**(12): p. 3311-3317.
213. Rodriguez-Sanchez, L. and E. Rial, *The distinct bioenergetic properties of the human UCP1*. *Biochimie*, 2017. **134**: p. 51-55.
214. Chevallet, M., S. Luche, and T. Rabilloud, *Silver staining of proteins in polyacrylamide gels*. *Nat Protoc*, 2006. **1**(4): p. 1852-8.
215. Alexandrov, A.I., M. Mileni, E.Y. Chien, M.A. Hanson, and R.C. Stevens, *Microscale fluorescent thermal stability assay for membrane proteins*. *Structure*, 2008. **16**(3): p. 351-9.
216. Majd, H., M.S. King, S.M. Palmer, A.C. Smith, L.D. Elbourne, I.T. Paulsen, D. Sharples, P.J. Henderson, and E.R. Kunji, *Screening of candidate substrates and coupling ions of transporters by thermostability shift assays*. *Elife*, 2018. **7**.
217. Klingenberg, M., E. Winkler, and S. Huang, *ADP/ATP carrier and uncoupling protein*. *Methods Enzymol*, 1995. **260**: p. 369-89.
218. Smirnova, I.A., P. Ädelroth, and P. Brzezinski, *Extraction and liposome reconstitution of membrane proteins with their native lipids without the use of detergents*. *Scientific Reports*, 2018. **8**(1): p. 14950.
219. Orosz, D.E. and K.D. Garlid, *A Sensitive New Fluorescence Assay for Measuring Proton Transport across Liposomal Membranes*. *Analytical Biochemistry*, 1993. **210**(1): p. 7-15.
220. Garlid, K.D., X. Sun, P. Paucek, and G. Woldegiorgis, *Mitochondrial cation transport systems*. *Methods Enzymol*, 1995. **260**: p. 331-48.
221. Consortium, T.U., *UniProt: the universal protein knowledgebase in 2021*. *Nucleic Acids Research*, 2020. **49**(D1): p. D480-D489.
222. Jabeen, A., A. Mohamedali, and S. Ranganathan, *Protocol for Protein Structure Modelling*, in *Encyclopedia of Bioinformatics and Computational Biology*, S. Ranganathan, et al., Editors. 2019, Academic Press: Oxford. p. 252-272.

223. Berman, H.M., J. Westbrook, Z. Feng, G. Gilliland, T.N. Bhat, H. Weissig, I.N. Shindyalov, and P.E. Bourne, *The Protein Data Bank*. Nucleic Acids Research, 2000. **28**(1): p. 235-242.
224. Webb, B. and A. Sali, *Comparative Protein Structure Modeling Using MODELLER*. Current Protocols in Protein Science, 2016. **86**(1): p. 2.9.1-2.9.37.
225. Pettersen, E.F., T.D. Goddard, C.C. Huang, G.S. Couch, D.M. Greenblatt, E.C. Meng, and T.E. Ferrin, *UCSF Chimera--a visualization system for exploratory research and analysis*. J Comput Chem, 2004. **25**(13): p. 1605-12.
226. Ko, J., H. Park, L. Heo, and C. Seok, *GalaxyWEB server for protein structure prediction and refinement*. Nucleic Acids Research, 2012. **40**(W1): p. W294-W297.
227. Williams, C.J., J.J. Headd, N.W. Moriarty, M.G. Prisant, L.L. Videau, L.N. Deis, V. Verma, D.A. Keedy, B.J. Hintze, V.B. Chen, S. Jain, S.M. Lewis, W.B. Arendall, 3rd, J. Snoeyink, P.D. Adams, S.C. Lovell, J.S. Richardson, and D.C. Richardson, *MolProbity: More and better reference data for improved all-atom structure validation*. Protein Sci, 2018. **27**(1): p. 293-315.
228. Studer, G., M. Biasini, and T. Schwede, *Assessing the local structural quality of transmembrane protein models using statistical potentials (QMEANBrane)*. Bioinformatics, 2014. **30**(17): p. i505-11.
229. Chondronikola, M., E. Volpi, E. Børshheim, C. Porter, M.K. Saraf, P. Annamalai, C. Yfanti, T. Chao, D. Wong, K. Shinoda, S.M. Labbé, N.M. Hurren, F. Cesani, S. Kajimura, and L.S. Sidossis, *Brown Adipose Tissue Activation Is Linked to Distinct Systemic Effects on Lipid Metabolism in Humans*. Cell Metab, 2016. **23**(6): p. 1200-1206.
230. Yoneshiro, T., Q. Wang, K. Tajima, M. Matsushita, H. Maki, K. Igarashi, Z. Dai, P.J. White, R.W. McGarrah, O.R. Ilkayeva, Y. Deleye, Y. Oguri, M. Kuroda, K. Ikeda, H. Li, A. Ueno, M. Ohishi, T. Ishikawa, K. Kim, Y. Chen, C.H. Sponton, R.N. Pradhan, H. Majd, V.J. Greiner, M. Yoneshiro, Z. Brown, M. Chondronikola, H. Takahashi, T. Goto, T. Kawada, L. Sidossis, F.C. Szoka, M.T. McManus, M. Saito, T. Soga, and S. Kajimura, *BCAA catabolism in brown fat controls energy homeostasis through SLC25A44*. Nature, 2019.
231. Maurer, S.F., T. Fromme, S. Mocek, A. Zimmermann, and M. Klingenspor, *Uncoupling protein 1 and the capacity for non-shivering thermogenesis are components of the glucose homeostatic system*. Am J Physiol Endocrinol Metab, 2019.
232. Grandoch, M., U. Flogel, S. Virtue, J.K. Maier, T. Jelenik, C. Kohlmorgen, K. Feldmann, Y. Ostendorf, T.R. Castaneda, Z. Zhou, Y. Yamaguchi, E.B.M. Nascimento, V.G. Sunkari, C. Goy, M. Kinzig, F. Sorgel, P.L. Bollyky, P. Schrauwen, H. Al-Hasani, M. Roden, S. Keipert, A. Vidal-Puig, M. Jastroch, J. Haendeler, and J.W. Fischer, *4-Methylumbelliferone improves the thermogenic capacity of brown adipose tissue*. Nat Metab, 2019. **1**(5): p. 546-559.
233. Lee, Y.-H., Y.-S. Jung, and D. Choi, *Recent advance in brown adipose physiology and its therapeutic potential*. Experimental & Molecular Medicine, 2014. **46**(2): p. e78-e78.
234. Tomas, P., J. Jimenez-Jimenez, P. Zaragoza, V. Vuligonda, R.A. Chandraratna, and E. Rial, *Activation by retinoids of the uncoupling protein UCP1*. Biochim Biophys Acta, 2004. **1658**(1-2): p. 157-64.
235. Ježek, P., M. Modrianský, and K.D. Garlid, *A structure-activity study of fatty acid interaction with mitochondrial uncoupling protein*. FEBS Letters, 1997. **408**(2): p. 166-170.
236. Jezek, P. and K.D. Garlid, *New substrates and competitive inhibitors of the Cl<sup>-</sup> translocating pathway of the uncoupling protein of brown adipose tissue mitochondria*. J Biol Chem, 1990. **265**(31): p. 19303-11.
237. Schilperoort, M., A.D. van Dam, G. Hoeke, I.G. Shabalina, A. Okolo, A.C. Hanyaloglu, L.H. Dib, I.M. Mol, N. Caengprasath, Y.W. Chan, S. Damak, A.R. Miller, T. Coskun, B. Shimpukade, T. Ulven, S. Kooijman, P.C. Rensen, and M. Christian, *The GPR120 agonist TUG-891 promotes metabolic health by stimulating mitochondrial respiration in brown fat*. EMBO Molecular Medicine, 2018. **10**(3): p. e8047.

238. Rainsford, K.D., *Anti-inflammatory drugs in the 21st century*. Subcell Biochem, 2007. **42**: p. 3-27.
239. Rainsford, K.D., *Ibuprofen: pharmacology, efficacy and safety*. Inflammopharmacology, 2009. **17**(6): p. 275-342.
240. Bushra, R. and N. Aslam, *An overview of clinical pharmacology of Ibuprofen*. Oman Med J, 2010. **25**(3): p. 155-1661.
241. Mazaleuskaya, L.L., K.N. Theken, L. Gong, C.F. Thorn, G.A. FitzGerald, R.B. Altman, and T.E. Klein, *PharmGKB summary: ibuprofen pathways*. Pharmacogenet Genomics, 2015. **25**(2): p. 96-106.
242. Keipert, S. and M. Jastroch, *Brite/beige fat and UCP1 — is it thermogenesis?* Biochimica et Biophysica Acta (BBA) - Bioenergetics, 2014. **1837**(7): p. 1075-1082.
243. Voet, D. and J.G. Voet, *Biochemistry*. 4th edition. ed. 2011: John Wiley & Sons.
244. Ježek, P., M. Jabůrek, and R.K. Porter, *Uncoupling mechanism and redox regulation of mitochondrial uncoupling protein 1 (UCP1)*. Biochim Biophys Acta Bioenerg, 2019. **1860**(3): p. 259-269.
245. Christiansen, E., S.V. Hansen, C. Urban, B.D. Hudson, E.T. Wargent, M. Grundmann, L. Jenkins, M. Zaibi, C.J. Stocker, S. Ullrich, E. Kostenis, M.U. Kassack, G. Milligan, M.A. Cawthorne, and T. Ulven, *Discovery of TUG-770: A Highly Potent Free Fatty Acid Receptor 1 (FFA1/GPR40) Agonist for Treatment of Type 2 Diabetes*. ACS Med Chem Lett, 2013. **4**(5): p. 441-445.
246. Locke, R.M., E. Rial, I.D. Scott, and D.G. Nicholls, *Fatty acids as acute regulators of the proton conductance of hamster brown-fat mitochondria*. Eur J Biochem, 1982. **129**(2): p. 373-80.
247. Strieleman, P.J. and E. Shrago, *Specific interaction of fatty acyl-CoA esters with brown adipose tissue mitochondria*. Am J Physiol, 1985. **248**(6 Pt 1): p. E699-705.
248. Donatello, S., T. Spennetta, P. Strieleman, G. Woldegiorgis, and E. Shrago, *Adaptive changes in individual acyl-CoA esters from hamster BAT during cold acclimation*. Am J Physiol, 1988. **254**(2 Pt 1): p. E181-6.
249. Jezek, P., J. Houstěk, and Z. Drahota, *Alkaline pH, membrane potential, and magnesium cations are negative modulators of purine nucleotide inhibition of H<sup>+</sup> and Cl<sup>-</sup> transport through the uncoupling protein of brown adipose tissue mitochondria*. J Bioenerg Biomembr, 1988. **20**(5): p. 603-22.
250. Woldegiorgis, G., T. Duff, L. Contreras, E. Shrago, and A.E. Ruoho, *Photoaffinity labeling of hamster brown adipose tissue mitochondria by an [125I] coenzyme A derivative: differential interaction with the uncoupling protein and ADP/ATP carrier*. Biochem Biophys Res Commun, 1989. **161**(2): p. 502-7.
251. Katiyar, S.S. and E. Shrago, *Differential interaction of fatty acids and fatty acyl CoA esters with the purified/reconstituted brown adipose tissue mitochondrial uncoupling protein*. Biochem Biophys Res Commun, 1991. **175**(3): p. 1104-11.
252. Ciapaite, J., G. van Eikenhorst, and K. Krab, *Application of modular control analysis to inhibition of the adenine nucleotide translocator by palmitoyl-CoA*. Mol Biol Rep, 2002. **29**(1-2): p. 13-6.
253. Cannon, B., U. Sundin, and L. Romert, *Palmitoyl coenzyme A: a possible physiological regulator of nucleotide binding to brown adipose tissue mitochondria*. FEBS Lett, 1977. **74**(1): p. 43-6.
254. Kopecký, J., P. Jezek, Z. Drahota, and J. Houstěk, *Control of uncoupling protein in brown-fat mitochondria by purine nucleotides. Chemical modification by diazobenzenesulfonate*. Eur J Biochem, 1987. **164**(3): p. 687-94.
255. Saito, M., Y. Okamatsu-Ogura, M. Matsushita, K. Watanabe, T. Yoneshiro, J. Nio-Kobayashi, T. Iwanaga, M. Miyagawa, T. Kameya, K. Nakada, Y. Kawai, and M. Tsujisaki, *High Incidence*

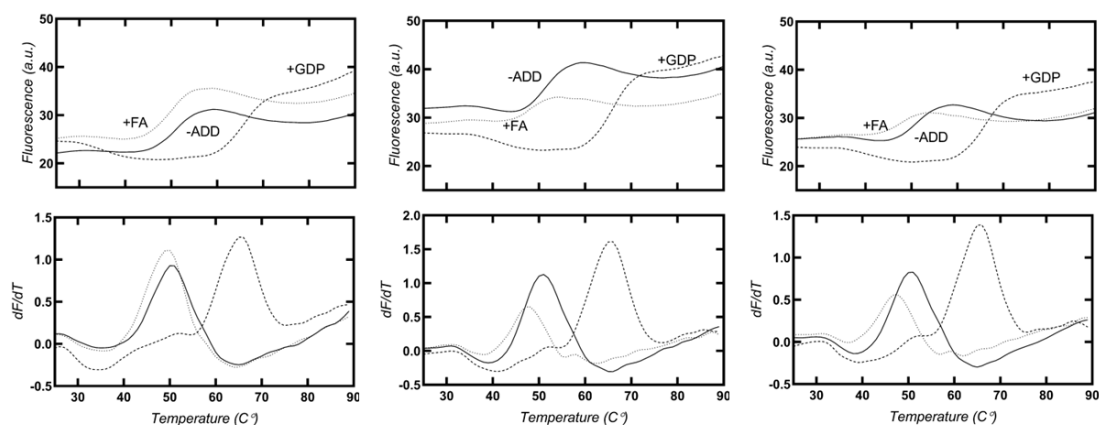
- of Metabolically Active Brown Adipose Tissue in Healthy Adult Humans*. Effects of Cold Exposure and Adiposity, 2009. **58**(7): p. 1526-1531.
256. Porter, C., D.N. Herndon, M. Chondronikola, T. Chao, P. Annamalai, N. Bhattarai, M.K. Saraf, K.D. Capek, P.T. Reidy, A.C. Daquinag, M.G. Kolonin, B.B. Rasmussen, E. Borsheim, T. Toliver-Kinsky, and L.S. Sidossis, *Human and Mouse Brown Adipose Tissue Mitochondria Have Comparable UCP1 Function*. Cell Metab, 2016. **24**(2): p. 246-55.
  257. WINKLER, E. and M. KLINGENBERG, *An improved procedure for reconstitution of the uncoupling protein and in-depth analysis of H<sup>+</sup>/OH<sup>-</sup> transport*. European Journal of Biochemistry, 1992. **207**(1): p. 135-145.
  258. Brunaldi, K., N. Huang, and J.A. Hamilton, *Fatty acids are rapidly delivered to and extracted from membranes by methyl-beta-cyclodextrin*. J Lipid Res, 2010. **51**(1): p. 120-31.
  259. Nury, H., C. Dahout-Gonzalez, V. Trezeguet, G. Lauquin, G. Brandolin, and E. Pebay-Peyroula, *Structural basis for lipid-mediated interactions between mitochondrial ADP/ATP carrier monomers*. FEBS Lett, 2005. **579**(27): p. 6031-6.
  260. Arechaga, I., S. Raimbault, S. Prieto, C. Levi-Meyrueis, P. Zaragoza, B. Miroux, D. Ricquier, F. Bouillaud, and E. Rial, *Cysteine residues are not essential for uncoupling protein function*. Biochem J, 1993. **296 ( Pt 3)**(Pt 3): p. 693-700.
  261. Murdza-Inglis, D.L., M. Modriansky, H.V. Patel, G. Woldegiorgis, K.B. Freeman, and K.D. Garlid, *A single mutation in uncoupling protein of rat brown adipose tissue mitochondria abolishes GDP sensitivity of H<sup>+</sup> transport*. J Biol Chem, 1994. **269**(10): p. 7435-8.
  262. Bienengraeber, M., K.S. Echtay, and M. Klingenberg, *H<sup>+</sup> transport by uncoupling protein (UCP-1) is dependent on a histidine pair, absent in UCP-2 and UCP-3*. Biochemistry, 1998. **37**(1): p. 3-8.
  263. Echtay, K.S., M. Bienengraeber, and M. Klingenberg, *Role of Intrahelical Arginine Residues in Functional Properties of Uncoupling Protein (UCP1)*. Biochemistry, 2001. **40**(17): p. 5243.
  264. Bouillaud, F., J. Weissenbach, and D. Ricquier, *Complete cDNA-derived amino acid sequence of rat brown fat uncoupling protein*. J Biol Chem, 1986. **261**(4): p. 1487-90.
  265. Lee, G.R., J. Won, L. Heo, and C. Seok, *GalaxyRefine2: simultaneous refinement of inaccurate local regions and overall protein structure*. Nucleic Acids Res, 2019. **47**(W1): p. W451-w455.
  266. Kunji, E.R.S. and A.J. Robinson, *Coupling of proton and substrate translocation in the transport cycle of mitochondrial carriers*. Current Opinion in Structural Biology, 2010. **20**(4): p. 440-447.
  267. Wang, G., J.G. Meyer, W. Cai, S. Softic, M.E. Li, E. Verdin, C. Newgard, B. Schilling, and C.R. Kahn, *Regulation of UCP1 and Mitochondrial Metabolism in Brown Adipose Tissue by Reversible Succinylation*. Mol Cell, 2019.
  268. Harborne, S.P., M.S. King, P.G. Crichton, and E.R. Kunji, *Calcium regulation of the human mitochondrial ATP-Mg/Pi carrier SLC25A24 uses a locking pin mechanism*. Sci Rep, 2017. **7**: p. 45383.
  269. Hirschberg, V., T. Fromme, and M. Klingenspor, *Test Systems to Study the Structure and Function of Uncoupling Protein 1: A Critical Overview*. Frontiers in Endocrinology, 2011. **2**(63).
  270. Winkler, E. and M. Klingenberg, *An improved procedure for reconstitution of the uncoupling protein and in-depth analysis of H<sup>+</sup>/OH<sup>-</sup> transport*. Eur J Biochem, 1992. **207**(1): p. 135-45.
  271. Jezek, P., J. Hanus, C. Semrad, and K.D. Garlid, *Photoactivated azido fatty acid irreversibly inhibits anion and proton transport through the mitochondrial uncoupling protein*. J Biol Chem, 1996. **271**(11): p. 6199-205.
  272. Skulachev, V.P., *Uncoupling: new approaches to an old problem of bioenergetics*. Biochim Biophys Acta, 1998. **1363**(2): p. 100-24.
  273. Kamp, F. and J.A. Hamilton, *pH gradients across phospholipid membranes caused by fast flip-flop of un-ionized fatty acids*. Proc Natl Acad Sci U S A, 1992. **89**(23): p. 11367-70.

274. Ashburn, T.T. and K.B. Thor, *Drug repositioning: identifying and developing new uses for existing drugs*. Nat Rev Drug Discov, 2004. **3**(8): p. 673-83.
275. Jumper, J., R. Evans, A. Pritzel, T. Green, M. Figurnov, O. Ronneberger, K. Tunyasuvunakool, R. Bates, A. Žídek, A. Potapenko, A. Bridgland, C. Meyer, S.A.A. Kohl, A.J. Ballard, A. Cowie, B. Romera-Paredes, S. Nikolov, R. Jain, J. Adler, T. Back, S. Petersen, D. Reiman, E. Clancy, M. Zielinski, M. Steinegger, M. Pacholska, T. Berghammer, S. Bodenstein, D. Silver, O. Vinyals, A.W. Senior, K. Kavukcuoglu, P. Kohli, and D. Hassabis, *Highly accurate protein structure prediction with AlphaFold*. Nature, 2021. **596**(7873): p. 583-589.
276. Varadi, M., S. Anyango, M. Deshpande, S. Nair, C. Natassia, G. Yordanova, D. Yuan, O. Stroe, G. Wood, A. Laydon, A. Žídek, T. Green, K. Tunyasuvunakool, S. Petersen, J. Jumper, E. Clancy, R. Green, A. Vora, M. Lutfi, M. Figurnov, A. Cowie, N. Hobbs, P. Kohli, G. Kleywegt, E. Birney, D. Hassabis, and S. Velankar, *AlphaFold Protein Structure Database: massively expanding the structural coverage of protein-sequence space with high-accuracy models*. Nucleic Acids Res, 2022. **50**(D1): p. D439-d444.

## Appendix

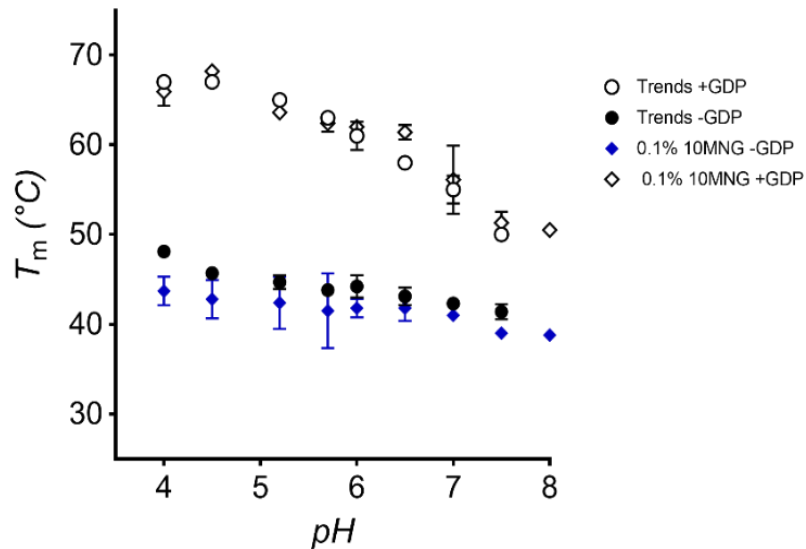
**Appendix table A1 Molecules excluded from thermostability screen**

Excluded molecules	Reason
1-OCTADECYL-LOPA	Unfolded UCP1 at 100 $\mu$ M
RSC-3388	Unfolded UCP1 at 100 $\mu$ M
PYRROPHENONE	Unfolded UCP1 at 100 $\mu$ M
ACITRETIN	Unfolded UCP1 at 100 $\mu$ M
PERFLUORONONANOIC ACID	Unfolded UCP1 at 100 $\mu$ M
DIDS	Unfolded UCP1 at 100 $\mu$ M
T4	Unfolded UCP1 at 100 $\mu$ M
CoA	Exposed thiol interfering with the assay
BOPY-FI ATP-g-S	Fluorescent moiety
BOPY-FI GDP-g-S	Fluorescent moiety

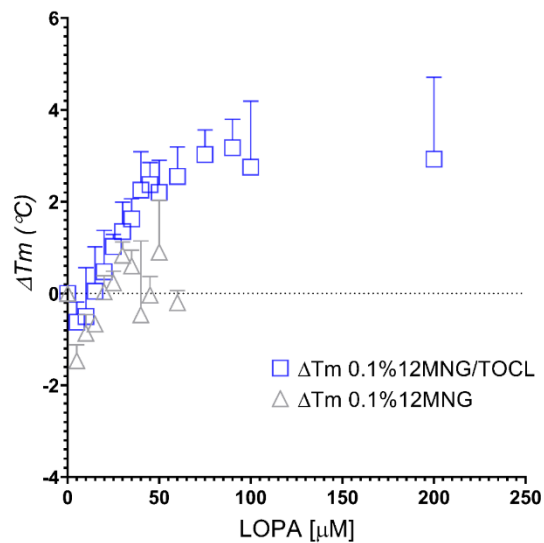


**Appendix figure A1. Variability in repeated tests of UCP1 with and without ligands (see Fig 3.1).** Assays performed at pH 7.5 in 0.1 %12MNG. (Upper panels) raw fluorescence traces of native ovine UCP1, without (-ADD; full line) or with oleic acid ( 25  $\mu$ M; FA, dots) or a purine nucleotide (1 mM; GDP, dashes), showing three repeats from separate runs. (Bottom panels) corresponding derivative peaks from which the melting

temperature ( $T_m$ ) was measured. Average  $T_m$  values for each condition: -ADD =  $51.5 \pm 0.4$  °C; +FA =  $44.1 \pm 1.8$  °C; +GDP =  $64.9 \pm 1.4$  °C.

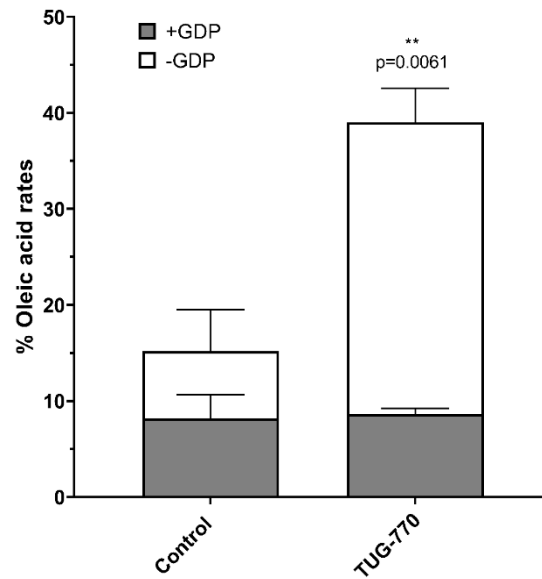


**Appendix figure A2. Native UCP1 pH titre.** Thermostability shift assay of native UCP1 pH 4.0 to 8.0 in 0.1 % 10MNG with 20 mM buffers gluconate and piperazine pH 4.0 to 5.5, pH 6.0 and 6.5 Bis-Tris, pH 7.0 to 8.0 Hepes.  $T_m$  of -GDP (coloured symbols) and +GDP (open symbols) shown. Comparing own data (diamond shapes), with data published in [169] (circles).

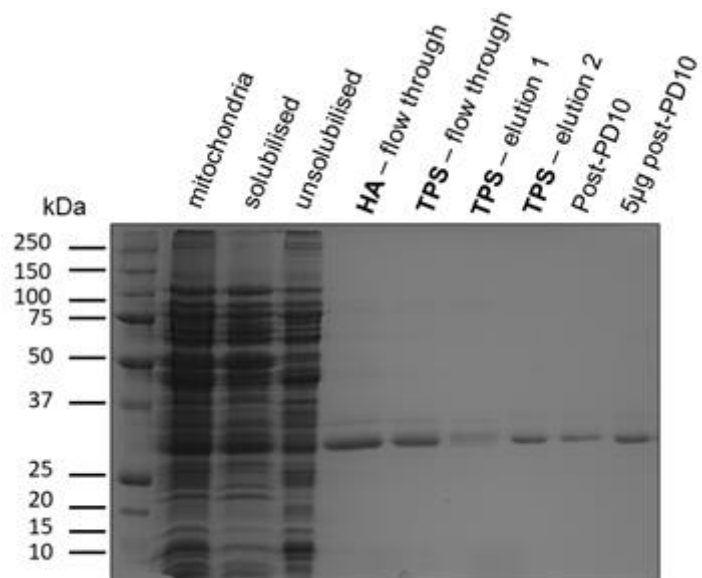


**Appendix figure OLPA thermostability assay titre.** Titre of lysophosphatidic acid (OLPA), in 0.1 % 12MNG, 20 mM Hepes pH 7.5, with (squares) and without (triangles) the

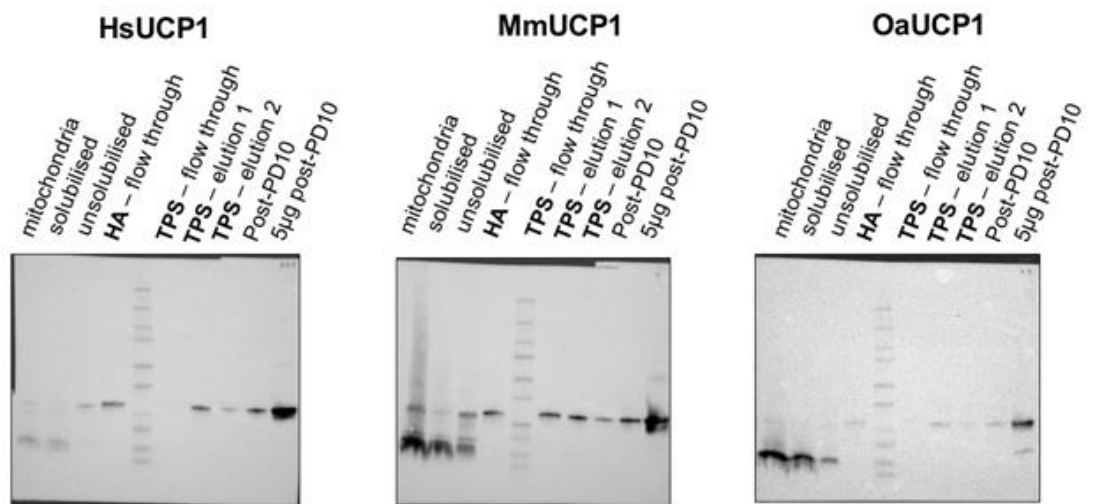
addition of cardiolipin (tetraoleoylcardiolipin-TOCL) in the assay buffer. Values given are averages ( $\pm$ SD) of three to four independent experiments.



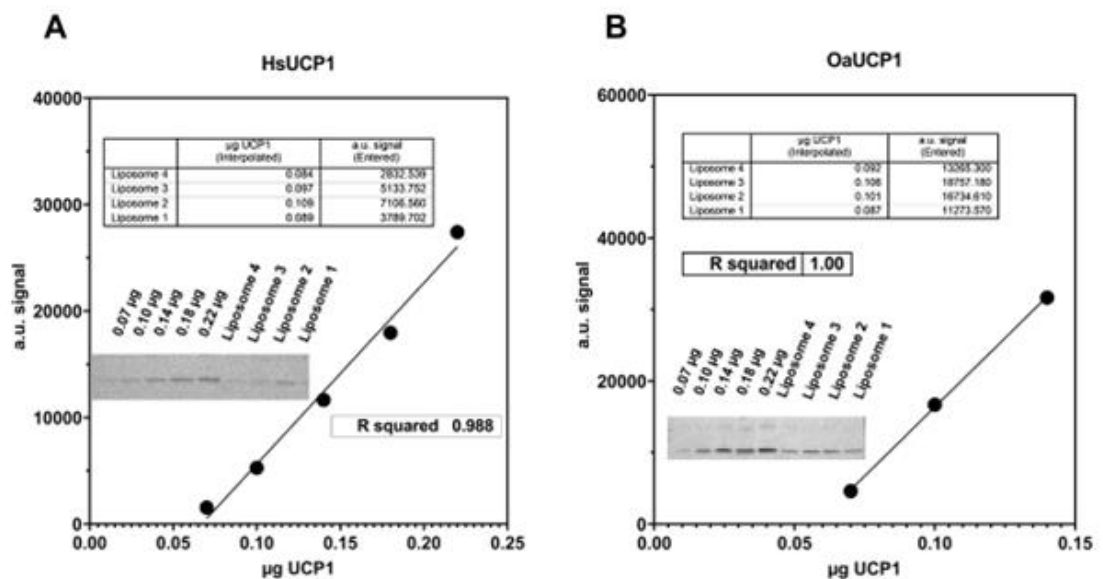
**Appendix figure A4. TUG-770 flux assay.** The free fatty acid receptor 1 (FFAR1) agonist TUG-770 activates UCP1-mediated proton transport. Values expressed as averages of three independent experiments  $\pm$ SD, statistical analysis performed by one-way ANOVA (\* $p$ <0.05, \*\* $p$ <0.02, \*\*\* $p$ <0.001).



**Appendix figure A5. Native ovine UCP1 purification profile.** HA=Hydroxyapatite; TPS=Thiopropyl Sepharose; PD10=desalting column. Gel profile stained with coomassie dye (Imperial Stain).



**Appendix figure A6. Western blots anti-UCP1 of purification profiles – full blots.** Western blots of the UCP1 isoforms purification profiles with anti-UCP1 antibodies, tracking the protein through the purification.



**Appendix figure A7. Determination of UCP1 reconstituted in liposomes. Panel A.** Western blot and standard curve of HsUCP1. **Panel B.** Western blot and standard curve of OaUCP1. The top two points of the standard curve indicated a saturation of signal and so were omitted.

**Appendix table A2. Summary statistics of homology models quality control – final models**

<i>Parameter</i>	<i>m-state OaUCP1</i>	<i>m-state MmUCP1</i>	<i>m-state HsUCP1</i>	<i>c-state OaUCP1</i>	<i>c-state MmUCP1</i>	<i>c-state HsUCP1</i>
<i>MolProbity (smaller is better)</i>	1.15	1.43	1.19	0.97	0.78	0.58
<i>Clash score (Goal:0)</i>	2.24	2.84	2	1.13	0	0
<i>Poor rotamers (&lt;0.3%)</i>	0.41%	0.00%	0.41%	0.00%	0.00%	0.82%
<i>Favoured rotamers (&gt;98%)</i>	99.18%	100.00%	99.59%	99.58%	99.20%	99.18%
<i>Ramachandran Outliers (&lt;0.05%)</i>	0.00%	1.02%	0.00%	1.06%	0.00%	0.00%
<i>Ramachandran Favoured (&gt;98%)</i>	97.21%	94.90%	96.55%	97.18%	95.93%	97.60%
<i>Rama distribution Z-score (Goal: &lt;2)</i>	0.81 ± 0.46	0.09 ± 0.45	0.27 ± 0.46	0.83 ± 0.46	0.42 ± 0.45	-0.01 ± 0.44

```

HsUCP1 1 MGGLTASDV--HP-----TLGVQLFSAGIAACLADVIITFPPLDTAKVR 40
MmUCP1 1 MVNPTTSEV--QP-----TMGVKIFISAGVSAACLADIIITFPPLDTAKVR 40
OaUCP1 1 MVGHAAITDV--PP-----TMAYKIFISAGVAACVADIIITFPPLDTAKVR 40
BtAAC1 1 MSDQAL-----SFLKDFLAGGVAAAISKTAVAPIERVKLL 35
ScAAC2 1 MSSNAQVKTLPLPPAPAPKKESENFLIDFLMGGVSAAVAKTAASPIERVKLL 50
ScAAC3 1 MSSDAKQKET-----NFAINFLMGGVSAAIKTAASPIERVKIL 39
TtAAC 1 MSNKQETKILGMP-----PFVVDFLMGGVSAAVSKTAAAPIERIKLL 42

HsUCP1 41 LQVQGECP TSSVI--RYKGVLTITAVVKTEGRMKLYSGLPAGLQRQISS 88
MmUCP1 41 LQIQGEGQASSTI--RYKGVLTITLAKTEGLPKLYSGLPAGIQRQISF 88
OaUCP1 41 LQIQGECLETSSAF--RYKGVLTITLAKTEGPVKLYSGLPAGLQRQISF 88
BtAAC1 36 LQVQ-HASKQISAEKQYKGIIDCVVRIPKEQGFSLFWRGNLANVIRYFPT 84
ScAAC2 51 IQNQDEMLKQGTLDKRYAGILDCFKRTATQEGVISFWRGNLANVIRYFPT 100
ScAAC3 40 IQNQDEMIKQGTLDKQYSGIVDCFKRTAKQEGLSFWRGNLANVIRYFPT 89
TtAAC 43 VQNQDEMIKAGRLDRRYNGIIDCFRRRTADEGLMALWRGNLANVIRYFPT 92

HsUCP1 89 ASLRIGLYD TVQEF LTAG-----KETAPSLGSKILAGLITGGVAVFIGQP 133
MmUCP1 89 ASLRIGLYDSVQEFYFSSG-----RETPASLGNKISAGLMTGGVAVFIGQP 133
OaUCP1 89 ASLRIGLYD TVQEFF TTG-----KE--ASLGSKISAGLITGGVAVFIGQP 131
BtAAC1 85 QALNFAFKDKYKQIFLGGVDRH--KQFWRYFAGNLASGGAAGATSLCFVYP 133
ScAAC2 101 QALNFAFKDKIKAMF--GFKKE-EGYAKWFAGNLASGGAAGALSLLFVYS 147
ScAAC3 90 QALNFAFKDKIKLMF--GFKKE-EGYGKWFAGNLASGGAAGALSLLFVYS 136
TtAAC 93 QALNFAFRDKFKAMF--GYKKDKDGYAKWMAGNLASGGAAGATSLLFVYS 140

HsUCP1 134 TEVVKVRLQAQ--SHLHGIKPRYTGTYNAYRIIATTEGLTGLWKGTTPNL 181
MmUCP1 134 TEVVKVRLQAQ--SHLHGIKPRYTGTYNAYRIIATTESLSTLWKGTTPNL 181
OaUCP1 132 TEVVKVRLQAQ--SHLHGPKPRYTGTYNAYRIIATTEGLTGLWKGTTPNL 179
BtAAC1 134 LDFARTRLAAD--VGKGAARQFTGLGNCITKIFKSDGRLGLYQGFNVSL 181
ScAAC2 148 LDYARTRLAADSKSSKGGARQFNGLIDVYKKTLSKSDGVAGLYRGFLPSV 197
ScAAC3 137 LDFARTRLAADAKSSKGGARQFNGLIDVYKKTLSKSDGIAGLYRGFMPSV 186
TtAAC 141 LDYARTRLANDAKSAKGGARQFNGLIDVYRKTLASDGIAGLYRGFGPSV 190

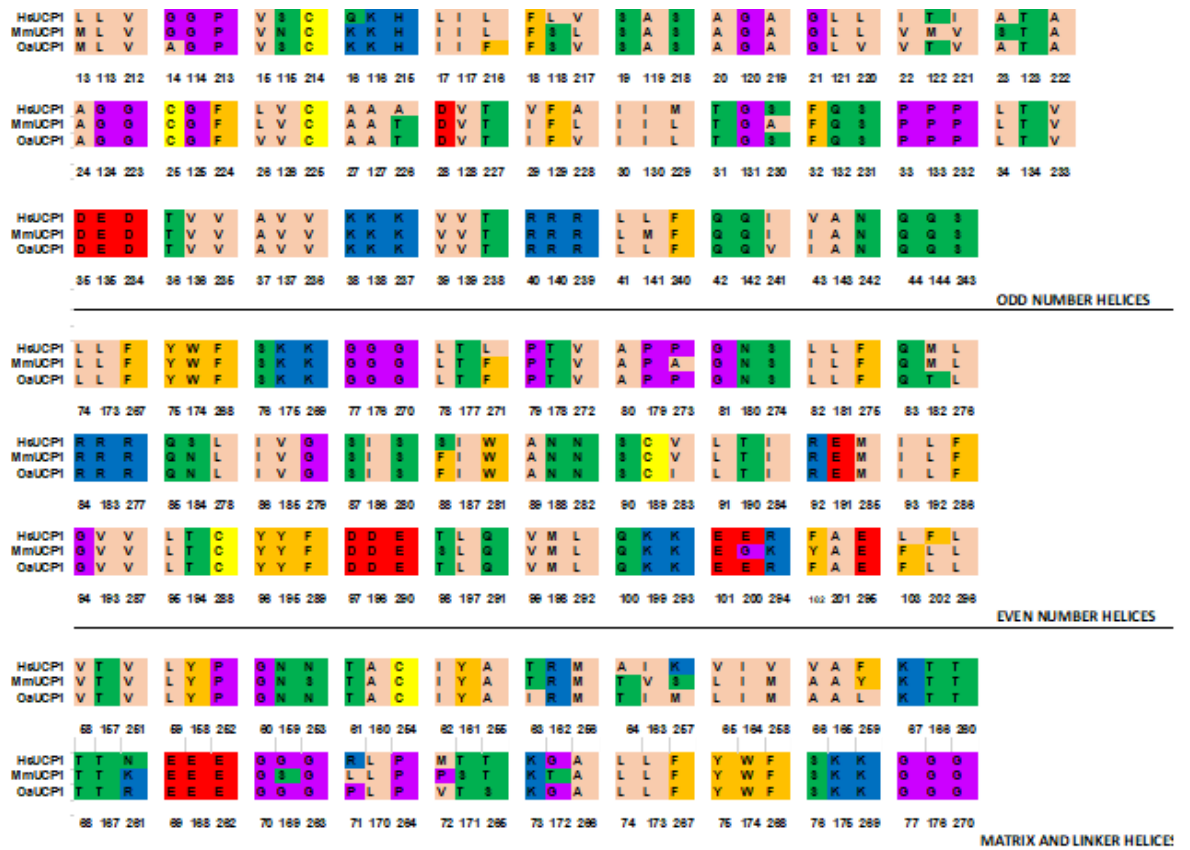
HsUCP1 182 MRSV IINCTELV TYDLMKEAFVKNNILADDVPCHLVSAL IAGFCATAMSS 231
MmUCP1 182 MRNVIINCTELV TYDLMK GALVNNKILADDVPCHLLSALVAGFCTLLAS 231
OaUCP1 180 TRNVIINCTELV TYDLMKEALVKNKLLADDVPCHLVSALVAGFCTIVLSS 229
BtAAC1 182 QGI I IYRAAYFGVYDTAKG-----MLPDPKNVHIVSWMIAQTVTAVAG 225
ScAAC2 198 VGIVVYRGLYFGMYDSLKPL-----LLTGSLEGSFLASFLLGWVVTTGAS 242
ScAAC3 187 VGIVVYRGLYFGMFDLKP-----VLTGSLDGSFLASFLLGWVVTTGAS 231
TtAAC 191 AGIVVYRGLYFGMYDSIKPV-----VLVGPLANNFLASFLLGWCVTTGAS 235

HsUCP1 232 ----PVDVVKTRFINSPPG-----QYKSPNCAMKVFTNEGPTAFFKGLV 272
MmUCP1 232 ----PVDVVKTRFINSLPG-----QYPSVPSCAMSMYTKEGPTAFFKGFV 272
OaUCP1 230 ----PVDVVKTRFVNSSPG-----QYTSVPNCAMMMLTREGPSAFFKGFV 270
BtAAC1 226 LVSYPFDTVRRRMMMQSGRKGADIMYTGTVDCWRKIAKDEGPKAFFKGAW 275
ScAAC2 243 TCSYPLD TVRRRMMMTSGQ---AVKYDGAFDCLRKIVAAEGVGS LFKGCG 289
ScAAC3 232 TCSYPLD TVRRRMMMTSGQ---AVKYNGAIDCLKKIVASEGVGS LFKGCG 278
TtAAC 236 IASYPLD TVRRRMMMTSGE---AVKYKSSIDAFRQIIAKEGVKSLFKGAG 282

HsUCP1 273 PSFLRLGSWNVI MFVCFEQLKRELSKSRQTMDCAT 307
MmUCP1 273 ASFLRLGSWNVI MFVCFEQLKKELMKSRQTVDCIT 307
OaUCP1 271 PSFLRLGSWNVI MFVCFEQLKRELMKSRQAMDCAT 305
BtAAC1 276 SNVLR-GMGGAFVLVLYDEIKKFFV----- 298
ScAAC2 290 ANILR-GVAGAGVISM YDQLQMI LFGKKFK----- 318
ScAAC3 279 ANILR-SVAGAGVISM YDQLQMI LFGKKFK----- 307
TtAAC 283 ANILR-GVAGAGVLSIYDQLKILLFGKAFKGGSG- 315

```

**Appendix figure A8. UCP1 isoforms alignment to AAC isoforms.** Human, mouse, and ovine UCP1 are here aligned to the AAC isoforms for which structures are currently available (alignment algorithm: MUSCLE, alignment performed in Jalview). HsUCP1=human UCP1; MmUCP1=mouse UCP1; OaUCP1=ovine UCP1; BtAAC1=bovine AAC; ScAAC2/3=yeast AAC isoforms; TtAAC=thermophilic fungus AAC. Positively charged residues are in blue, negatively charged in red, polar residues in green, hydrophobic residue in pink and aromatic residues in orange. Proline and glycine (helix breakers) are shown in violet and cysteines in yellow.



**Appendix figure A9. UCP1 isoforms triplet alignment.** Alignment of HsUCP1, MmUCP1 and OaUCP1 by triplet symmetry, based on the alignment in [137]. Aminoacid numbering of HsUCP1. Positively charged residues are in blue, negatively charged in red, polar residues in green, hydrophobic residue in pink and aromatic residues in orange. Proline and glycine (helix breakers) are shown in violet and cysteines in yellow.

**Appendix Table A3. Example of systematic analysis of HsUCP1 triplet alignment**

<b>C-state</b>	<b>Residue</b>	<b>In literature</b>	<b>Contact</b>	<b>Residues Contacting</b>	<b>M-state</b>	<b>Residue</b>	<b>In literature</b>	<b>Contacts</b>	<b>Residues Contacting</b>
T	5	n	n		T	5	n	n	
A	105	n	n		A	105	n	n	
K	204	n	n		K	204	n	n	
	6	n	n		A	6	n	n	
G	106	n	n		G	106	n	n	
N	205	n	n		N	205	n	n	
S	7	n	n		S	7	n	n	
K	107	n	n		K	107	n	n	
N	206	n	n		N	206	n	n	
D	8	n	n		D	8	n	n	
E	108	n	n		E	108	n	n	
I	207	n	n		I	207	n	n	
V	9	n	n		V	9	n	n	
T	109	n	n		T	109	n	n	
L	208	n	n		L	208	n	n	
H	10	n	n		H	10	n	n	
A	110	n	n		A	110	n	n	
A	209	n	n		A	209	n	n	
P	11	n	n		P	11	n	n	
P	111	n	n		P	111	n	n	
D	210	YES	n		D	210	YES	n	
T	12	n	n		T	12	n	n	
S	112	n	n		S	112	n	n	
D	211	YES	n		D	211	YES	n	
L	13	n	n		L	13	n	n	
L	113	n	n		L	113	n	n	
V	212	n	n		V	212	n	n	
G	14	n	n		G	14	n	n	
G	114	n	n		G	114	n	n	
P	213	n	n		P	213	n	n	
V	15	n	n		V	15	n	n	
S	115	n	n		S	115	n	n	
C	214	n	n		C	214	n	n	

Q	16	n	n		Q	16	n	n	
K	116	n	n		K	116	n	n	
H	215	YES	n		H	215	YES	n	
L	17	n	n		L	17	n	n	
I	117	n	n		I	117	n	n	
L	216	n	n		L	216	n	N	
F	18	n	n		F	18	n	n	
L	118	n	n		L	118	n	n	
V	217	n	n		V	217	n	n	
S	19	n	n		S	19	n	n	
A	119	n	n		A	119	n	y	thr123
S	218	n	n		S	218	n	n	
A	20	n	n		A	20	n	n	
G	120	n	n		G	120	n	n	
A	219	n	n		A	219	n	n	
G	21	n	n		G	21	n	n	
L	121	n	n		L	121	n	y	v185
L	220	n	n		L	220	n	n	
I	22	n	n		I	22	n	n	
T	122	n	n		T	122	n	n	
I	221	n	n		I	221	n	n	
A	23	n	n		A	23	n	n	
T	123	n	n		T	123	n	y	leu95
A	222	n	n		A	222	n	n	
A	24	n	N		A	24	n	y	A89
G	124	n	n		G	124	n	n	
G	223	n	n		G	223	n	y	v283/thr227
C	25	n	n		C	25	n	n	
G	125	n	n		G	125	n	n	
F	224	n	n		F	224	n	n	
L	26	n	n		L	26	n	n	
V	126	n	n		V	126	n	n	
C	225	n	n		C	225	n	n	
A	27	n	n		A	27	n	n	
A	127	n	n		A	127	n	n	
A	226	n	y	thr194	A	226	n	n	
D	28	n	N		D	28	n	y	phe32
V	128	n	n		V	128	n	y	ser184
T	227	n	n		T	227	n	y	gly223

V	29	n	n		V	29	n	n	
F	129	n	y	thr177	F	129	n	n	
A	228	n	n		A	228	n	y	ser231
I	30	n	n		I	30	n	n	
I	130	n	n		I	130	n	n	
M	229	n	n		M	229	n	n	
T	31	n	n		T	31	n	n	
G	131	n	n		G	131	n	n	
S	230	n	y	thr190	S	230	n	n	
F	32	n	n		F	32	n	y	thr26/asp28
Q	132	n	y	thr177/asn180	Q	132	n	y	asn180/val136
S	231	n	n		S	231	n	y	ser274
P	33	n	n		P	33	n	n	
P	133	n	n		P	133	n	n	
P	232	n	n		P	232	n	n	
L	34	n	n		L	34	n	n	
T	134	n	n		T	134	n	n	
V	233	n	n		V	233	n	n	
D	35	n	y	lys34	D	35	n	n	
E	135	n	n		E	135	n	n	
D	234	n	n		D	234	n	y	lys3237
T	36	n	n		T	36	n	y	leu74/phe32/arg40
V	136	n	y	arg140	V	136	n	y	gln32
V	235	n	n		V	235	n	n	
A	37	n	n		A	37	n	n	
V	137	n	n		V	137	n	y	leu141
V	236	n	n		V	236	n	y	phe240
K	38	n	y	asp35	K	38	n	y	gln42
K	138	n	n		K	138	n	n	
K	237	n	n		K	237	n	y	asn180
V	39	n	n		V	39	n	y	val43
V	139	n	n		V	139	n	n	
T	238	n	n		T	238	n	n	
R	40	n	n		R	40	n	y	thr36
R	140	n	y	val136/ala160	R	140	n	n	
R	239	n	n		R	239	n	y	ser243
L	41	n	n		L	41	n	n	
L	141	n	n		L	141	n	n	
F	240	n	n		F	240	n	n	

Q	42	n	n		Q	42	n	y	lys38
Q	142	n	n		Q	142	n	n	
I	241	n	n		I	241	n	n	
V	43	n	n		V	43	n	y	arg40
A	143	n	n		A	143	n	n	
N	242	n	n		N	242	n	n	
Q	44	n	y	gln40	Q	44	n	y	pro48
Q	144	n	y	ser50	Q	144	n	y	his148
S	243	n	n		S	243	n	y	arg239

C-state	Residue	In literature	Contact	Residues Contacting	M-state	Residue	In literature	Contacts	Residues Contacting
V	58	n	n		V	58	n	n	
T	157	n	n		T	157	n	n	
V	251	n	n		V	251	n	n	
L	59	n	n		L	59	n	n	
Y	158	n	n		Y	158	n	n	
P	252	n	n		P	252	n	y	met256
G	60	n	n		G	60	n	y	thr63
N	159	n	n		N	159	n	y	tyr155
N	253	n	n		N	253	n	n	
T	61	n	n		T	61	n	y	gly57
A	160	n	y	arg140	A	160	n	y	tyr154
C	254	n	n		C	254	n	y	val258
I	62	n	n		I	62	n	n	
Y	161	n	n		Y	161	n	n	
A	255	n	n		A	255	n	n	
T	63	n	n		T	63	n	n	
R	162	n	n		R	162	n	n	
M	256	n	n		M	256	n	n	
A	64	n	n		A	64	n	n	
I	163	n	n		I	163	n	n	
K	257	n	n		K	257	n	n	
V	65	n	n		V	65	n	n	
I	164	n	n		I	164	n	n	
V	258	n	n		V	258	n	n	
V	66	n	n		V	66	n	n	
A	165	n	n		A	165	n	n	
F	259	n	n		F	259	n	n	

K	67	n	n		K	67	n	n	
T	166	n	n		T	166	n	n	
T	260	n	n		T	260	n	n	
T	68	n	n		T	68	n	n	
T	167	n	n		T	167	n	n	
N	261	n	n		N	261	n	n	
E	69	n	n		E	69	n	n	
E	168	n	n		E	168	n	n	
E	262	n	n		E	262	n	n	
G	70	n	n		G	70	n	n	
G	169	n	n		G	169	n	n	
G	263	n	n		G	263	n	n	
R	71	n	n		R	71	n	n	
L	170	n	n		L	170	n	n	
P	264	n	n		P	264	n	n	
M	72	n	n		M	72	n	n	
T	171	n	n		T	171	n	n	
T	265	n	n		T	265	n	n	
K	73	n	n		K	73	n	n	
G	172	n	n		G	172	n	n	
A	266	n	n		A	266	n	n	
L	74	n	n		L	74	n	y	thr136
L	173	n	n		L	173	n	n	
F	267	n	n		F	267	n	n	
C-state	Residue	In literature	Contact	Residues Contacting	M-state	Residue	In literature	Contacts	Residues Contacting
V	58	n	n		V	58	n	n	
T	157	n	n		T	157	n	n	
V	251	n	n		V	251	n	n	
L	59	n	n		L	59	n	n	
Y	158	n	n		Y	158	n	n	
P	252	n	n		P	252	n	y	met256
G	60	n	n		G	60	n	y	thr63
N	159	n	n		N	159	n	y	tyr155
N	253	n	n		N	253	n	n	
T	61	n	n		T	61	n	y	gly57
A	160	n	y	arg140	A	160	n	y	tyr154
C	254	n	n		C	254	n	y	val258
I	62	n	n		I	62	n	n	
Y	161	n	n		Y	161	n	n	

A	255	n	n		A	255	n	n	
T	63	n	n		T	63	n	n	
R	162	n	n		R	162	n	n	
M	256	n	n		M	256	n	n	
A	64	n	n		A	64	n	n	
I	163	n	n		I	163	n	n	
K	257	n	n		K	257	n	n	
V	65	n	n		V	65	n	n	
I	164	n	n		I	164	n	n	
V	258	n	n		V	258	n	n	
V	66	n	n		V	66	n	n	
A	165	n	n		A	165	n	n	
F	259	n	n		F	259	n	n	
K	67	n	n		K	67	n	n	
T	166	n	n		T	166	n	n	
T	260	n	n		T	260	n	n	
T	68	n	n		T	68	n	n	
T	167	n	n		T	167	n	n	
N	261	n	n		N	261	n	n	
E	69	n	n		E	69	n	n	
E	168	n	n		E	168	n	n	
E	262	n	n		E	262	n	n	
G	70	n	n		G	70	n	n	
G	169	n	n		G	169	n	n	
G	263	n	n		G	263	n	n	
R	71	n	n		R	71	n	n	
L	170	n	n		L	170	n	n	
P	264	n	n		P	264	n	n	
M	72	n	n		M	72	n	n	
T	171	n	n		T	171	n	n	
T	265	n	n		T	265	n	n	
K	73	n	n		K	73	n	n	
G	172	n	n		G	172	n	n	
A	266	n	n		A	266	n	n	
L	74	n	n		L	74	n	y	thr136
L	173	n	n		L	173	n	n	
F	267	n	n		F	267	n	n	

<b>C-state</b>	Residue	In literature	Contact	Residues Contacting	<b>M-state</b>	Residue	In literature	Contacts	Residues Contacting
----------------	---------	---------------	---------	---------------------	----------------	---------	---------------	----------	---------------------

L	74	n	n		L	74	n	n	
L	173	n	n		L	173	n	n	
F	267	n	n		F	267	n	n	
Y	75	n	n		Y	75	n	n	
W	174	n	n		W	174	n	y	leu170
F	268	n	n		F	268	n	n	
S	76	n	n		S	76	n	n	
K	175	n	y	gln243/ile237 /gly168	K	175	n	n	
K	269	n	n		K	269	n	n	
G	77	n	n		G	77	n	n	
G	176	n	n		G	176	n	y	asn180
G	270	n	n		G	270	n	n	
L	78	n	y	intraloop leu74	L	78	n	y	intrahelix leu82
T	177	n	y	phe125/gln128	T	177	n	y	leu181
L	271	n	n		L	271	n	n	
P	79	n	n		P	79	n	n	
T	178	n	n		T	178	n	n	
V	272	n	n		V	272	n	n	
A	80	n	n		A	80	n	n	
P	179	n	y	arg183	P	179	n	n	
P	273	n	n		P	273	n	n	
G	81	n	n		G	81	n	n	
N	180	n	y	gln132/	N	180	n	y	lys237/ser184 /gln132
S	274	n	y	intrah leu278	S	274	n	y	ser231
L	82	n	n		L	82	n	y	intrahelix ile 86 leu78
L	181	n	n		L	181	n	y	val185
F	275	n	n		F	275	n	n	
Q	83	n	n		Q	83	n	n	
M	182	n	n		M	182	n	n	
L	276	n	y	trp281 intrah	L	276	n	y	ser 280 intrahelix
R	84	n	n		R	84	n	n	
R	183	n	y	pro turn under to the bottom	R	183	n	y	arg277/ile187
R	277	n	n		R	277	n	y	arg183
Q	85	n	n		Q	85	n	n	
S	184	n	n		S	184	n	y	val128/ile187 /asn188
L	278	n	y	ser274 intrah	L	278	n	y	asn282 intrah
I	86	n	n		I	86	n	y	ser 90 leu 82 intrahelix but doublecheck ser90
V	185	n	n		V	185	n	y	leu121/leu181

G	279	n	n		G	279	n	y	val283
S	87	n	n		S	87	n	n	
I	186	n	n		I	186	n	y	thr190
S	280	n	n		S	280	n	y	leu276 intrah
S	88	n	n		S	88	n	n	
I	187	n	n		I	187	n	y	glu191/ and ser184 on same helix
W	281	n	y	leu276	W	281	n	n	
A	89	n	n		A	89	n	y	ala24
N	188	n	n		N	188	n	y	arg92/ser 184 same helix
N	282	n	n		N	282	n	y	leu278/phe286 intrah
S	90	n	n		S	90	n	y	ile86 leu17
C	189	n	n		C	189	n	y	val193 same helix
V	283	n	n		V	283	n	y	val287/gly279 intrah
L	91	n	n		L	91	n	n	
T	190	n	y	ser230	T	190	n	y	194/187, h-bonds alpha helix
I	284	n	n		I	284	n	y	cys288 intrah
R	92	n	n		R	92	n	y	asn188/ thr 123on same helix
E	191	n	n		E	191	n	y	ile187/ tyr 195
M	285	n	n		M	285	n	n	
I	93	n	n		I	93	n	y	phe289
L	192	n	n		L	192	n	n	
F	286	n	n		F	286	n	y	asn282 intrah
G	94	n	n		G	94	n	n	
V	193	n	n		V	193	n	y	lys116
V	287	n	n		V	287	n	y	val283 intrah
L	95	n	n		L	95	n	y	thr123\
T	194	n	y	ala226	T	194	n	y	one turn up and down intrahelix
C	288	n	n		C	288	n	y	leu292 /ile284 intrah
Y	96	n	n		Y	96	n	y	gln100 intrahelix
Y	195	n	n		Y	195	n	y	intrahelix glu191
F	289	n	n		F	289	n	y	ile93
D	97	n	n		D	97	n	y	lys293/glu101 only intrahelix
D	196	n	n		D	196	n	n	
E	290	n	n		E	290	n	y	lys199
T	98	n	n		T	98	n	y	leu13
L	197	n	n		L	197	n	y	intrahelix val193
Q	291	n	n		Q	291	n	n	
V	99	n	n		V	99	n	y	intrahelix leu95

M	198	n	n		M	198	n	y	intrahelix 194
L	292	n	n		L	292	n	y	cys288 intrah
Q	100	n	y	thr104	Q	100	n	y	all intra thr104 /tyr96
K	199	n	n		K	199	n	y	glu290
K	293	n	n		K	293	n	y	asp97
E	101	n	y	intra ala105	E	101	n	y	intra asp97
E	200	n	n		E	200	n	n	
R	294	n	y	ser297 intrah	R	294	n	n	
F	102	n	n		F	102	n	n	
A	201	n	n		A	201	n	n	
E	295	n	n		E	295	n	n	
L	103	n	n		L	103	n	y	glu108
F	202	n	n		F	202	n	n	
L	296	n	n		L	296	n	n	